Energy Storage Materials 68 (2024) 103361

Contents lists available at ScienceDirect

Energy Storage Materials

journal homepage: www.elsevier.com/locate/ensm

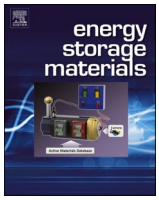

Emerging trends and prospects in aqueous electrolyte design: Elevating energy density and power density of multivalent metal-ion batteries

Yi-Yen Hsieh [1], Hsing-Yu Tuan [1,*]

Department of Chemical Engineering, National Tsing Hua University, Hsinchu 30013, Taiwan

ARTICLE INFO

Keywords:
Batteries
Energy storage
Aqueous electrolyte
Interfacial chemistry
Multivalent metal-ion batteries

ABSTRACT

Aqueous batteries, using multivalent metallic charge carriers (Zn^{2+}, Mg^{2+}, Ca^{2+}, Al^{3+}), show promise as next-generation electrochemical energy storage due to their adequate energy density, high power density, and cost-effectiveness. The electrolyte, serving as a bridge between the cathode and anode, plays a crucial role in functionality. However, the use of aqueous electrolytes introduces issues such as limited voltage range, slow kinetics of multivalent cations, and side reactions on metal surfaces. Electrolyte engineering has emerged as a key solution to overcome major challenges in multivalent metal-ion batteries. This innovative approach involves optimizing factors such as electrolyte concentration, specific additives, pH management, and manipulating the ligand effect of cation salts. Additionally, incorporating anti-freezing agents is crucial. A systematic review of this domain is crucial for further development and refinement of electrolyte engineering strategies. This review should primarily focus on assessing how these modifications can enhance energy and power densities, broaden the operational range of the batteries (by adjusting water activity and LUMO/HOMO energy levels), improve cation transport (via enhanced ion conductivity, dielectric constant, transference number, and solvation structure), and effectively mitigate detrimental side reactions, such as metal deposition, interphase formation, and hydrogen bonding regulation. The electrolyte design strategies in multivalent metal-ion systems are outlined in terms of their effectiveness in smoothing metal dendrites, managing solvation shells and free water molecules, and minimizing side reactions between the metal surface and electrolyte. The article proposes future innovation directions and development prospects for enhancing electrolyte design engineering in these systems.

1. Introduction

Lithium-ion batteries (LIBs) are prevalent in mobile devices and electric vehicles but concerns over limited lithium reserves (77 K tons) are driving research into alternatives. Sodium-ion batteries (SIBs) and potassium-ion batteries (PIBs) are promising contenders because the demand is growing for battery technologies with plentiful metal resources and superior energy density. These monovalent metal-ion batteries have been widely developed as cathodes for aqueous monovalent-ion batteries because of their low cost and high theoretical capacity [1]. Multivalent metal-ion batteries (), using abundant elements like zinc (Zn, 13 M tons), calcium (Ca, 4.1 % of Earth's crust), magnesium (Mg, 29.1 M tons), and aluminum (Al, 64 M tons), are promising alternatives to lithium-ion batteries [2]. The electrochemical reaction of aqueous batteries are driven by multivalent charge carriers (divalent ions like Zn^{2+}, Mg^{2+}, Ca^{2+}, and trivalent ions like Al^{3+}) moving between anodes and cathodes during cycling, accompanied with the transport of protons [3]. The similarities between multivalent metal-ion batteries and monovalent metal-ion batteries allow for leveraging existing knowledge and manufacturing practices for quicker industry adoption of these new systems. Metals like Zn, Ca, Mg, and Al offer greater air stability and lower reactivity than Li, Na, and K. The viability of these multivalent metal-ion batteries depends on whether they offer sufficient advantages over LIBs to be considered favorable alternatives [4,5]. Numerous reported literatures has presented a complete system of cathode and anode materials to emphasize their electrochemical performance on aqueous batteries [6–9]. Therefore, this review explores aqueous electrolytes in multivalent metal-ion battery systems, focusing on their potential for wide working window, reversible capacity, and fast ion transport. It examines how the electrolytes influence the performance of aqueous energy storages and expand their applicability to match those of LIBs. Key challenges, direct impacts, critical factors, and design strategies will

* Corresponding author.
E-mail address: hytuan@che.nthu.edu.tw (H.-Y. Tuan).

[1] This review is written jointly by Yi-Yen Hsieh and Hsing-Yu Tuan with data cited from the literature.

https://doi.org/10.1016/j.ensm.2024.103361
Received 25 December 2023; Received in revised form 15 March 2024; Accepted 20 March 2024
Available online 21 March 2024

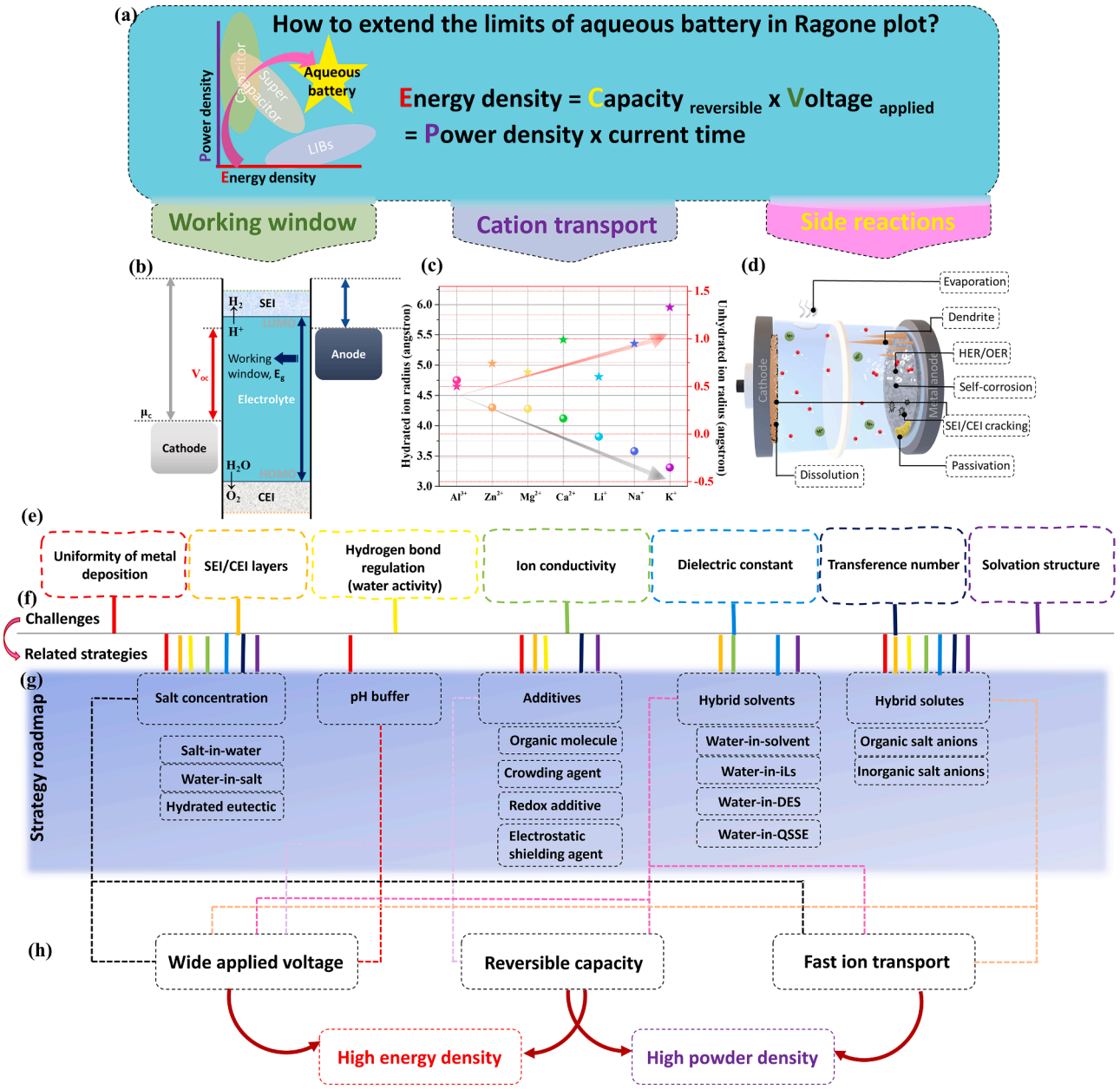

Fig. 1. (a) The core concepts and scheme of this review article. (b) Principle of working window of electrolyte. (c) Hydrated and unhydrated cation ratio of triple-valent, double-valent, and monovalent metal ions. (d) Challenges and shortcomings of aqueous batteries. (e) The crucial factors and directions we will discuss in this review. (f) The challenges faced in aqueous batteries correspond to related strategies. (g) Strategy roadmap and the categories of each strategy and the problems they address, shown by color-coded lines connecting key factors in (e). (h) The relationship between the ultimate goals (high energy and power density) corresponding to these electrolyte design strategies.

be analyzed, particularly in terms of energy density and power density (Fig. 1a). According to the relationships of energy density and power density, critical parameters are dominated by the side-reaction inhibition, working window, and cation transport kinetics of battery system. The side reactions can be divided into seven parts, including electrolyte evaporation, metal dendrite, hydrogen evolution, electrode corrosion, SEI cracking, surface passivation, cathode dissolution. Meanwhile, cation transport kinetics are controlled by ion conductivity, dielectric constant, transference number, and solvation structure. We will mention the concerns of aqueous batteries, further discussing the working principle, related equations, and its solutions. After understanding the critical factors of electrochemical performances, the properties and design strategies of electrolytes are critically reviewed with an emphasis on metal deposition/corrosion, solid-electrolyte interphase (SEI), hydrogen bonding between water molecules, ionic conductivity, dielectric constant, transference number, and solvation structure. We summarize the solutions and characterization for each critical aspect of aqueous batteries toward the electrochemical behavior, highlighting electrolyte design strategies, which can enable high-performance multivalent metal-ion batteries. The final section will propose feasible pathway to overcome the current obstacles in academic research and practical applications.

2. Working principle and design aspects of electrolytes in aqueous electrolytes

The electrolyte design will focus on three key aspects: working window, cation transport kinetics, and side reactions. The discussion

begins with the fundamental electrochemistry and transport kinetics of electrolytes. This includes operational cell voltage, solid-electrolyte interphase (SEI) formation, ionic conductivity, dielectric constant, and transference number, which are related to radius of un-/hydrated cations, viscosity, and charge-transfer impedance.

2.1. Principle of working window and characterization of electrolytes

In electrolyte design, the crucial factor is the electrolyte's working window, which influences the choice of electrode materials and battery safety (Fig. 1b). Before exploring design strategies for optimizing the electrolyte system, it's essential to identify the parameters or requirements that significantly impact the electrolyte's electrochemical performance. For storage capability, a suitable electrolyte should prioritize the migration, convection, and diffusion of both cations and anions, guided by the Nernst-Planck equation.

$$J(x) = -D\frac{\partial C(x)}{\partial x} - \frac{\partial F}{RT}DC\frac{\partial \Phi(x)}{\partial x} + Cv(x) \quad (1)$$

Where J, z, D, C, R, T, F and Φ are respectively the flux of species in the solution, valence of ionic species, diffusion coefficient, concentration, gas constant, temperature, Faradaic constant, and electrical potential in the solution. The $-D\frac{\partial C(x)}{\partial x}$, $DC\frac{\partial \Phi(x)}{\partial x}$, and $Cv(x)$ are diffusion, migration, and convection factors, respectively. In both coin-cell and pouch-type batteries, stirring at the electrode surface is ineffective, rendering forced convection negligible. During charging and discharging, metal cations (counterions) migrate towards the opposite electrodes. This movement is influenced by factors like concentration, viscosity, steric effect, sheath force, counterion effect, and the polarity of electrolyte salts and solvents. Electrochemical performances such as rate capability, cyclability, and reversibility can be improved by altering solvation effects, dissociation, mobility, reactivity, polarization, conductivity, and stability of electrolyte properties. This section will explore the diverse impacts and properties of various electrolytes on electrochemical reactions. In general, three key reaction interfaces exist: electrolyte, active materials, and the current collector. The most critical factor on control of physical properties is the interface between active materials and electrolyte. When materials contact with electrolytes, chain reactions of solvents and solutes occur. A passivating SEI layer provides kinetic stability, creates a barrier to electron transfer between electrodes and electrolytes, and prevents redox reactions of electrolytes. The open circuit potential (V_{oc}) of a battery cell are determined by the work function difference between the cathode and anode as follows [10].

$$e * V_{oc} = \mu_a - \mu_c < E_g \quad (2)$$

Here e is the charge of electron (1.602×10^{-19} C). The working window of an electrolyte is defined by the energy gap between its lowest unoccupied molecular orbital (LUMO) and highest occupied molecular orbital (HOMO). The electrochemical potentials of the anode (μ_a) and cathode (μ_c) are based on their Fermi levels. Effective battery operation requires the electrodes' chemical potentials to align with the electrolyte's working window. If the anode's μ_a exceeds the LUMO, it may reduce the electrolyte, unless prevented by a SEI layer, which blocks electron transfer from the anode to the LUMO. Similarly, a cathode with μ_c below the electrolyte's HOMO risks oxidizing the electrolyte, unless a passivation layer prevents electron transfer from the HOMO to the cathode. Electrons from the anode's Fermi level donated to the electrolyte's LUMO can catalyze water and hydrogen evolution reactions (HER) if the anode's potential is higher than the LUMO. Conversely, if the cathode's μ_c is lower than the electrolyte's HOMO, oxygen evolution reactions (OER) occur, with electrons moving from the electrolyte to the cathode. Therefore, designing an electrolyte with a wide potential window is crucial to encompass the potential range between the cathode and anode. In addition, the V_{oc} can be determined by voltametric measurements such as linear sweep voltammetry (LSV) and cyclic voltammetry (CV) under three-electrode system. The applied current (I_{app}) and enclosed area (capacitance, Q) of CV curves can be divided into two parts as follows:

$$I_{app} = I_c + I_p$$
$$Q = (I_c + I_p) * t \quad (3)$$

Where I_c and I_p are capacitive current (non-faradaic current) and peak current (faradaic current), representing adsorption/desorption phenomena and redox process respectively. The I_c is generally close to zero when I_{app} determines the potential window without any polarization and decomposition of electrolyte. The area enclosed by CV curves can be divided into cathodic and anodic reactions, allowing for the calculation of their contribution ratios. This measurement can indicate the occurrence of undesirable redox reactions in the electrolyte.

2.2. Transport kinetics of metal cations

The kinetic reactions and diffusion behavior through electrode surface and bulk electrolytes are respectively governed by the dehydration and hydration radii of cations. During the transport process in bulk electrolyte, cations will be solvated by anions due to their opposite charge. The relationship between the cation radius and its Stokes radius is depicted in Fig. 1c. The hydrated radius of a cation is influenced by its oxidation state and unhydrated radius. Generally, under the same oxidation state, a smaller unhydrated cation radius result in a larger solvation radius. As a cation's oxidation state increases, so does its hydration radius. Consequently, an increase in hydration radius and associated sheath force leads to reduced mobility of cations in the electrolyte, posing challenges for achieving high-current durability in aqueous batteries [11,12]. That is, the ionic mobility (μ_i) depends on the ionic size and interactive environment with surrounding species such as counterions, solvent species, and polar groups of solvent molecules, as shown below [13].

$$\mu_i = \frac{Z_i F\ D_i}{RT} \quad (4)$$

$$D = \frac{k_B\ T}{6\pi\ \eta\ r} \quad (5)$$

$$\mu_i = \frac{1}{6\pi\ \eta\ r} \quad (6)$$

The r, k_B, and η are respectively solvation radius of metal cations, Boltzmann's constant, and viscosity of electrolyte. After inserting the Eqs. (2) into (1), the related formula (3) demonstrates that the ion mobility is inversely proportional to the viscosity of electrolyte and solvation radius of cations. Low viscous solvents can enhance the ionic mobility and ameliorate the concentration polarization according to the Stokes–Einstein relation. Besides, the diffusion coefficient of cations in a solvent can be measured by CV curves at various scan rates (Randles–Sevcik equation) and galvanostatic intermittent titration technique.

Considering the solvation phenomena, the dielectric constant (ε) of the solvents is also critical factor, which determines number of free charge carriers, solubility, and viscosity [14]. In other words, a cation in a high-ε solvent have a higher probability of remaining free, thereby avoiding the ion pairing of transferred cations with base electrolyte anions or molecules [15]. As the transport media of ionic motion, water can possess a higher dielectric constant and ionic mobility than most organic solvents. When we apply an electric field to a material with a high dielectric constant, the electric charges within the material will become polarized, allowing the material to store more electrical energy. The higher polarity and dipole moment of molecules are, the better dielectric constant a solvent has. The common solvents with present of cyclocarbonate structures, such as ethylene carbonate (EC), propylene carbonate (PC), has a high dielectric constant accompanied with high

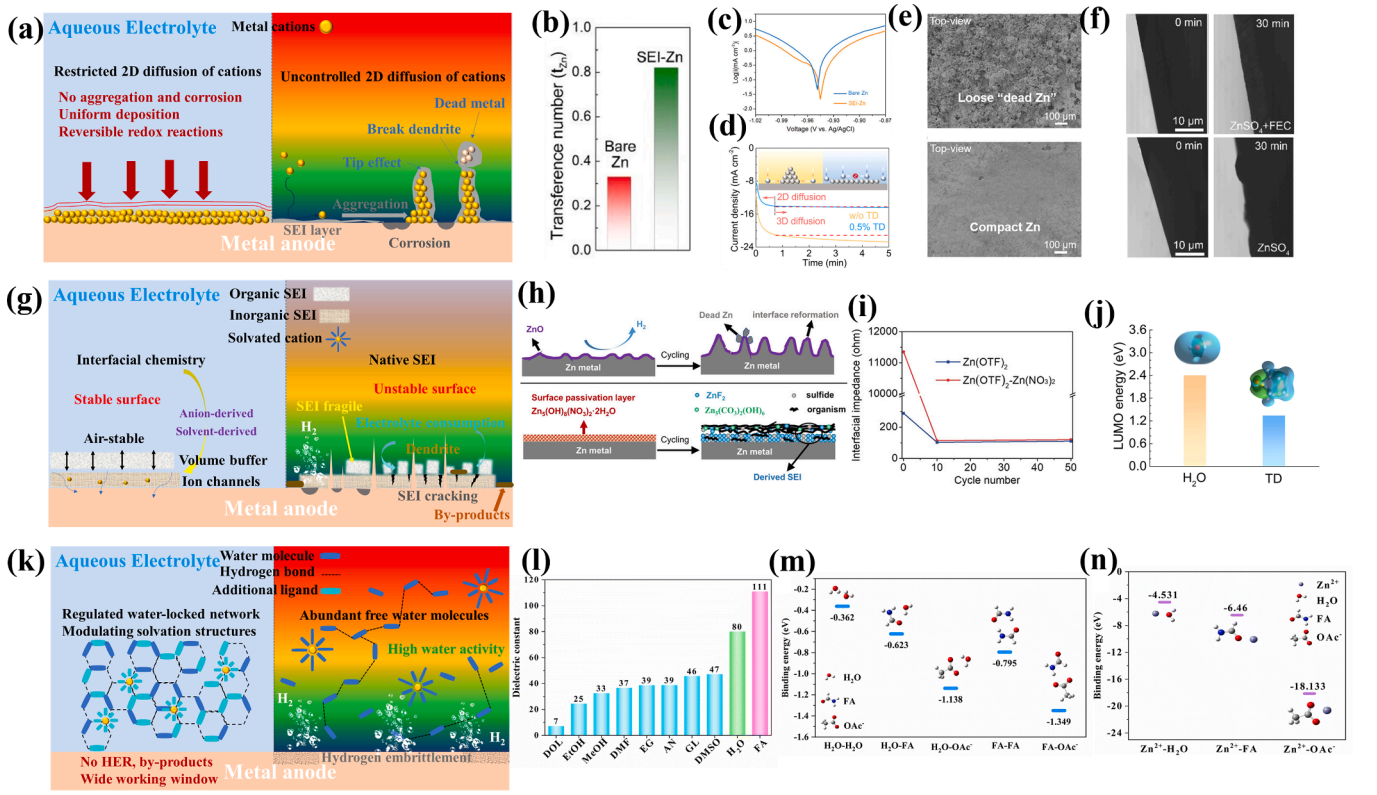

Fig. 2. Aqueous electrolyte issues of multivalent metal-ion batteries. (a) Scheme of metal deposition and its side reactions. (b) The Zn^{2+} transference numbers of bare Zn and SEI-Zn electrodes. Reprinted with permission from Ref. [36] Copyright 2021 Elsevier. (c) Linear polarization curves for describing the corrosion of Zn electrodes. Reprinted with permission from Ref. [31] Copyright 2021 Wiley-Blackwell. (d) Chronoamperograms and scheme of 2D and 3D diffusion behavior. Reprinted with permission from Ref. [43] Copyright 2023 Elsevier. (e) SEM images of Zn electrodes after cycling for 400 h in the baseline electrolyte (upper) and the designed electrolyte (lower). Reprinted with permission from Ref. [31] Copyright 2021 Wiley-Blackwell. (f) In situ optical microscope observations of the Zn deposition process in $ZnSO_4$ and $ZnSO_4$ + FEC electrolytes. Reprinted with permission from Ref. [19] Copyright 2023 Wiley-Blackwell. (g) Scheme of SEI formation and its side reactions. (h) Illustration of surface evolution mechanism with and without modification. (i) Interfacial impedance measured from Zn//Zn cells in Zn $(OTf)_2$-$Zn(NO_3)_2$ and $Zn(OTf)_2$ electrolytes under cycling. Reprinted with permission from Ref. [33] Copyright 2023 Wiley-Blackwell. (j) The LUMO energy levels of H_2O and TD molecules. Reprinted with permission from Ref. [43] Copyright 2023 Elsevier. (k) Scheme of hydrogen bond network and its side reactions. (l) Comparison of the dielectric constant for different organic solutions used in low-temperature aqueous electrolytes. (m) DFT calculated binding energies of H_2O–H_2O, H_2O–FA, H_2O–OAc^-, FA–FA, and FA–OAc^- pairs. (n) Calculated binding energies of Zn^{2+}–H_2O, Zn^{2+}–FA, and Zn^{2+}–OAc^-. Reprinted with permission from Ref. [50] Copyright 2023 Royal Society of Chemistry.

viscosity. While the chain carbonates (e.g., diethyl carbonate (DEC), dimethyl carbonate (DMC) and ethyl methyl carbonate (EMC)) have a low dielectric property and low viscosity. According to the Eq. (3), the increased viscosity of solvents will lead to low charge mobility and diffusion coefficient. The high ion mobility of molecules can further enhance the ionic conductivity of electrolytes, which facilitates the facile migration of charges. This is why the commercial electrolyte are the mixture composed of both EC and DEC [16].

Different electrolytes affect electrochemical reactions, including mass transfer, surface kinetics, and redox behavior, during cation transport from bulk solution to electrode surface. This charge transfer mechanism involves the dissociation/solvation of metal cations and proton transport. Additionally, the migration and dissociation of ionic complexes and solvated ions are linked to ionic conductivity (σ). The Nernst-Einstein equation, derived from solvation and migration behavior, illustrates these relationships.

$$\sigma = F\sum_{i=0}^{n}(C_i\mu_i\ z_i) \tag{7}$$

The n_i, C_i, and z_i are number of charge carriers, molar concentration, and valence of ionic species, respectively. The higher ionic conductivity an electrolyte has, the lower series resistance (R_s) it will be. Therefore, we can use EIS technique and LSV curves to further calculate the ionic conductivity based on the Ohm's law [17].

$$\sigma = \frac{l}{R_s A} \tag{8}$$

where l and A represent the thickness of sample and contact surface area.

A lower viscosity leads to a higher ion mobility, while a lower solvation degree of cation leads to a higher mobility. Due to the influence of solvation effect, different oxidation state and unhydrated radius of metal cations are related to the transference number (t_i), which is the fraction of current carried by ionic species in the solution, as follows:

$$t = \frac{C_i\mu_i\ z_i}{\sum_{i=0}^{n}(C_i\mu_i\ z_i)} \Rightarrow_{All\ u\ the\ same} t = \frac{C_i z_i}{\sum_{i=0}^{n}(C_i z_i)}$$

In liquid electrolytes for metal ion batteries, the transference number is crucial for electrochemical performance. It's defined as the ratio of electric current carried by the cation to the total current. A transference number near 1 indicates cation-dominated ion conduction in the electrolyte. A high transference number reduces concentration polarization during charging and discharging, leading to higher power density [18]. The transference number of cations can be determined using Nyquist plots and current-time curves in symmetric cells, as shown in the following equation.

$$t_{cation} = \frac{I_s(\Delta V - I_o R_o)}{I_o(\Delta V - I_s R_s)}$$

The I_0, R_0, I_s, R_s, and ΔV are designated as initial current, initial resistance, steady-state current, steady-state resistance, and applied voltage [19]. To select an appropriate electrolyte for batteries, it's crucial to find one that alters the kinetics and diffusion of charge carriers. An ideal electrolyte should have high dielectric constant (ε), low viscosity (η), and good conductivity (σ), which is challenging in organic solvents. Water is a promising alternative due to its inherent properties, ion concentrations, and solvation degree, enhancing ionic conductivity for high power density. Consequently, many aqueous electrolytes have been formulated and utilized in different types of energy storages.

3. Challenges and strengths/weaknesses of aqueous batteries

Recent advancements in energy storage have led to the development of various metal-ion based systems. Organic electrolytes, chosen for their effective wettability, solubility, and ionic conductivity, are increasingly used in both academic and industrial applications. Aqueous rechargeable batteries, in comparison to non-aqueous ones, offer similar capacity and energy density. Meanwhile, their air stability significantly improves the safety of electric vehicles and devices. However, the working window of aqueous systems (< 1.5 V) is narrower than that of commercial organic solvents (2.0~3.0 V) used in LIBs, SIBs, and PIBs. Exceeding this voltage range can decompose water-based electrolytes, causing HER and OER. This leads to the expansion of coin-type or pouch-type cells, raising safety concerns during cycling. We will begin by discussing the development of monovalent metal-ion aqueous batteries over recent decades. Our focus will then shift to the development of electrolytes for multivalent metal-ion batteries. Finally, recent publications will be summarized on each type of aqueous battery. Besides, due to unique interactions with electrode materials, metal-ion system differs significantly in electrochemical nature and performance from the system of non-metallic charge carrier [7,20,21]. Therefore, our discussion will primarily focus on metal-ion batteries.

3.1. Challenges for aqueous batteries

In aqueous batteries, several side reactions are listed in Fig. 1d. Modifying hydrogen bonds between water molecules and other solvents or electrolyte anions can alter the water activity [22,23]. Second, drastic changes in pH are often caused by the formation of by-products [24]. Evaporation of aqueous electrolytes is also a problem for battery cycle life. On the cathode side, the dissolution of cathodes in aqueous batteries (e.g., $ZnMn_2O_4$ [25], V_2O_5 [26]) will occur, resulting in loss of active material and structural degradation, resulting in rapid capacity fading. On the metal anode side of batteries, common issues include dendrites, self-corrosion, and surface passivation, leading to short circuits, reduced redox reactivity, and low surface activity. Additionally, the repeated breaking and regrowth of SEI and CEI layers can cause excessive electrolyte consumption and material structural damage [27]. To take appropriate steps, we need to figure out what problems we face and why. In this section, we review the challenges faced in aqueous multivalent metal-ion batteries, focusing on uniformity of metal deposition, SEI/CEI layers, and hydrogen bond regulation (see Fig. 1e).

3.1.1. Uniformity of deposition on metal anode

To be compatible with satisfactory aqueous batteries, metal anode as the essential component has been modified from various perspectives and strategies, which includes interphase, substrate, and bulk design [28]. Dendrite growth is mainly caused by the uncontrollable 2D diffusion of metal cations on the anode surface, influenced by uneven electric field distribution (refer to Fig. 2a). This de-solvation process causes the initial formation of dendrite induced by accumulation of cations at specific active sites. Furthermore, post-plated Zn ions tend to deposit on dendrite bulges, where the tip effect increases charge density in the prominently curved areas [29]. The tip effect leads to increased uneven surface energy, promoting further dendrite growth and fragility, resulting in dead metal formation. The metal deposition on dendrites during the next stripping process causes irreversible oxidation and anode corrosion, worsening the electric field distribution. These corrosion sites without SEI layer protection are further corroded by electrolyte components (e.g., sulfide and water), triggering HER and the formation of passivating by-products [30]. Dendrite growth and surface corrosion significantly impact the transference number, as depicted in Fig. 2b. A lower transference number increases the concentration gradient of metal ions at the electrode/electrolyte interface, creating a strong interfacial electric field that exacerbates dendrite growth. The transference number of SEI-Zn is higher than that of bare Zn, suggesting that a pre-formed high-ion-conductivity SEI interphase helps to facilitate cation transport and inhibit detrimental ions. Fig. 2c uses Tafel plots to illustrate the corrosion status of metal surfaces. The tailored SEI-Zn anode, with a higher corrosion potential and lower corrosion current, shows a reduced tendency for surface corrosion. Additionally, Fig. 2d demonstrates 2D and 3D diffusion behaviors of metal ions through current-time measurements. In symmetric cells lacking proper SEI growth, a continuous increase in current density over time indicates ongoing 2D diffusion. In contrast, modified SEI surfaces exhibit a brief period of 2D diffusion followed by 3D diffusion with a lower current density, indicating uniform metal deposition without a significant increase in specific area. To observe dendrite formation during cycling, ex-situ and in-situ electron and optical microscopes are used to directly monitor metal deposition behavior (refer to Figs. 2e and 2f). The loose structures of metal anode are induced by massive amounts of dendrites-induced dead Zn metal. Meanwhile, corrosion and parasitic reactions on the metal surface are inevitably because of the direct contact between the aqueous electrolyte and unstable anode surface, resulting in the increase of local pH and the accumulation of by-products. However, the Zn metal with architectural SEI films (e.g., hopeite [31] and metal halides [19]) displayed a compact and uniform surface without any dendrites, revealing the present of smooth and stable Zn^{2+}-conductive SEI layer, thereby maintaining its protective function during sequential cycling test. It is imperative to delve into and comprehend advanced anode construction methods from the perspective of crystallinity, including mechanical processing, template-mediated method, field simulation, interphase induction, and most importantly, electrolyte effect [32].

3.1.2. SEI/CEI formation

The compositions of organics and inorganics in SEI and CEI typically are ionic conductor and electronic insulator with multi-layers, inhibiting uneven interactions between electrolytes and electrodes, and facilitating the transport of cations through the passivation layer toward the electrode surface. Organic layers (e.g., metal hydroxycarbonate [19,33]) often have porous and flexible structures at the outer layer, which is close to the electrolyte. Inner inorganic layers (e.g., metal-F [34], metal-phosphate, [35], hybrid inorganics [36]) often have wide stable potential window, high Young's modulus, and ion conductive properties. In aqueous batteries, solvents, salts, water, and gas can affect composition of SEI layers. Optimizing the SEI's capabilities, including volume buffering, structural/interfacial protection, side reaction inhibition, mechanical strength, and pH mediation, can be achieved by altering electrolyte salts or adding suitable organic solvents or different electrolyte liquids. Additionally, a compact and stable SEI layer, enhanced by a capping agent on the electrode surface, can limit 2D diffusion of metal ions, thereby inhibiting dendrite growth [37,38]. Furthermore, hybrids SEI with both inorganics and organics have been reported to protect metal anode, showing significantly improved cycling stability and dendrite suppressing effect [36,39,40]. In Fig. 2g, due to the metal anode's more negative reduction potentials compared to HER, water electrolysis to H_2 occurs during Zn deposition. The increased pH near the metal surface will lead to anode corrosion and by-product formation. The uneven morphology of the native SEI layer on the metal anode contributes to dendrite formation, causing repeated

exposure of new active surfaces to electrolytes and subsequent SEI layer regrowth. As shown in Fig. 2h, Li et al. designed a low-concentration aqueous electrolyte with the mixture of $Zn(OTf)_2$ and $Zn(NO_3)_2$ to in-situ grow a robust inorganic/organic hybrid SEI with multiple components (i.e., ZnF_2, $Zn_5(CO_3)_2(OH)_6$, and other organics). The inorganic inner layer facilitated Zn-ion diffusion while the organic outer layer prevented water penetration, further suppressing the gas evolution and stabilizing the surface activity. To prove the increasing of Zn-ion conduction of from $Zn_5(OH)_8(NO_3)_2{\cdot}2\ H_2O$ to $Zn_5(CO_3)_2(OH)_6$, EIS impedances gradually decreased after 10 cycles of Zn plating/stripping, proving the transformation of ion-insulating $Zn_5(OH)_8(NO_3)_2{\cdot}2\ H_2O$ into a fast-ion conducting $Zn_5(CO_3)_2(OH)_6$ (see Fig. 2i). Remarkably, the stable SEI film will effectively suppress the formation of metal dendrites and HER on metal foil. The relatively uniformity and high mechanical strength of SEI layers were found that stabilizing the structural integrity and reversibility of electrode surface is a crucial step for prolonged lifespan and enhanced capacity performance [41]. Furthermore, the critical thickness of SEI layer can estimate the electron tunneling barrier followed by the electronic tunneling probability equation [42]. During the competitive decomposition among solute anions, H_2O molecules, and dissolved gas (CO_2 and O_2), the thicker but moderate SEI film will lead to partially penetrate the passivating layer, which can effectively suppress the side reactions of H_2O molecules. Besides, the LUMO energy level of electrolyte also can be calculated to estimate the dissociation rate between water and solvents. As displayed in Fig. 2j, an interface stabilizer 2,3,4,5-tetrahydrothiophene-1,1-dioxide (TD) exhibits lower LUMO level compared to H_2O, suggesting its capability of reduction before water at metal surface during cycling, thereby benefitting the SEI formation composed of organic sulfone/sulfonate species and inorganic salts [43]. Hence, developing a suitable SEI composition on both cathode and anode is also an important part to optimize battery's efficiency and cyclability. However, the pure water will not induce the formation of SEI or CEI on electrode surfaces. As a result, the addition of solutes and solvents are an important factor to construct a desired electrolyte interphase on electrodes. Additionally, the specific properties and functions of SEI/CEI depends on their organic/inorganic composition, which are determined by the electrolyte components [44,45]. Therefore, the addition of anions as active receptors in the aqueous electrolytes can successfully change the interfacial chemistry from a solvent-derived to an anion-derived one [46].

3.1.3. Hydrogen bond regulation and solvation structure

The issues mentioned above are typically addressed by employing various strategies such as adding organic solvents, mixing electrolytes, altering the types of salt solutes, and adjusting the electrolytes concentrations. The solvation structure, hydrogen bonding regulation and surrounding chemistry (i.e., hydrogen bond donor (HBD) and hydrogen bond acceptor (HBA)) will be alternated (see Fig. 2k), further changing the cation mobility, SEI composition, and water activity. Toward the high-energy, and high-power aqueous batteries, the main targets in this section are in terms of (I) rapid mobility of solvated cations with weak dissociation energy of anion ligands;(II) confined free water molecules by weakened hydrogen bonds between water molecules;(III) determination of binding energies between H_2O-H_2O, H_2O-Metal ions, HBD/HBA-H_2O, and HBD/HBA-Metal ions. To identify the coordination chemistry, the ^1H NMR, Raman, X-ray absorption spectroscopy (XAS) and Fourier-transform infrared spectroscopy (FTIR) [47–49] are used to prove the existence of coordination between molecules and metal ions. The DFT calculation of binding energy is also an analysis tool to verify the solvation energies. As mentioned in Section 2.2, the dielectric constant depends on molecule's polarity and viscosity, determining the salt dissolution and ion diffusion. High dielectric-constant electrolytes can easily regulate the hydrogen bond network and solvation architecture as a regulator to alternate the [H_2O]-coordinated complexes. Therefore, as shown in Fig. 2l, You et al. reported the introduction of high-polar formamide (FA), which is a high dielectric constant co-solvent as both HBA and HBD [50]. There is higher binding energies between H_2O and FA as well as H_2O and OAc^- (see Fig. 2m), indicating the stronger hydrogen bond interactions between FA and H_2O. Both H_2O-FA and H_2O-OAc^- complexes own higher binding energy than that of H_2O-H_2O. Obviously, due to the addition of polar molecules, the disruption and reorganization of the original hydrogen bond network among H_2O molecules will occur, thereby effectively inhibiting the water decomposition accompanied with hydrogen embrittlement. Furthermore, solvation structures with metal ions can be calculated in Fig. 2n. The binding energy of Zn ions to FA is far more negative than that of Zn^{2+} to H_2O, revealing that FA has stronger coordination with Zn ions. The H_2O molecules located in the Zn-solvated shell is preferable to be exchanged by FA molecules, leading to successively regulate [$Zn(H_2O)_6$] structure into [$Zn(H_2O)_m(FA)_n(OAc)_k$] solvation configurations in the electrolyte. The FA-based solvation shell will inhibit the metal corrosion and the HER, further widening the working window.

3.2. Electrolyte issue in multivalent metal-ion system

This section will discuss the merits and drawbacks of aqueous batteries in various multivalent metal-ion systems, following an understanding of the side reactions and their principles. Multivalent cations transport more electrons per ion compared to monovalent ions during cycling. This results in less ion storage needed per unit of a lattice host for a given reversible capacity, leading to reduced lattice distortion in host materials. Multivalent metal-ion batteries potentially outperform commercial LIBs in energy and power density, attributed to their higher capacity and water-based electrolytes. The increased charge density of multivalent metal ions creates a stronger electric field, leading to a larger solvation sheath and a more substantial diffusion barrier in the electrolyte. This phenomenon causes higher desolvation energy and slower ion transport before insertion into the electrode [51]. Recent literature and applications highlight the growing interest in aqueous batteries, particularly zinc-ion batteries (ZIBs), in academia and industry. Their appeal lies in the abundant and cost-effective nature of zinc, and the metallic nature of their charge carriers offers superior energy storage advantages compared to systems with non-metallic charge carriers [52]. In addition to ZIBs, other multivalent metal-ion batteries like magnesium-ion (MIBs), calcium-ion (CIBs), and aluminum-ion (AIBs) are being explored for large-scale battery systems. However, aside from ZIBs, these batteries predominantly use non-aqueous electrolytes. This preference is due to challenges like highly reactive electrolyte salts (e.g., $AlCl_3$), low solubility of certain electrolytes (e.g., $Ca(PF_6)_2$), formation of passivation layers on metal surfaces (e.g., $Mg(ClO_4)_2$, $Mg(BF_4)_2$), and metal oxide precipitation in water-based electrolytes, all of which hinder the development of aqueous versions of these batteries [53]. To advance aqueous batteries, it's crucial to identify their challenges and optimize them through electrolyte design. For example, in CIBs, the transport kinetics of solvated calcium ions are quicker compared to zinc, magnesium, and aluminum ions. This is attributed to their lower charge density, which correlates with the trend in unhydrated ion radius (Fig. 1c). However, irreversible calcium deposition tandem with sluggish kinetics of Ca ions with low coulombic efficiency and shielding effect of Ca ions by the high-polar water molecules are the critical problem in aqueous CIBs [54,55]. Second, in MIBs, unlike LIBs, there's a lack of Mg-based electrolytes with high ionic conductivity that allow complete reversibility of Mg ions. While concentrated electrolytes can expand the working window and reduce side reactions, their high viscosity, desolvation energy, and cost limit practical applications [56,57]. Third, in AIBs, Al metal is the preferred choice for negative electrode due to its high theoretical specific capacity (2980 mAh g^{-1}) [58]. However, HER and low plating/stripping efficiency of aluminum at the anode contribute to irreversibility, resulting in low coulombic efficiency and poor cyclability [59]. An effective solution is the formation of a protective SEI layer through electrolyte decomposition during the de-solvation process,

Table 1
Overview of recent publications and their design strategies and electrochemical performances in aqueous multivalent metal-ion batteries.

Battery system	Strategy	Electrolyte	Potential Window (V)	Specific capacity (mA h g^{-1})	Retention/cycles/ current density	Ref.
MIBs	Hydrated eutectic electrolytes	$Mg(NO_3)_2{\cdot}6H_2O$ + acetamide	1.0~0.3 0.0~1.2	130 34	65.5 %/1500/10C 91.5 %/2000/10C	[64]
MIBs	Crowding agent	0.8 M $Mg(TFSI)_2$–85 %PEG-15 %H_2O	2.1	326	80 %/100/50mA	[57]
MIBs	WIS Anion effect	$MgCl_2{\cdot}6H_2O$:H_2O mass ratio of 25:1	2.1	25	99 %/700/0.5A	[65]
MIBs	WIS, crowding agent, pH buffer, redox pair	Saturated $MgCl_2$ + 1 M $MnCl_2$ in H_2O: PEG = 1:1 with 0.0018 M H_2SO_4	~1.7	500	100 %/1200/5C	[66]
MIBs	Hybrid solvent	1 M Mg $(ClO_4)_2{\cdot}6H_2O$ in TEGDME and water	2.0	150	67 %/1000/1.5A	[67]
MIBs	Dual ion Hybrid electrolyte	1 M $MgCl_2$ + 0.5 M NaCl	1.7	90	100 %/1000/0.5A	[68]
MIBs	Anion effect	1 M Mg $(CH_3COO)_2$	1.2	175	81.5 %/3000/5A	[69]
MIBs	Dual ion Hybrid electrolyte	1.9 M Na_2SO_4 and 2.4 M $MgSO_4$	0.5	65	88 %/100/1C	[70]
MIBs	Redox pair additive	1 M $MgSO_4$ + 0.02 M KBr in DI	2.5	79.6	~90 %/5000/10 A	[71]
MIBs	Hybrid anions	$Mg(TFSI)_2$ and $MgSO_4$ in DI	0.8	110	87 %/500/1C	[72]
MIBs	Anion effect	0.5 M $Mg(ClO_4)_2$	1.6	150	–/160/1A	[73]
ZABs	WiIL	$Zn(TFSI)_2$ in BMITFSI with 20 % water content	0.25~1.75	75	100 %/1000/1A	[74]
ZIBs	HEE	Methylsulfonylmethane:$Zn(ClO_4)_2{\cdot}6H_2O$ + water (molar ratio=3.6:1.2:3)	0.4~1.5V	250	100 %/1600/1A	[75]
ZIBs	WiDES	$ZnCl_2$ + acetamide + water	0.8	70	85.7 %/10,000/1A	[76]
ZIBs	WIBS Additive	4 M $ZnSO_4$ + 2 M Li_2SO_4 in DI with 10 % DME	1.2	168	~100 %/63/91mA	[77]
ZIBs	Crowding agent	$Zn(TFSI)_2$ in DI With 70 wt % PEG400	0.1V~1.7V	260	78 %/1000/0.29 A	[78]
ZIBs	additive	2 M $ZnSO_4$ in DI With 100 mM trehalose	0.8~1.8V	200	89 %/1000/1A	[79]
ZIBs	additive	2 M $ZnSO_4$ in DI with 50 mM tranexamic acid	1.0 V	180	87.7 %/1000/3 A	[80]
ZIBs	WiDES	2 M $Zn(OTf)_2$ in DI with ethylene glycol	1.5V	436 385	75 %/300/0.5A 70 %/600/1 A	[81]
ZIBs	Redox pair additive	1 M $ZnSO_4$ + 0.1 M $MnSO_4$	1.3V	225 150	–/200/0.1A –/400/1A	[25]
ZIBs	Co-solvent	2 M $ZnSO_4$ and 0.2 M $MnSO_4$ in dimethyl sulfoxide (DMSO)/water mixture	1.05 V	250	~70 %/5000/2 A	[82]
ZIBs	Co-solvent	2 M $Zn(OTf)_2$ in Tetramethyl urea/water mixture	1.0 V	165	95.2 %/1000/1 A	[83]
ZIBs	additive	2 M $ZnSO_4$ in DI with 10 wt.% sorbitol	0.85	150	86.8 %/500/1A	[84]
ZIBs	Co-solvent	1 M $Zn(OTf)_2$ in DOL/water mixture	1.4	~250	94 %/1500/2A	[85]
ZIBs	additive	1 M $ZnSO_4$ in DI with 5 % TMB additives	1.4	~300	~80 %/1000/1A	[86]
ZIBs	Water-in-Swelling-Clay	2 M $ZnSO_4$ in DI with bentonite	1.0	120 160.7 318	88.29 %/5000/3A 96.64 %/2000/1A 90.4 %/200/0.1A	[87]
ZIBs	Additive pH buffer	2 M $ZnSO_4$ + 50 mM taurine in DI	1.4	~200	–/1600/3A	[88]
ZIBs	Additive pH buffer	2 M $ZnSO_4$ and 0.1 M $MnSO_4$ in DI with 20 mM taurine	1.0	~285	–/1000/1A	[89]
AIBs	Redox pair additive	2 M $Al(OTf)_3$ + 0.5 M $MnSO_4$	1.35	320	–/65/0.1A	[90]
AIBs	WIS	$AlCl_3{\cdot}6H_2O$	1.4	165	95 %/1000/0.5A	[91]
AIBs	WIS	5 M $Al(OTf)_3$	1.5	–	–	[92]
AIBs	WIS	5 M $Al(OTf)_3$	2.65	75	97.6 %/100/150 mA	[93]
AIBs	PEG additive pH buffer	2 g PEG add 9 mL of a 1.0 M $Al(ClO_4)_3{\bullet}9H_2O$ with 1 g perchloric acid	1.4	100	90 %/20,000/500 mA	[59]
AIBs	WIS	5 M $Al(OTf)_3$	1.6	~60 (mA h cm^{-2})	–	[94]
AIBs	Anion	1 M $AlCl_3$, 1 M $Al(NO_3)_3$, and 0.5 M $Al_2(SO_4)_3$ aqueous solutions	1.3	159	~100 %/350/2.5A	[95]
AIBs	WIS	$AlCl_3$	1.3	140	85 %/250/1A	[96]
AIBs	Al(TFSI)3-based WIS with redox pair additive (MnSO4)	3 M $Al(TFSI)_3$ in DI with 70 mM $MnSO_4$	~1.4	450	>100 %/400/0.15 A g^{-1}	[97]
AIBs	DES additive	2 M $Al(OTf)_3$ in DI	1.5	85	97.1 %/150/0.1 A g-1	[98]
ASBs	Hybrid salts pH buffer	$Al(OTf)_3$ + LiTFSI + HCl	0.8	420	97 %/30/0.2A	[99]
AIBs	WIS Dual ion system	4.4 M $AlCl_3$ + 1 M $MnCl_2$ in H_2O with 0.05 M HCl	0.8	493	100 %/1000/10 mA cm^{-2}	[100]
AIBs	WIS Dual ion system	0.5 M $AlCl_3$/12 M LiTFSI	1.5	120	64.4 %/300/4A	[101]
CIBs	Concentration	8.37 M $Ca(NO_3)_2$ in DI	1.1	~70	~94 %/150/2C	[102]
CIBs	WIS	15 M $Ca(NO_3)_2$ in DI	1.3	~410 (based on weight of anodes)	~80 %/1800/3A	[103]
CIBs	Concentration	6.25 M $Ca(TFSI)_2$ in DI	1.8	49	–/50/0.1A	[104]
CIBs	Concentration	6.25 M $Ca(TFSI)_2$ in DI	1.6	75	–/100/0.1A	[105]
CIBs	Anion effect	1 m $CaCl_2{\cdot}2H_2O$ in DI	1.7	85.7	73.7 %/1600/3A	[106]

(*continued on next page*)

Table 1 (*continued*)

Battery system	Strategy	Electrolyte	Potential Window (V)	Specific capacity (mA h g^{-1})	Retention/cycles/ current density	Ref.
CIBs	Anion effect, crowding agent	8.37 M $Ca(NO_3)_2$ in DI with 10 wt% polyvinyl alcohol	~2.0	75	83 %/150/0.335A	[107]
CIBs	Concentration	2.5 M $Ca(NO_3)_2$ in DI	1.3	125 (based on anode)	95 %/200/0.8A	[108]
CIBs	WIS	5 M $Ca(OTf)_2$ in DI	1.4	137 (mAh m^{-2})	85 %/260/0.1 mA cm^{-2}	[109]
CIBs	WIS	5 M $Ca(OTf)_2$ in DI	1.7	77.8 (based on cathode)	94.4 %/30,000/1A	[110]

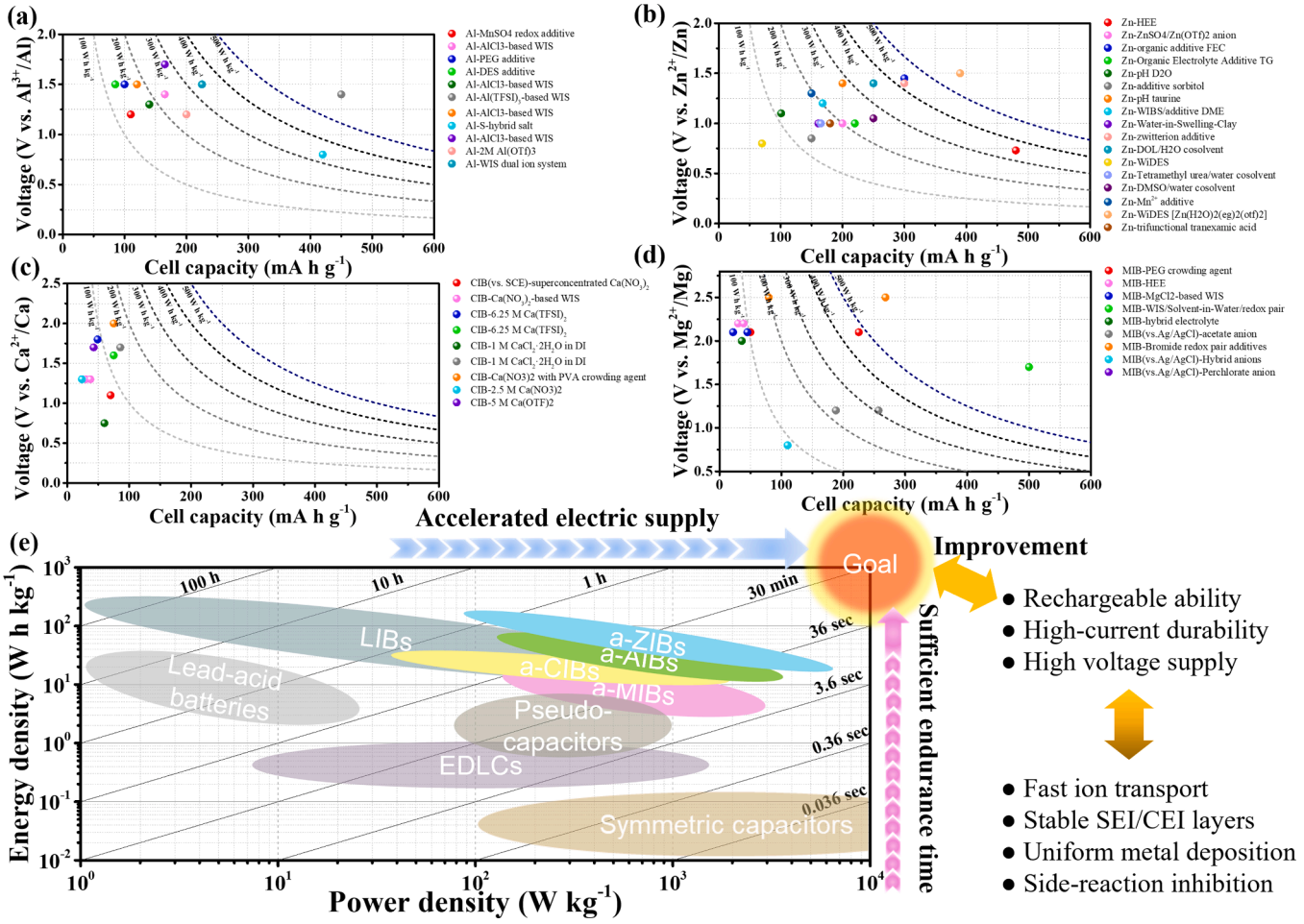

Fig. 3. The applied voltage-cell capacity plots of full-cells and half-cells in (a) AIBs, (b) ZIBs, (c) CIBs, and (d) MIBs. (e) The Ragone plot of multivalent metal-ion batteries compared with other battery systems. The right side of the (e) is the improvement and crucial factor for high-energy and high-power aqueous batteries.

which mitigates side reactions from rapid kinetics and prevents aluminum corrosion [59]. Fourth, in ZIBs, Zn exhibits superior electrochemical reversibility as an anode compared to most metals, which are unsuitable for direct use as negative electrodes in aqueous media. However, ZIBs face a significant challenge with tree-like dendrite formation, more severe than in other multivalent metal-ion batteries. These dendrites can penetrate separators, leading to short circuits [60]. Except for ZIBs, other aqueous multivalent metal anodes usually form dense and thick insulating layers, thereby reducing active sites on the anode surface and inhibiting the reversible metal deposition. Common challenges in aqueous batteries like ZIBs, MIBs, CIBs, and AIBs include a limited working window, irreversible capacity, and sluggish cation transport, are caused by dendrite growth, unstable SEI formation, and hydrogen evaluation (see Fig. 1e). Meanwhile, ionic conductivity, dielectric constant, and transference number of electrolytes play a critical factor for efficient transport of protons, multivalent ions, and anions during the cycling process. It strongly depends on the regulations of solvents, salts, and additives. Moreover, five directions of electrolyte design are respectively salt concentration, pH buffer, additives, hybrid solvent, and hybrid solutes (see Fig. 1f). The rainbow color lines correspond to each problem we faced in aqueous batteries. For instance, the red line represents that what strategies can solve the uniformity of metal deposition during a cycling process. The orange, yellow, green, blue, dark blue, and purple lines are designated as SEI/CEI layer, hydrogen bond regulation, ion conductivity, dielectric constant, transference number, and solvation structure, respectively. The line located on the top of these five strategies means that this strategy can affect these electrochemical properties and phenomena. For example, the salt concentration strategy can regulate hydrogen bonding, inhibit dendrite growth, and change solvation structure, leading to low water activity, reversible metal

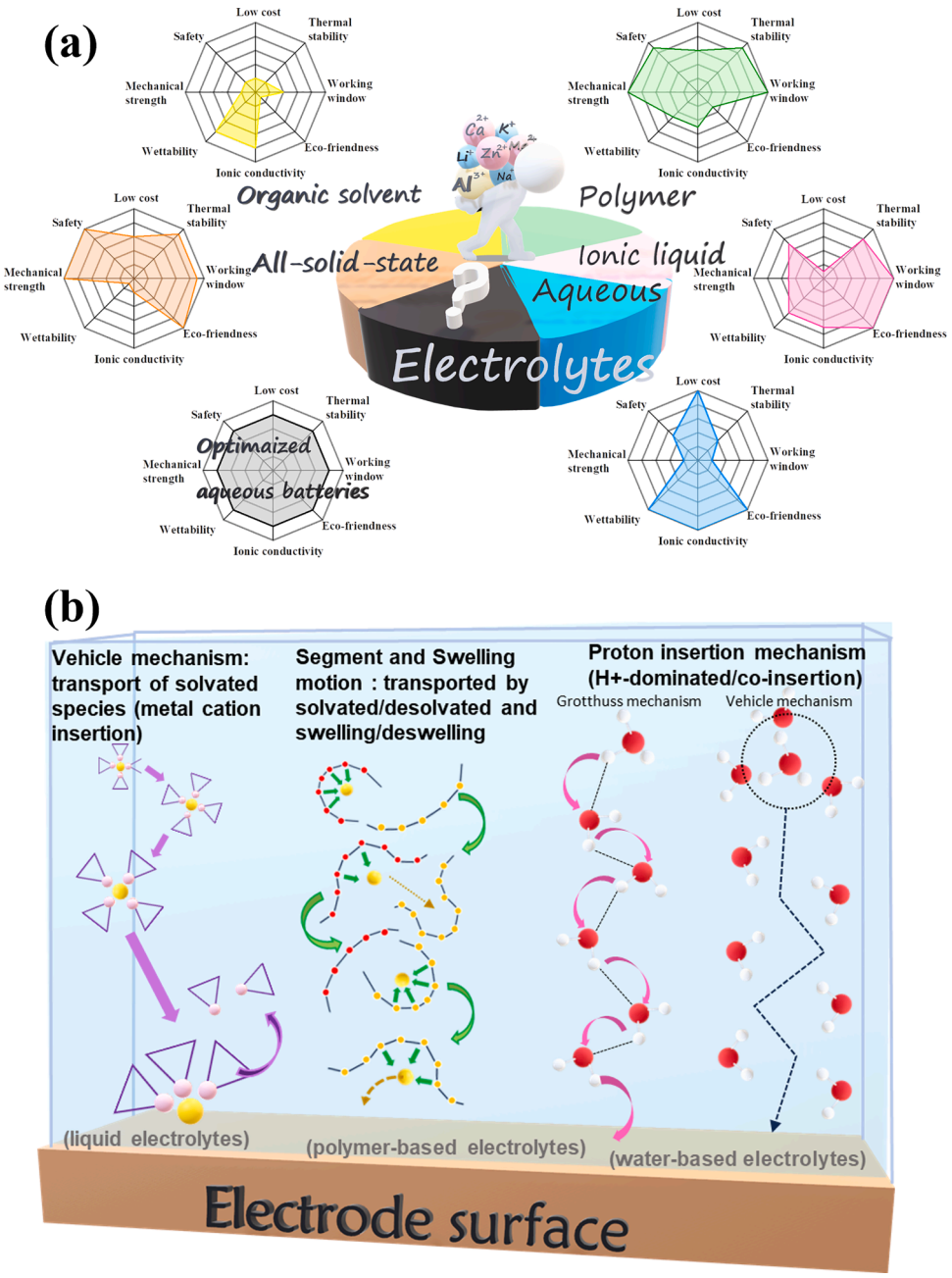

Fig. 4. (a) Advantages and disadvantages of various electrolyte. (b) Scheme of transport mechanism of metal cations and protons in different electrolytes.

plating/stripping, high ionic conductivity, and large transference number, and so on. The strategy roadmap indicates what steps researchers should be taking to solve the corresponding problems associated with aqueous electrolytes (Fig. 1g). These dashed lines in different strategies represent the relationship between strategies (salt concentration, pH buffer, additives, hybrid solvents, and hybrid solutes) and results (wide applied voltage, reversible capacity, and fast ion transport). Each direction of electrolyte design can be divided into various strategies listed below the strategy title. The "additives" strategy contains the addition of organic molecule, crowding agent, redox anion/cation, electrostatic shielding agent, etc. The "salt concentration" involves salt-in-water (low concentration), water-in-salt (high-concentration), and hydrated eutectic electrolytes, while the "hybrid solvent" and "hybrid solutes" means combination of various solvents and electrolyte salts. The working principle and utilization of all of strategies will be descripted and discussed thoroughly based on recent excellent research articles.

Hence, the choice of aqueous electrolytes in battery cells is critical, as inappropriate selections can cause gas generation and reduced lifespan. While safer and more affordable aqueous electrolytes are preferred, they often restrict operating voltage and practicality. Recent studies on these electrolytes, design strategies, and the electrochemical performance in multivalent metal-ion batteries are detailed in Table 1 and Figs. 3a-d. Essentially, reaching the apex in the Ragone plot for energy storage involves three key factors: reversible capacity, applied voltage, and fast ion transport shown in Fig. 1h. In addition to ultralong cycle life, the sufficient energy density of aqueous batteries is essential and determined by both specific capacity and applied voltage. Thereof, the applied voltage is relevant to battery's working window and discharge plateau. The power density of aqueous batteries is dominated by applied voltage and current density. The current density is calculated from the capacity divided by current time. That is, cations or protons transported more efficient will help the battery's current durability, meaning that

aqueous batteries still perform a promising capacity under current abuse. The relationship between aqueous multivalent metal-ion batteries and other commercial energy storage systems is depicted in Fig. 3e. In other words, wide applied voltage, reversible capacity, and fast ion transport are main pursues for standard energy density and power density, which need to arise toward 200 Wh kg^{-1} (energy density of commercial LIBs: 100∼250 Wh kg^{-1}) and 1000 W kg^{-1} (power density of commercial LIBs: ∼100 W kg^{-1}) based on overall weight of battery cells [61]. The high dielectric constant of water-based electrolytes in these batteries results in higher intrinsic ion mobility, enabling them to achieve significant power density compared with that of LIBs. However, the aqueous batteries belong to the Faradaic reaction system; therefore, it cannot reach to the power density similar to commercial supercapacitors (19.6 kW kg^{-1}∼35.4 kW kg^{-1}) [62]. Despite the high-performance potential of half-cells in aqueous multivalent metal-ion batteries, full-cell LIBs still demonstrate greater stability and higher specific capacity in both academic and industrial application. Moreover, the energy density of aqueous full cells in multivalent metal-ion batteries hasn't yet surpassed commercial standards, with applied voltages over 3.6 Vs and energy densities exceeding 250 W h kg^{-1}, especially at sufficient mass loading [63]. In recent, the working window of most research regarding to electrolyte design are ranged from 0.5 to 1.8 V. Therefore, to increase the energy density of aqueous batteries, the electrochemical window of electrolytes needs to be improved and operated up to 2.0 V. Optimizing electrolytes with five strategies - enhancing ion transport, stabilizing SEI/CEI layers, enabling uniform metal deposition, suppressing side reactions, and improving rechargeability and durability under high current condition - can significantly boost the performance of aqueous batteries for large-scale energy storage.

3.3. Characteristics and transport mechanism of various types of electrolytes

In developing water-based electrolytes for energy storage, trade-offs are made between electrolyte types due to their unique advantages and drawbacks. Recently, there's an increasing focus on hybrid-electrolyte approaches, such as water-organic solvents [67], water-ionic liquid (or deep eutectic solvent) [74,76], water-polymer [111–113], and water-inorganic solid electrolyte [114–116], etc. Water-based electrolytes in energy storage offer fast ion transport, high ionic conductivity, and solubility, but struggle with forming stable SEI, inhibiting side reactions, and maintaining stability and mechanical strength. We summarized the advantages and disadvantages of each electrolyte, including cost, thermal stability, working window, eco-friendliness, ionic conductivity, wettability, mechanical strength, and safety (Fig. 4a). Developing novel aqueous electrolytes can balance electrochemical stability and conductivity for enhanced performance in energy storage. How to develop an optimized electrolyte system to satisfy the demands of high performances is an importance target in the field of energy storages.

3.3.1. Liquid electrolytes

Liquid electrolytes, such as organic/inorganic solvents (e.g., EC, DEC, dimethyl ether, dimethyl carbonate, H_2SO_4, H_2ClO_4) and water, are known for their high ionic conductivity, SEI formation ability, excellent wettability, low viscosity, and commercial availability. In these electrolytes, both Shannon's ionic and Stokes radii significantly influence metal ion diffusivity. Specifically, smaller atoms can strongly attract surrounding counter ions, forming larger hydrated species radii [117]. The larger an ion's Stokes radius, the more challenging its diffusion. Cation transport in bulk electrolytes involves solvation with counter ions, forming solvated species in both aqueous and organic solutions. Due to high ionic conductivity of liquid electrolytes, metal ions transport typically follows the Vehicle mechanism (Fig. 4b), where charge species move with surrounding counterions to the electrode surface. In recent, the competitive proton insertion in cathodes is unavoidable in water-based electrolytes, which will be discussed in Section 3.3.4. As soon as the solvated cations arriving the negative surface of electrode during the reduction process, the solvating anions will dissociate from the metal cations and release back to the bulk electrolyte. Nevertheless, there are still many drawbacks such as volatile and flammable for organic solvent, and corrosion for inorganic solvent, as well as narrow working voltage for aqueous solution.

3.3.2. Ionic liquids and deep eutectic solvents

Alternative components/classes of electrolytes have been proposed. Among them, ionic liquids (ILs) appear as some of the most promising. The ILs generally consist of both anions (e.g., bis(fluorosulfonyl)imide (FSI^-), bis(trifluoromethansulfonyl)imide ($TFSI^-$), hexafluorophosphate (PF_6^-) and tetrafluoroborate (BF_4^-)) and cations (e.g., imidazolium and pyridinium) [118], and it can be freely selected to tune their physicochemical properties of being suitable for different battery systems. Ionic liquids, due to their mobile anions and cations, exhibit high ionic conductivity without additives. Their wide voltage stability windows, thermal stability, and low vapor pressure (10^{-10} torr) help prevent hydrogen embrittlement and gas evolution, thereby expanding the operational temperature range and enhancing safety [119]. Besides, the branch degree and structure of organic cations can affect the viscosity and ionic conductivity of ILs and diffusivity of solvated species [120]. That is, a suitable counter ion will improve the charge transfer resistance (R_{ct}) and activation energy of ion diffusion (E_a), enhancing the electrochemical performances and rate capability. Also, the components of electrolyte are beneficial for the growth of robust SEI layers to prevent the excessive side reactions between electrolyte and electrode materials, giving a stable and reversible capacity during a long-term cycling process.

Deep eutectic solvents (DESs), a new type of room-temperature ionic liquid, are gaining attention in electrochemical research. DESs are eutectic mixtures of anionic and cationic Lewis/Brønsted acids, comprising ions and molecules like quaternary ammonium salts and HBDs, such as amides, carboxylic acids, and alcohols, including ethylene glycol, urea, 1,6-hexanediol, and acetamide [121]. Furthermore, the physical properties of DESs are usually determined by characteristics and polarity of HBD, improving the solubility for solutes, potential window, and conductivity. Especially, the quaternary ammonium cation and HBDs will form a metal complex to change the solvation sheath and dissociation energy, stabilizing the deposition/stripping of metal and alleviating the formation of metal dendrite during discharge/charge process. Therefore, choosing a suitable cation, anion, and even neutral molecules is a key point for applying on the different battery systems and electrode materials. In addition to the wide potential window, nonflammability, and low vapor pressure, the DESs are equipped with biocompatibility, air stability, and economic friendliness compared to ionic liquids. Furthermore, the transport mechanisms of both ILs and DESs in aqueous batteries are similar to water-based aqueous electrolytes.

3.3.3. Polymer electrolytes (gel polymer and solid polymers)

To address safety concerns and thermal runaway in liquid electrolytes, attention is shifting toward solid-state (SSEs) and quasi-solid state (QSSEs) electrolytes for energy storage, offering greater electrochemical stability and leakage prevention. The main challenge in polymer electrolytes lies in enhancing their ionic conductivity and cation diffusivity. A crucial question is how metal cations transport through the quasi-static framework during the charge/discharge process, a process that varies depending on the types of polymers used. There are different kinds of polymer electrolytes, including gel polymer, solid polymer, and even hybrid polymer electrolytes. For instance, the usual electrolyte polymers such as poly(ethylene oxide) (PEO), Poly(vinylidenefluoride) (PVDF), polysiloxane (PS), carboxymethyl cellulose (CMC), gelatin, etc. have been widely used in aqueous batteries [122]. Thereof, these polymers typically feature hydrophilic groups, which can effectively

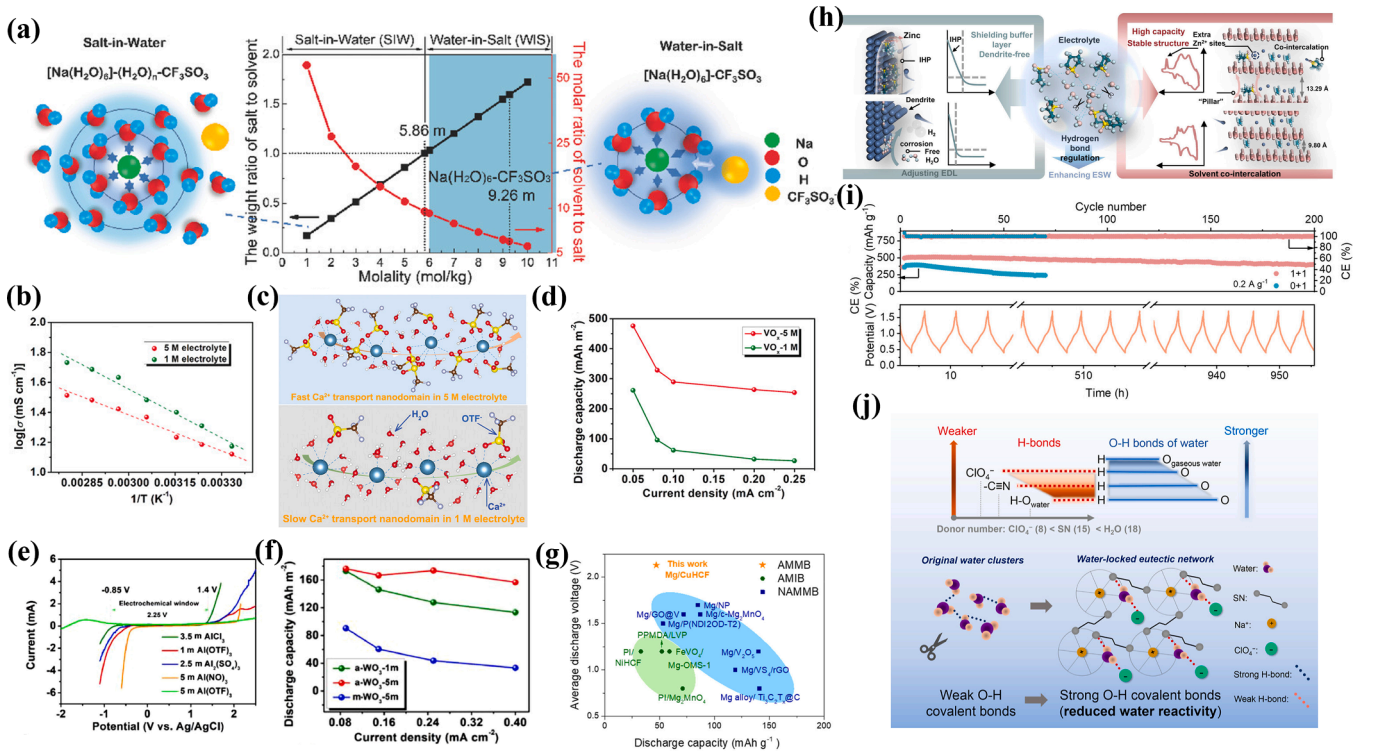

Fig. 5. (a) The cation–anion and ion–solvent interactions in WIS electrolyte. The molar and weight salt/solvent ratios in NaOTf–H_2O binary system, whose corresponding temperature dependences of ion conductivities. Reprinted with permission from Ref. [140] Copyright 2017 Wiley-Blackwell. (b) Ionic conductivity of aqueous 1 and 5 M $Ca(OTf)_2$ electrolytes as a function of temperature. (c) The illustrations of hydrated Ca-ions transport nanochannels in 1 M and 5 M electrolytes. (d) Rate performance of the VO_x films in the aqueous 1 and the 5 M Ca $(OTf)_2$ electrolytes. Reprinted with permission from Ref. [109] Copyright 2021 Wiley-Blackwell. (e) The LSV of aqueous electrolytes on titanium mesh in a three-electrode system in various electrolytes. (f) Rate performance of the a-WO_3 and the m-WO_3 films in the aqueous $Al(OTf)_3$ electrolytes. Reprinted with permission from Ref. [94] Copyright 2022 Elsevier. (g) Electrochemical performance of WIS aqueous MIBs compared with other rechargeable Mg batteries, including nonaqueous Mg metal batteries and aqueous Mg-ion batteries. Reprinted with permission from Ref. [65] Copyright 2022 American Chemical Society. (h) Schematic illustration of the triple-function hydrated eutectic electrolyte. (i) Cyclic performances of NVO with and without HEE network. Reprinted with permission from Ref. [144] Copyright 2023 Wiley-Blackwell. (j) Schematic illustration of the design principle and the solvation structure for WLE. Reprinted with permission from Ref. [23] Copyright 2022 American Chemical Society.

complex with metal cations. The cations interact with donor sites in the polymers' polar groups, facilitating their transport to the surface of active materials. This transport occurs through polymer chain segment motion or a swollen gelled phase, depending on whether the polymer is solid or gel [123,124]. In solid-state polymer electrolytes (SPEs), ionic conductivity is facilitated by a segment motion mechanism. Here, solvated sites are covalently linked through hydrogen bonds, preventing macroscopic displacement of the ligand-cation complex. Cation motion takes place along the backbone of the polymer chain, involving a cooperative movement between the polymer segment and the coordinated cation. Ultimately, the polymer complex dissociates sequentially, facilitating the transfer of metal ions to adjacent polymer segments until they reach the electrode surface [125]. Besides, gel polymers, also known as quasi-solid-state electrolytes (QSSEs), absorb and desorb solvent molecules as a result of incorporating liquid plasticizers or solvents into the polymer-salt system. If the polymer's donor number surpasses that of the solvent, solvent drag does not occur. Conversely, stronger solvent-cation than polymer-cation interactions result in solvent drag during ion transfer. This makes the transport mechanism in gel polymers distinct from SPEs. Metal cation transfer in gel polymer electrolytes depends on the volume change in the swollen gelled phase, endowing QSSEs with excellent mechanical strength, liquid electrolyte retention, and electrochemical stability [126]. QSSEs enhance ionic conductivity in aqueous batteries by capturing liquid electrolytes, transferring metal cations through a swelling/deswelling process. The ionic conductivity of these polymers increases with the incorporation of more hydrophilic groups and the promotion of an amorphous structure. These factors enhance water content and reduce diffusion barriers. Lower glass transition temperatures (Tg) facilitate polymer chain segment motion, thereby improving ionic conductivity and flexibility. Moreover, cross-linked polymer electrolytes resist crystallization and offer robust mechanical properties, rendering them suitable for flexible pouch-type batteries [127].

3.3.4. Water contented electrolyte (proton-dominated/co-insertion mechanism)

There are three types of electrochemical mechanisms according to published literatures, which includes (1) cation intercalation, (2) proton/cation, and (3) conversion [128]. Due to small atomic radius and weak columbic repulsion, competitive H^+ co-insertion with metal cations will participate in the electrochemical mechanism during the cycling process in both polymer and water-based electrolytes. The transport mechanism dominated by solvated metal cations are described in Section 3.3.1. First, the large metal cations will be difficult to intercalate into cathode materials with narrow tunnels or interlayers. Therefore, the protons will be prior inserted into cathodes, further resulting in H^+ insertion and H^+ conversion reactions [129,130]. In diluted water-based electrolytes, especially acid solution and ZnSO4-based salt, the protons will be the main charge carriers and transport through the Vehicle mechanism, where the zinc hydroxide sulfate hydrate (ZHS) by-products will form accompanied with proton insertion reaction [131]. Otherwise, when protons transport through a polymer media or high-concentration salt electrolyte, the Grotthuss mechanism will control all proton transport in the cycling process. The Grotthuss mechanism, also called ion hopping, depends on the formation and breaking of hydrogen bonds; thus, any factor that leads to an

increase in the average hydrogen bond energy or a disruption in the hydrogen bonding network will be detrimental to this transport mechanism [132]. Although proton insertion also can deliver a capacity of 100~200 mA h g^{-1}, it is lower than Zn-ion insertion and co-insertion mechanism. To control the transport mechanism, regulating hydrogen bonding network is one way to change the interaction between protons and other molecules in aqueous electrolytes. In addition, the formation of ZHS will affect the pH of electrolyte condition, which is tunable through the ligand effect and additive strategy (see Subsections 4.3 and 4.4). In addition to structural design of cathodes, [133]. Zhao et al. proposed a strategy for blocking the proton transport by end-capping of hydrogen bonds using N-methyl-2-pyrrolidone (NMP) [134]. Due to abundance of hydrogen bond acceptor (e.g., C═O), the hydrogen bond propagation can be effectively inhibited by weakening the hydrogen bonding interaction of water molecules. This resulted in low water activity and high dissociation energy of water molecules, thereby leading to lack of protons for inserting into cathode materials. Meanwhile, divalent charge carriers will dominate the insertion and conversion reaction. It is also possible that partial dissociated protons can assist with Zn-ion insertion, leading to co-insertion mechanism, thus enhancing structural stability and capacity performance at same time [135–137]. Therefore, different types of electrolytes (e.g., water-based and polymer-based aqueous electrolytes), electrolyte salts, pH conditions, and concentration will change the hydrogen bonding network and charge carrier mobility (i.e., protons and metal ions), which will be discussed in detail in next section.

4. Functional modeling and design direction of aqueous electrolytes for optimizing the electrochemical performances in aqueous energy storages

Electrolytes in energy storage systems are tailored to match the electrode electrochemistry and structure during both charging and discharging processes. Despite the diverse requirements of electrodes, common challenges for electrolytes include a narrow potential window, structural corrosion from hydrogen embrittlement, and the dissolution of active intermediates due to water's high dielectric constant. To ensure battery cyclability, stability, and reversibility, it's crucial to address issues not covered by unmodified electrolyte systems. A carefully selected electrolyte influences gas evolution, polarization, and reinforces the passivating layer. This helps reduce the formation and cracking of SEI films while minimizing electrolyte consumption during charge/discharge cycles. Over the past decade, researchers have developed strategies to achieve aqueous batteries with working voltages exceeding 3 V, comparable to those in organic solvents [138]. The design concepts discussed in this review encompass versatile approaches, categorized into concentration, hybrid solvent, hybrid salts, additives, acidic/basic control, aimed at optimizing aqueous electrolytes. These concepts form a comprehensive network with various working mechanisms, tailored to different electrode materials for enhanced performance. Subsequently, the review will delve into the modification factors and their respective working mechanisms, further discussing their role in improving the performance of aqueous multivalent-ion batteries within each subsection.

4.1. Concentration modulation

4.1.1. High concentration electrolyte

Improving electrode stability can be achieved straightforwardly by increasing salt concentration. In dilute aqueous electrolytes, the challenge lies in forming a stable SEI layer, as water's higher reduction potential compared to salt anions presents a hurdle, unlike in conventional carbonate-based electrolytes. Thus, higher salt concentrations can promote salt anion reduction reactions and reduce the number of free water molecules [139]. Facilitating the reduction reaction of salt anions can suppress water splitting and free water activity, thereby extending the electrolyte's working window. Moderately increasing the electrolyte salt concentration can enhance SEI formation and raise the potential threshold for H_2O decomposition Fig. 5a illustrates that in salt-in-water (SIW) electrolytes, typically below 5.86 mol/kg, metal ions bind with H_2O molecules due to strong Coulombic attraction and minimal steric effects on Lewis's base. Conversely, at higher concentrations, like 9.26 M, there are insufficient H_2O molecules and weaker hydrogen bond interactions to complex with metal cations [140]. The "water-in-salt" (WIS) concept, proposed for aqueous batteries, offers inherent moisture tolerance, a higher working window, and enhanced energy density, making it a promising electrolyte system. In WIS, metal ions exhibit strong coordination with salt anions (like FSI^-, $TFSI^-$, or derivatives), rather than solely with water molecules. This results in the formation of metal-water-anion complexes. This facilitates the development of an SEI film rich in fluorine, which contains metal cations in super-concentrated aqueous electrolytes [141]. Super-concentrated electrolytes not only promote the formation of a robust SEI protective layer but also limit oxygen solubility from air and decrease electrolyte evaporation due to their high salinity. Additionally, the slow diffusion of water molecules in the WIS system enhances electrolyte decomposition before water decomposition, which is attributed to the sluggish kinetics of OER/HER [141,142]. Furthermore, according to the Arrhenius equation (see Fig. 5b), the ion diffusion activation energy of the 5 M $Ca(OTf)_2$ is lower than that of the 1 M $Ca(OTf)_2$. The different electrochemical windows and the ion diffusion activation energies indicate that there are significant differences between the 1 M and the 5 M $Ca(OTf)_2$ in terms of cation–anion–water interactions [109]. Therefore, in the WIS electrolyte, solvated Ca ions can easily transport due to the electrostatic interaction between electronegative OTf^- channels and electropositive hydrated Ca ions. In contrast, the diffusion of H_2O-based solvated Ca ions in 1 M $Ca(OTf)_2$ electrolyte is slower, hindered by the Coulombic force between free H_2O and hydrated cations (Fig. 5c). As shown in Fig. 5d, its discharge areal capacity in the 5 M electrolyte is much larger than that in the 1 M electrolyte. Similarly, in aqueous AIBs (Fig. 5e and 5f), the wide working window (< 2.25 V vs. Ag/AgCl) for the WIS electrolyte. This value is much wider than those of other electrolytes, indicating the advantages of $Al(OTf)_3$-based WIS electrolyte, thereby delivering the better rate capability and retention. This design strategy is also suitable for MIBs given in Fig. 5 g. Compared with other aqueous/non-aqueous MIBs, the aqueous MIBs in WIS electrolyte exhibited an exceptional voltage performance. Furthermore, adding a high concentration supporting salts is one way to improve the reversibility of Zn metal due to the much stronger binding of water and $TFSI^-$ by Zn^{2+} as compared to Li^+ [143]. The hybrid metal ion system with high-concentration LiTFSI is a highly effective strategy to address the Zn dendrite and water activity, leading to high CE and cyclability.

4.1.2. Hydrated eutectic electrolyte

A high-concentration electrolyte design strategy involves the use of hydrated eutectic electrolytes (HEE) to tackle challenges like O_2/H_2 evolution and cost in WIS electrolytes. HEEs, characterized by their hydrogen bond networks of donors and acceptors, help mitigate water's side reactions. Zhu et al. created a HEE using $Mg(NO_3)_2{\cdot}6H_2O$ and acetamide, offering high ionic conductivity despite a high viscosity and a 1:2 Mg/acetamide atomic ratio [64]. Modifying the hydrogen bond network is a method to improve the stability of aqueous electrolytes. The solvation ability of hydrogen bond acceptors depends on their dielectric constant and dipole moment, which indicates their capability to bind free water molecules through hydrogen bonds. Zhong et. al. introduced tetramethylene sulfone into aqueous electrolyte to reconstruct the hydrogen bond network with strong interaction between sulfone and H_2O [144]. As shown in Fig. 5h, this "hydrogen-bond-regulation" strategy can effectively promote redox capacity and cycle lifespan with stable working window, inhibiting the dendrite formation and electrode corrosion. During the cycling tests, higher specific capacity (512.2 mA h g^{-1}) and better capacity retention (>80 %) in aqueous electrolyte with

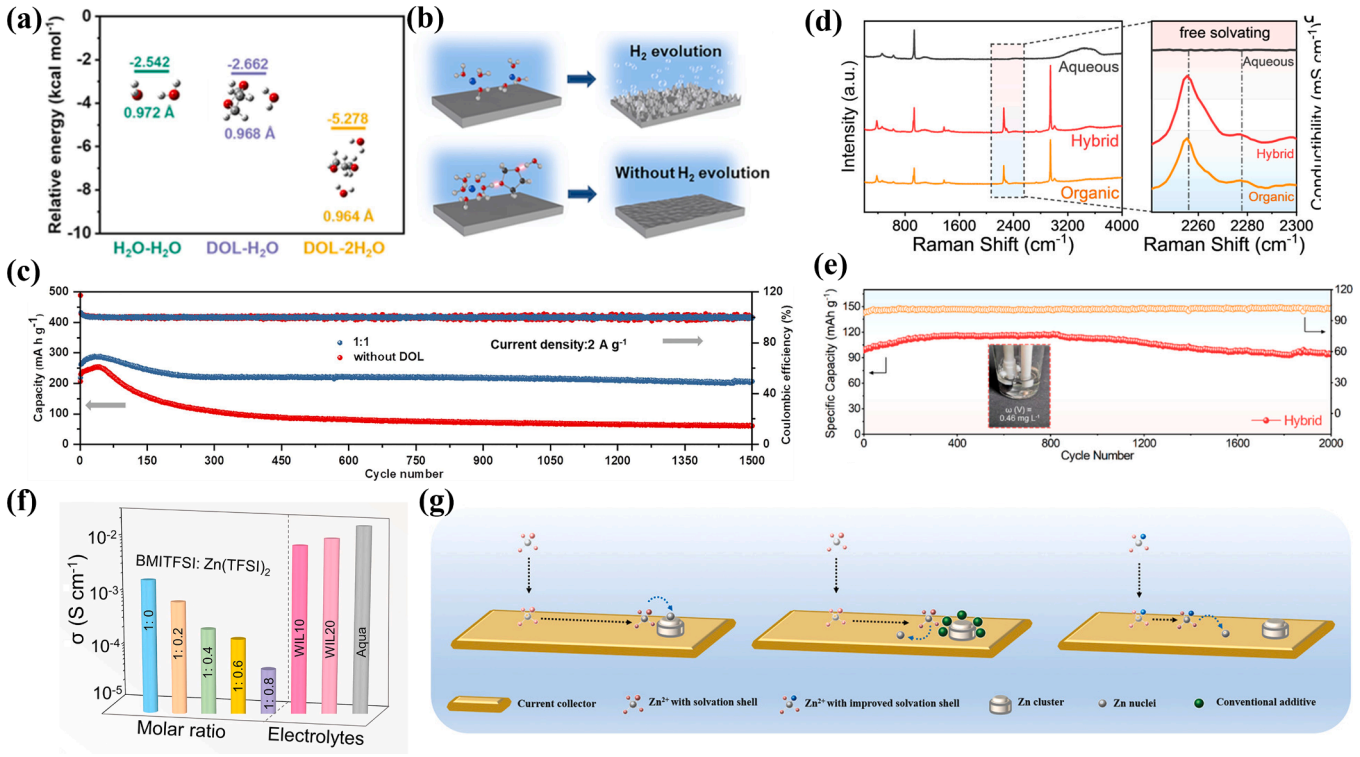

Fig. 6. (a) Relative binding energy for DOL with H_2O molecules obtained from DFT calculations. (b) Improving zinc reversibility schematic illustration by hydrogen bond in DOL-H_2O hybrid electrolyte. (c) Cycling stability of Zn/V_2O_5 on the hybrid electrolyte with a current density of 2 A g^{-1}. Reprinted with permission from Ref. [85] Copyright 2022 Elsevier. (d) Raman spectra of CVO in aqueous (i.e., 1 M $Ca(ClO_4)_2$ in pure H_2O), hybrid (i.e., 1 M $Ca(ClO_4)_2$ in AN: H_2O = 8:2), and AN electrolyte (i.e., 1 M $Ca(ClO_4)_2$ in pure AN). (e) Cycle performance of CIBs in aqueous hybrid electrolytes at 1 A g^{-1}. Reprinted with permission from Ref. [154] Copyright 2023 American Chemical Society. (f) Ionic conductivities of pure ILs with different salt ratios, the WILs, and Aqua at 20 °C. Reprinted with permission from Ref. [74] Copyright 2022 American Chemical Society. (g) Schematic illustration of Zn nucleation and growth process without modification, with electrostatic shielding mechanism and with improved solvation shell, respectively. Reprinted with permission from Ref. [76] Copyright 2021 Wiley-Blackwell.

tetramethylene sulfone, which is better than that in aqueous electrolyte without a HEE-network formation (Fig. 5i). Constructing the strong O—H covalent bonds can greatly reduce water reactivity through the water-locked eutectic network. Liu et. al. presented a hydrated eutectic electrolyte featuring a water-locked effect, the coordination of metal ions inhibits O atom of H_2O as proton acceptors and brings SN, ClO_4^- and H_2O in close proximity to promote the formation of a weak hydrogen bond network (Fig. 5j) [23]. Increasing the reversibility of redox reactions can be achieved by incorporating additives with large dielectric constants, high dipole moments, and abundant sulfonyl groups, which can coordinate with cations. Han et al. developed an optimized HEE system using methylsulfonylmethane, facilitating the formation of a eutectic network between water molecules and metal cations to enhance cycle reversibility [75].

However, at critical salt concentrations, the ionic conductivity of the electrolyte decreases significantly due to significant cation-anion aggregation and coordination. Additionally, reduced water content may lead to challenges related to electrode/electrolyte contact and wettability [145]. While water-in-salt (WIS) electrolytes offer promising solutions for addressing challenges associated with water splitting and narrow working windows, their use of expensive salts (i.e., TFSI, FSI, OTf-based salt), highly toxic fluorinated salts (i.e., PF_6^- [146]) as well as corrosive and oxidized halides (i.e., metal chlorides) fails to meet the requirements for safe, cost-effective, and environmentally friendly energy storage solutions. Although the "water-in-ionomer" electrolyte, which is metal salts with anionic moiety bound to the polymer backbone [147], is a candidate to alternate the fluorine-free electrolyte due to achieved output voltage and initial energy density, the high-salt-content system still have insufficient kinetic behaviors.

4.1.3. *Hybrid solvent electrolytes (water-in-ionic liquid/ water-in-quasi-solid-state/water-in-DESs)*

The introduction of co-solvents into a WIS electrolyte can enhance its ionic conductivity, ion mobility, and temperature tolerance. By blending two solvents in a specific ratio, the combined properties of WIS and dilute aqueous electrolytes can be optimized [148]. Hence, a new aqueous electrolyte is proposed, comprising a hydrogen bond network formed by the interaction between water and 1,3-dioxolane (DOL). This innovation expands the potential of the HER, while maintaining high coulombic efficiency in zinc redox reactions and ensuring high conductivity [85]. In Fig. 6a and 6b, Du et al. proved through DFT calculations that the interaction between water and DOL inhibits H_2 evolution and smoothens the electrode surface. Based on these results, the Zn/V_2O_5 full cell can stably work beyond 1500 cycles with ~94 % capacity retention (Fig. 6c). Fig. 6d shows Raman spectroscopy used to distinguish solvation in 1 M $Ca(ClO_4)_2$ across pure water, acetonitrile, and their hybrid solution. The absence of the Raman peak at ~3400 cm^{-1} in aqueous electrolytes signifies weakened hydrogen bonds, confirming stabilized free water molecules. Meanwhile, this is attributed to the formation of mutual hydrogen bonding between H_2O and acetonitrile molecule, which results in a reduced electrochemical reactivity of H_2O molecules. Its capacity of ~120 mA h g^{-1} with a retention of 95 % after 2000 cycles at 1.0 A g^{-1}, which is a record-high performance for CIBs reported so far (Fig. 6e). Dou et. al. showed that the absence of Raman vibration mode of O—H stretching proved the maintained merits of WIS electrolyte, including the reduced water activity, coordinated metal ion-$(H_2O)_x$ complex, and stable working window, in an "acetonitrile/water-in-salt" hybrid electrolytes [149]. Yuan et. al. displayed that hybrid solvent (i.e., DMF/H_2O) not only can inhibit the water activity but also nonflammability and low viscosity properties, thereby

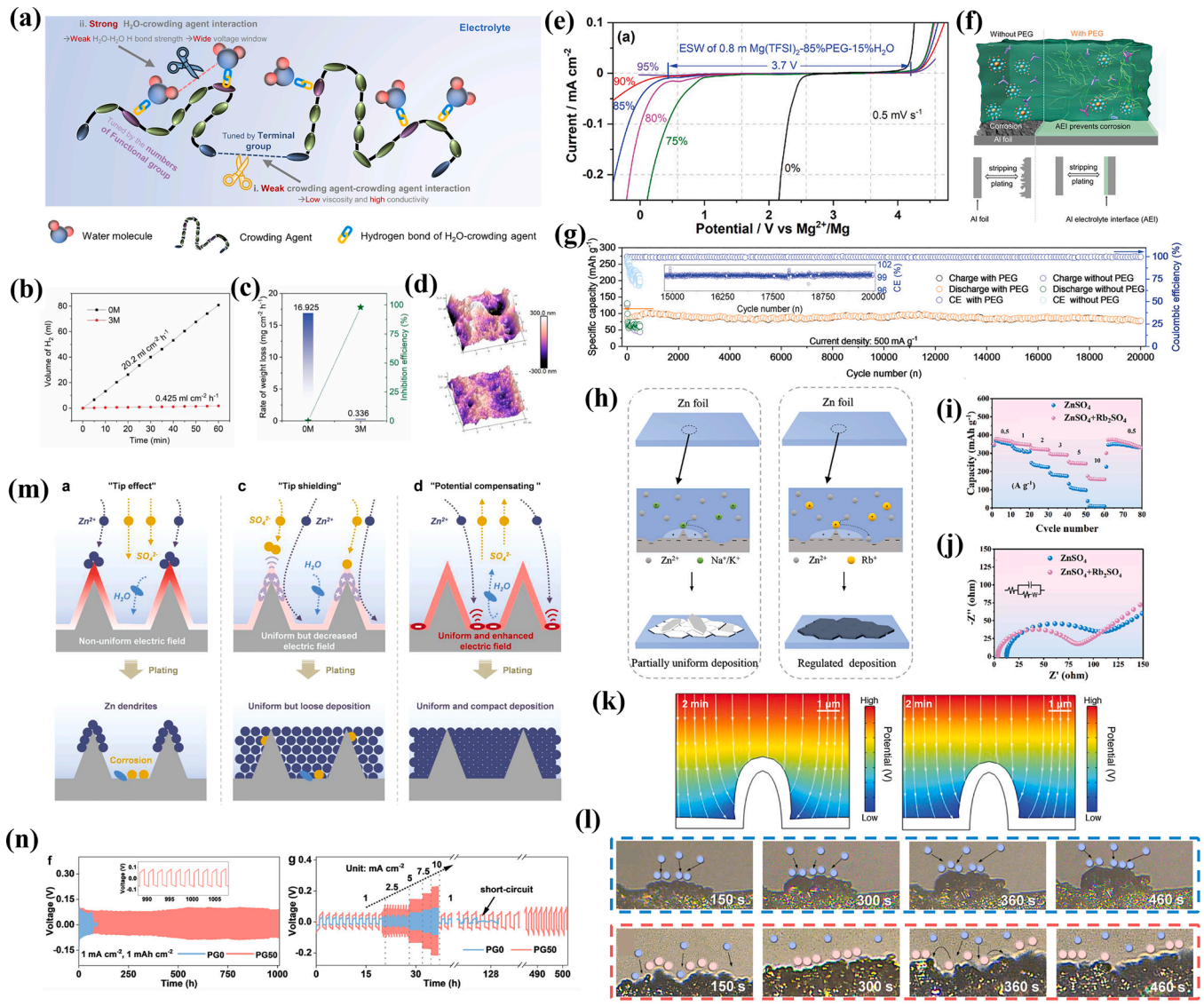

Fig. 7. **(a)** Schematic illustration of intermolecular interactions of H_2O–crowding agent, crowding agent–crowding agent, H_2O–H_2O. Reprinted with permission from Ref. [161] Copyright 2021 American Chemical Society. (b) Hydrogen evolution curves of the Al anodes in different electrolytes. (c) Rate of weight loss of Al anodes in the 0 M and 3 M electrolyte and inhibition efficiency. (d) AFM images of Al anodes after immersed in 0 M (upper), and 3 M electrolytes (lower). Reprinted with permission from Ref. [164] Copyright 2022 Elsevier. (e) The LSV of 0.8 M $Mg(TFSI)_2$-xPEG-(1-x)H_2O (x = 0 %, 75 %, 80 %, 85 %, 90 %, and 95 %) on glassy carbon between −3.0 and 2.2 V versus Ag/AgCl at 0.5 mV s^{-1}. Reprinted with permission from Ref. [57] Copyright 2022 Wiley-Blackwell. (f) Schematic illustration of electrolyte with and without PEG, indicating Al electrolyte interface is formed on Al and plays as a protective layer. The enlarged part is the schematic images of electrolyte on molecular level. (g) Cycling performance of the full-cell with PEG and without PEG at 500 mA g^{-1}. Insert is the detail of CE during the cycling process with PEG. Reprinted with permission from Ref. [59] Copyright 2023 Wiley-Blackwell. (h) Schematic diagram of Zn deposition cycled in $ZnSO_4$ + Na_2SO_4/K_2SO_4 (left) and $ZnSO_4$ + Rb_2SO_4 (right) electrolytes. (i) Rate capabilities of Zn//VO_2 full cells in different electrolytes at current densities from 0.5 to 10 A g^{-1}. (j) EIS curves of Zn//VO_2 full cells in different electrolytes. Reprinted with permission from Ref. [167] Copyright 2023 Wiley-Blackwell. (k) The potential and current distribution of Zn deposition at simulation time of 2 min in $ZnSO_4$ electrolyte (left) and $ZnSO_4$/Ce electrolyte (right); the gray lines with the arrows and the black lines at the bottom represent the current and the initial surface of the Zn anode. Reprinted with permission from Ref. [166] Copyright 2022 Wiley-Blackwell. (l) Locally magnified in-situ microscopy images of Zn anodes deposited in $ZnSO_4$ (upper) and $ZnSO_4/Y^{3+}$ (lower) electrolytes. Reprinted with permission from Ref. [170] Copyright 2023 Elsevier. (m) Proposed mechanisms for tip effect (left), tip shielding effect tip effect (left), and potential compensating effect (right), as well as corresponding Zn deposition behaviors. (n) Long-term cyclability (left) and rate capability (right) of symmetrical cells with different electrolytes. Reprinted with permission from Ref. [30] Copyright 2023 Wiley-Blackwell.

promoting the reversibility and cyclability of aqueous batteries [150]. This design strategy presents a novel approach to expand the working window and mitigate water decomposition. However, there are still shortcomings associated with the low-salt and high-solvent content of aqueous electrolytes. One of water's advantages lies in its high ionic conductivity and mobility, which need improvement in electrolytes with high organic solvent concentrations. In recent years, in addition to introducing organic solvent as co-solvent, water-in-ionic liquid (WiIL) [74,151,152], water-in-deep eutectic solvent (WiDES) [76], and water-in-eutectogel (WiETG) [113,153] have been reported to manipulate ion solvation and water reactivity, helping establishment of high-performance stable batteries. Thereof, as given in Fig. 6f, the ionic conductivity will fluctuate according to the change of molar ratio and electrolytes. Especially in mixture of ionic liquid and water, although the ionic conductivity of WiIL system still cannot be comparable to that of pure water, it has been significantly affected due to half times of ionic

conductivity of pure ionic liquid (green bar). Besides, the presence of BMI cations with large imidazole ring and long side chain can well disperse the charge distribution, which can benefit the mutual solubility between supporting salts and metal salts [74]. Furthermore, DFT simulation of WiDES system, which contains $ZnCl_2$, water, and acetamide, has been used to investigate the influence of solvation during the transport process [76]. Shi et al. found that there is the lowest activation energy of $[ZnCl(acetamide)_2(H_2O)]^+$ and its corresponding desolvation process compared with that of other complexes. The solvation structure in WiDES electrolyte can promote the uniform growth of zinc metal. This corresponds to the reduced nucleation overpotential and dissociation energy of this complex (Fig. 6 g). This solvation structure in WiDES electrolyte promotes uniform Zn metal growth, reducing nucleation overpotential and the complex's dissociation energy. This approach yields smooth metal deposition, akin to the electrostatic shielding effect of cation additives described in Section 3.3. Hou et al. developed a new WiETG system by combining DESs with a CMC-crosslinked PAM polymer, resulting in a quasi-solid-state aqueous electrolyte. This electrolyte uniquely offers a wide voltage window, non-flammability, and high ionic conductivity [113]. The presence of abundant ions, hydrophilic molecules, and the screening effect of TFSI anions in these electrolytes inhibit water molecule migration towards the electrode surface, thereby increasing the overpotential for HER and OER side reactions. Although high-water-content electrolytes are desirable for their ionic conductivity, they pose risks of water decomposition and limited application feasibility during the charge-discharge process. Enhancing the practicality of aqueous electrolytes in battery systems can be achieved by incorporating additives that improve metal corrosion resistance and increase the overpotential for HER and OER.

4.2. Additives

An effective and economical method for enhancing electrolyte properties involves adding an additive, typically under 10 % by weight [155,156]. These additives, including stabilizers, chelating agents, antifreeze, and crowding agents, improve electrolyte stability and functionality. They help minimize water decomposition, hydrogen bonding, evaporation, and dendrite growth in the electrolyte. Extensive research has led to the development of tailored additives that effectively reduce side reactions, curtail gas production, pH polarization, and prevent the formation of by-products like ZHS. For instance, to produce a Metal-F rich SEI film not merely derived from fluorinated salts, usual hydrolysate of organic solvent (i.e., FEC) is usually applied in the non-aqueous batteries to conduct the defluorination and form the metal-F inorganics. It is of great significance to design FEC-containing electrolyte and explore the potential mechanism of FEC in inhibiting formation of metal dendrites and avoiding undesirable parasitic reactions. The metal-F rich SEI layer, including LiF [157], ZnF_2 [19], can suppress the gas evolution, metal corrosion, and dendrites growth on the anode side. Besides, most of reported literatures possessed that additives should satisfy the multifunctional requirements, including charge of solvation structure, growth of stable CEI/SEI layer, inhibition of water activity. Therefore, the design of tailored electrolyte additives is crucial for optimizing performance in various multivalent metal-ion batteries.

4.2.1. Crowding agent

When compared to the effects of salt concentration and co-solvent strategies discussed in Subsections 3.1 and 3.2, the crowding phenomenon brings about significant alterations in the electrolyte system, particularly noticeable at concentrations surpassing 80 mg ml^{-1} of crowding agents [158]. With the addition of crowing agents (e.g., PEG [78,159,160], PEGDME 450 [161], PEO [162], sodium polyacrylate [163], glucose [164]), the water activity will be reduced through regulation of hydrogen bond networks, thereby inhibiting water decomposition and extending the working window. As shown in Fig. 7a, three main intermolecular interactions in a molecular crowding electrolyte are respectively crowding agent-crowding agent, H_2O-H_2O, and H_2O-crowding agent. Weakening the bond strength between H_2O molecules and crowding agents results in changes in viscosity and ionic conductivity. This effect can be achieved by introducing additional crowding agents and adjusting the number of functional groups they possess. After that, the enhanced intermolecular bonding strength between H_2O and crowding agent will further inhibit the water activity and decomposition. Furthermore, the decomposition of crowding agents can facilitate the formation of protective layer on the electrode surface to prevent the electrode's self-corrosion [164]. As given in Fig. 7b and 7c, adding glucose reduces water decomposition and hydrogen production while protecting metal foil from corrosion and weight loss in basic solutions. The AFM images (Fig. 7d) illustrate that surfaces treated with additives exhibit smoother Al surfaces compared to untreated ones. Additionally, increasing PEG 400 agent, as seen in Fig. 7e, changes and widens the solvation configurations of Mg ions and the working window of MIBs, pushing the potentials of HER/OER beyond water's thermodynamic stability. To further prevent the side reactions happening on the Al anode, Tao et al. also utilized the PEG to mitigate the reactive Al surface caused by the rapid kinetic in aqueous electrolyte. Importantly, PEG can polymerize hydroxide bonds amongst itself to produce chain macromolecules, inducing a SEI film formed on the Al anode during charging process (see Fig. 7f). It can not only inhibit the corrosion of Al anode under acidic conditions but also disrupt the hydrogen bond network between water molecules. This widens the working window and extends the lifespan of AIBs to over 20,000 cycles. (see Fig. 7 g).

4.2.2. Electrostatic shield effect and repulsion layer

In battery systems, controlling the formation of metal dendrites is critical for ensuring safety and stability. Ding et al. proposed a self-healing electrostatic shield to mitigate dendrite growth by introducing cations [165]. This mechanism utilizes cations with a lower reduction potential than Li ions. Upon deposition, these cations form a positively charged electrostatic shield around the protrusions of the initial Li deposition layer, effectively impeding dendrite growth. Consequently, further deposition of Li metal occurs in adjacent regions, thereby eliminating dendrite growth in LIBs. Hence, trying to add different cations into aqueous battery is a worthy noting strategy to optimize the electrolyte system, such as $CeCl_3$, [166] Rb_2SO_4, [167] $LiCl_3$, [168] La $(NO_3)_3$, [169] $Y_2(SO_4)_3$, [170] Rb cations, with their larger volume and spatial potential resistance, provide stronger electrostatic shielding and a more effective repulsion layer compared to Li/Na/K cations. This leads to more uniform metal deposition and reduced dendrite growth in aqueous electrolytes (Fig. 7h) [167]. The addition of Rb_2SO_4 greatly improved the capacity performance and current durability of the $Zn//VO_2$ full cell, while the full cell without Rb cations cannot exceeded current density of 2 A g^{-1}(Fig. 7i). The series and charge transfer resistance of full cell (refer to Fig. 7j) reduced significantly with present of Rb cations. To verify the existence and influence of electrostatic shielding, the finite element modeling simulation can be used to demonstrate the trend and position of metal deposition. In Fig. 7k, the deposition of Zn ions preferentially concentrates around the sharp edges according to the tip effect. With the addition of Ce^{3+} cation, the cations will tend to absorb on the tip of Zn protuberance, and therefore Zn ions are enabled to deposit on the smooth region of anode surface. To investigate how the Y^{3+} cations impact on the Zn deposition, the 3D laser scanning microscopy confocal analysis (Fig. 7l) showed that there were distinct differences in electrode surface with and without the addition of Y^{3+} [170]. In addition, Wang et al. have displayed that introducing polar molecules, which contained glycine and alanine functional groups, can effectively exhibit electrostatic shielding, thus suppressing electrode dissolution, in tandem with dendrite growth and generation of protective layer [171]. Other organic cation or polymer additives, like TMA_2SO_4, PEO, PSS, PAM, have been used in smoothening the Zn deposition associated with their polarity of functional groups, which will affect the binding strength between salt anions and

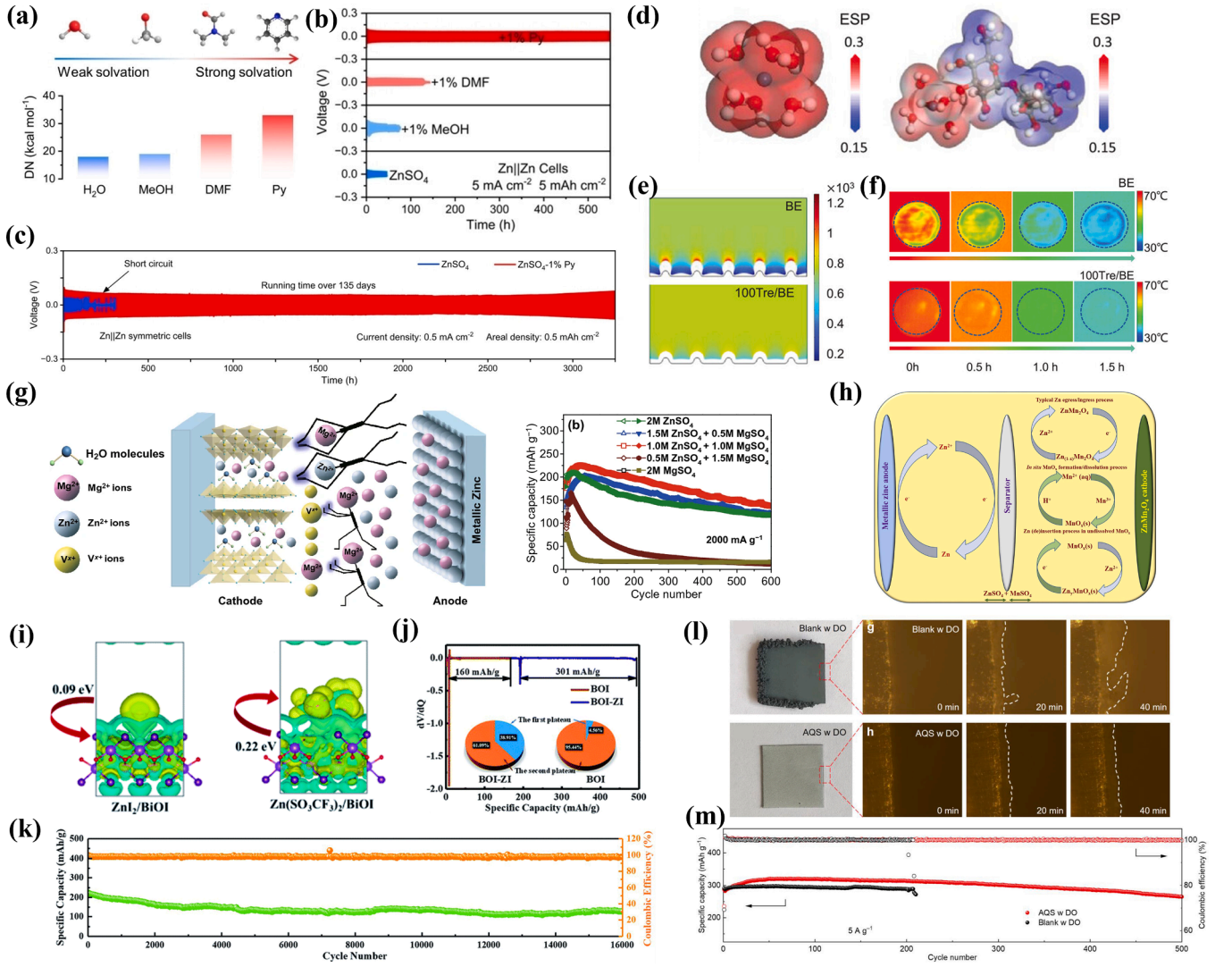

Fig. 8. (a) Summary of coordination power of additives. (b) Cycling lifespan of symmetric cells in different electrolytes under 1 % addition amount (c) Long-term galvanostatic cycling performances of Zn//Zn cells in $ZnSO_4$ and $ZnSO_4$–1 % Py electrolytes at 0.5 mA cm^{-2}, 0.5 mAh cm^{-2}. Reprinted with permission from Ref. [174] Copyright 2023 Wiley-Blackwell. (d) Electrostatic potential mapping of the original Zn^{2+}-$6H_2O$ in comparison to Zn^{2+}-$5H_2O$-trahalose. (e) Simulated electric field distributions on the Zn anode in the presence and absence of trehalose. (f) Infrared thermography images of zinc anode in BE and 100Tre/BE at 5 mA cm^{-2} with a capacity of 1 mAh cm^{-2} after 50th plating. Reprinted with permission from Ref. [79] Copyright 2023 Wiley-Blackwell. (g) Scheme of the Mg^{2+} functional mechanism for hybrid electrolyte. Reprinted with permission from Ref. [184] Copyright 2020 Springer Nature. (h) Electrochemical reactions inside $ZnMn_2O_4$//Zn cell in ZMS electrolyte. Reprinted with permission from Ref. [25] Copyright 2020 Elsevier. (i) Electron density difference maps for $Zn(I_3)_2$/Bi (left) and $Zn(SO_3CF_3)_2$/Bi (right) systems. (j) Differential voltage (dV/dQ) curves at 0.5 A g^{-1}. Inset: anion–cation contribution ratio at 0.5 A g^{-1}. (k) Long-term cycling performance of Zn–BiOI battery with addition of ZnI_2 at 3 A g^{-1}. Reprinted with permission from Ref. [185] Copyright 2022 Royal Society of Chemistry. (l) Optical photographs and operando optical microscope images of the Zn anode during deposition process in the electrolytes with and without sodium anthraquinone-2-sulfonate (AQS). (m) Long-term cycling performance of Zn//ZVO full cells using the electrolytes with and without AQS at 5 A g^{-1}. Reprinted with permission from Ref. [186] Copyright 2023 Wiley-Blackwell.

polymer additives [172,173]. In addition, certain anion additives can create a synergistic effect, helping to stabilize the pH fluctuations caused by the introduction of non-metal cations. Furthermore, mitigating the distribution of interface electric fields is crucial for preventing short circuits and addressing dendrite-induced failures. Li et al. reported that achieving homogeneous electric fields on metal anodes with elevated potential intensity can be effectively accomplished through the selective adsorption of highly polarized propylene glycol molecules. This process facilitates the formation of dense and uniform Zn deposition films (see Fig. 7m). In Fig. 7n-left, a stable voltage hysteresis was sustained for 1000 h in the presence of PG50, whereas dendrite-induced short-circuits were detected after only 67 h without the addition of PG50. The rate capability of Zn//Zn cells are investigated by more harsh conditions ranging from 1 to 10 mA cm^{-2} (Fig. 7n-right), demonstrating that the addition of PG enhances the cycling durability and rate capability of ZIBs compared to the base electrolyte.

4.2.3. *Organic molecule additives*

Ion mobility and ionic conductivity can be regulated not only through anion ligands and hybrid solvent strategies, but also by incorporating functional organic solvents. The polarized functional groups of these solvents serve a dual purpose: selective adsorption on metal surfaces and alteration of the original hydrogen bond network and solvation shell. Besides, the difference between hybrid solvents and organic molecular additives strategies is the amount compared to the wt% or vol % of water. The former is usually at solvent/water ratio from 2:1 to 1:3, whereas the latter is located at 1∼10 wt%. Luo et al. proposed the idea of whether the structural change of the inner Helmholtz plane can

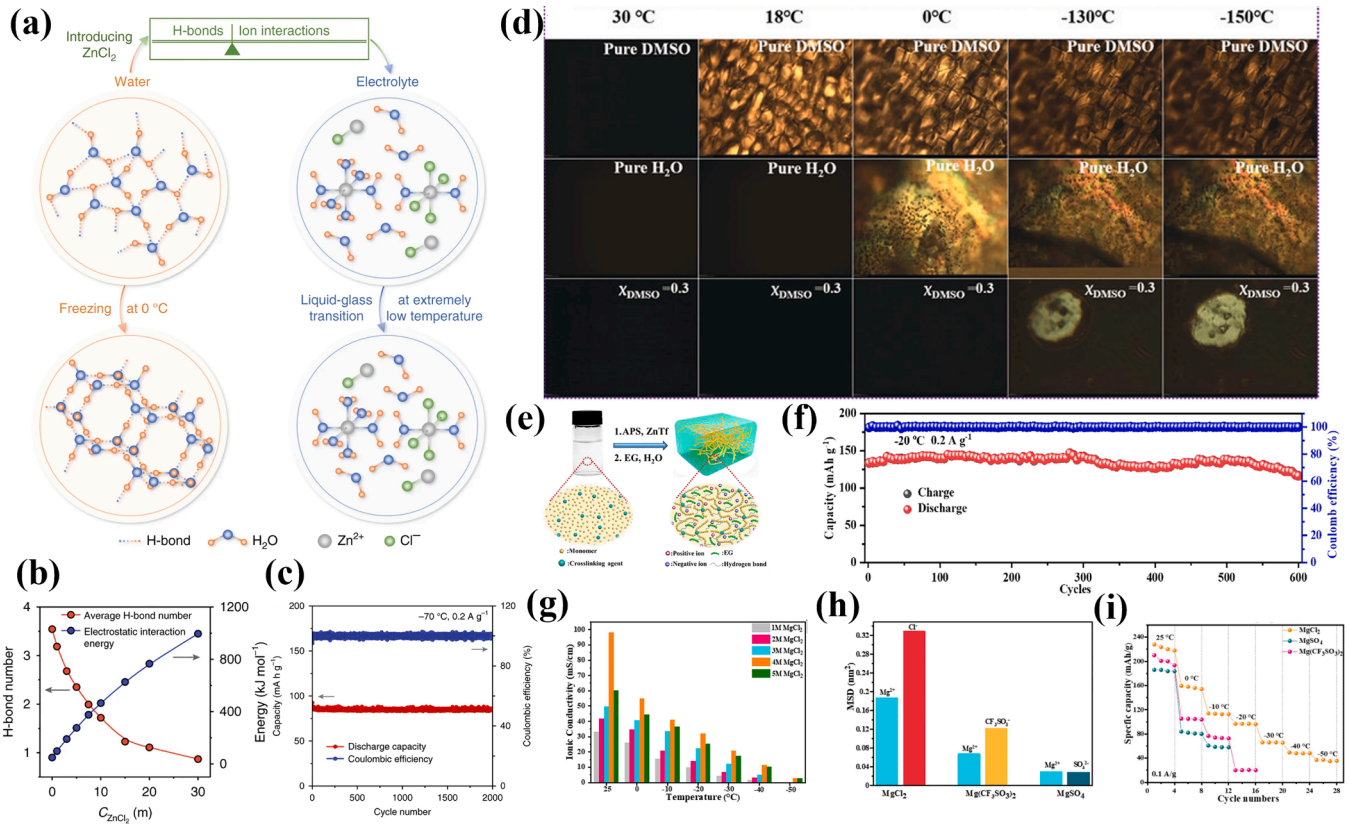

Fig. 9. (a) The schematic of the structure evolutions of water and electrolyte, and the design of low-T_t solution. (b) The hydrogen bond number and the electrostatic interaction energies obtained by Molecular dynamic simulation. (c) Cycling performance of PANI/LTE/Zn batteries at −70 °C. Reprinted with permission from Ref. [189] Copyright 2020 Springer Nature. (d) Polarized light microscopes images at different temperatures. Reprinted with permission from Ref. [188] Copyright 2019 Wiley-Blackwell. (e) The preparation process, self-healable feature, and anti-freezing property of the AF-SH single bond CPAM polyelectrolyte. (f) The cycle performance of AF-SH-ZIB under −20 °C. Reprinted with permission from Ref. [202] Copyright 2022 Elsevier. (g) Ionic conductivities of the $MgCl_2$ aqueous solution with various concentration from −50 to +25 °C. (h) The mean square displacement values of $MgCl_2$, $MgSO_4$, and $Mg(CF_3SO_3)_2$. (i) Specific capacities of MIBs with different electrolytes at different temperatures. Reprinted with permission from Ref. [200] Copyright 2023 Elsevier.

improve the reversibility of the metal anode. They suggested using a universal high donor number additive, such as pyridine, with just 1 vol. % addition in water to design the inner Helmholtz plane. Organic molecules with high donor numbers, indicating high binding energy to cations, can enhance the coordination capability of Zn ions. Fig. 8a illustrates organic solvents with varying donor numbers, ranging from low to high values in the order of H_2O, MeOH, DMF, and pyridine. This suggests that pyridine additives may be more effective than DMF and methanol in substituting the [H_2O]-based solvation structures of zinc ions. The symmetric cell (Zn//Zn) are put forward to evaluate the effect of versatile additives depicted in Fig. 8b. Due to the solvation structure variation, the 1 % pyridine in $ZnSO_4$ aqueous electrolyte can enhance the transference number, further achieving superior cyclability over 500 h. Reversely, the symmetric cells with 1 % DMF and 1 % methanol show a better performance than original electrolyte without additives, but it still far inferior to that of 1 % pyridine [174]. With the present of only 1 % pyridine, the symmetric cell can deliver a stable cycling for over 135 days, while pyridine-free $ZnSO_4$ electrolyte can only cycled for 80 h with suffering from an irreversible voltage rise (Fig. 8c).

Moreover, other organic molecules such as NH_2 [175], pyrrolidine-series [176,177], ether [178], acetamide [179,180] are also applied in the system of aqueous batteries. Thereof, the hydroxyl groups play a significant role in the solvation shell of cations in $ZnSO_4$-based aqueous electrolytes, which will interact with free water molecules and SO_4^{2-} anions and further modify the solvation sheath. Liu et al. reported that trehalose is more prone to electron loss, it can be easy to replace the [H_2O]-solvated shell of cations. As simulated in Fig. 8d, when one trehalose molecule replaces a water molecule in the Zn^{2+}-6H_2O, the electrostatic potential obviously decreases, suggesting a relief in electrostatic repulsion around Zn cations, therefore boost the rapid transportation and ionic conductivity. Simultaneously, this organic additive also can control the uniformity of Zn deposition shown in Fig. 8e. The COMSOL simulation presented the evident that the chemisorption of polyhydroxy trehalose will homogenize the interfacial electric field, resulting in an even Zn nucleation and high anti-corrosion impedance compared to that in the original electrolyte without additives. The infrared thermography images can be used to reveal the formation and distribution of by-products, which depend on the thermal conductivity difference between by-products and Zn metal (See Fig. 8f). Under the protection of the trehalose additive, the Zn anode displayed a more homogenous thermal distribution after 50th plating, indicating that the trehalose additive effectively alleviated side reactions.

4.2.4. *Redox anion/cation additives*

The incorporation of redox couples as electrolyte additives plays a pivotal role in enhancing uniform deposition, ionic conductivity, and overall capacity in battery systems. These additives not only contribute to the capacity but also facilitate the main charge ions, fostering electrochemical synergy during cycling tests. Both inorganic cations and anions can serve as redox pairs in this context. Notably, Zhang's group pioneered the utilization of divalent Mg ions as electrolyte additives, which has led to a significant improvement in the electrochemical performance of ZIBs. As given in Fig. 8 g, the addition of Mg^{2+} into the electrolyte will impede the continuous dissolution of electrode materials, thus maintain the structural stability and cyclability. During the charging and discharging process, the Mg^{2+} have been found to deposit

on the Zn anode and dissolved back into the electrolyte, respectively, revealing that this redox mediator can serve as co-insertion cations and interaction cations along with the Zn^{2+}. Another type of redox cation additives is Mn^{2+}, which can form the intermediate (i.e., MnO_x) to support the reversibility and prevent the mass loss of cathode materials. On the right side of Fig. 8h, the redox reactions involving Mn^{3+}, Mn^{2+}, and MnO_x aid the Zn egress/ingress and (de)insertion processes in undissolved MnO_x. This contributes to maintaining the structural integrity of the cathode and suggests a certain degree of manganese conversion in the electrolyte. In addition to redox cations, the inclusion of redox anion additives also enhances the performance of aqueous systems. Charge density differences and Bader analysis show that the pre-addition of ZnI_2 alters electron distribution and transfer between BiOI and ZnI_2 (Fig. 8i-left). Compared with the case of $Zn(CF_3SO_3)_2$ to BiOI (Fig. 8i-right), ZnI_2 acts as a redox mediator, effectively enhancing the kinetics of the Bi redox reaction. This enhances the multi-electron conversion's synergistic effect in aqueous ZIBs, leading to improved reversibility of BiOI with ZnI_2 compared to pure BiOI. As shown in Fig. 8j, the dV/dQ curves were displayed. Obviously, when ZnI_2 additive was added, the discharge capacity of the cation reaction increased to 301 mA h g^{-1}, showing that the Bi^{3+}/Bi^0 redox reaction releases more capacity in the presence of the ZnI_2 additive. With the addition of redox pair, a reversible capacity (~220 mA h g^{-1}) was reached, even after 16,000 cycles, and a 60 % capacity retention was achieved, revealing the good electrochemical energy storage performance of the battery (Fig. 8k). A novel redox additive, sodium anthraquinone-2-sulfonate (AQS), can tackle the oxygen-dissolved hazards through chemical self-deoxygenation strategy. The presence of the AQS additive resulted in clearly uniform Zn deposition, contrasting with non-uniform deposition and notable dendrite growth observed on the Zn anode in the blank electrolyte due to OH-derived by-products. (refer to Fig. 8l). As displayed in Fig. 8m, the Zn//V_2O_5 full cell with AQS demonstrated a significant improvement in cyclability compared to the AQS-free case. Additionally, there are other redox additives available, such as $K_3[Fe(CN)_6]$ [181], trimethyl-sulfoxonium iodide (TMSI) [182], KI [183], and so on.

4.2.5. *Anti-freezing and boiling-point-extended agents*

Climatic zones, including tropical, temperate, and frigid, experience distinct environmental temperatures. Energy storage systems deployed in these areas must address challenges such as temperature volatility in tropical climates and electrolyte solidification in frigid zones. Hence, the selection of electrolytes with suitable boiling and freezing points is crucial for the effective application of battery systems across different countries. The large-scale-developed aqueous batteries will be utilized in the extremely climate conditions, thereby suffering from severe capacity decay and poor ionic conductivity because of the high freezing point and low boiling point of water-based electrolyte. We necessarily consider the feasibility of aqueous batteries used in the cold environment due to the freezing situation of water at 0 °C. A large number of hydrogen bonds lead to the freezing of aqueous electrolyte below 0 °C, which limits its ionic conductivity and battery's performance under extreme environment [187]. Organic solvents can promote the formation of hydrogen bonds between the solvent and water molecules, which competes with hydrogen bond formation between water molecules. Consequently, these solvents interfere with hydrogen bonding in water, making it difficult for water molecules to bind.

To broaden the operational temperature range of aqueous batteries, several efforts have been directed towards modifying their solvation sheath and structure to meet the demands of extreme cold environments, which includes addition of aprotic solvent with high polarity (e.g., DMSO and acetonitrile) [188], anion salt [189,190], cryoprotective agent [191], hydrogel formation [192,193], and so on. Firstly, concerning the impact of salt concentration, the liquid-glass transition state decreases with increasing salt concentration. Fig. 9a illustrates how Zhang et al. modulated hydrogen bonds and cation-anion interactions by adjusting $ZnCl_2$ concentration and the solid-liquid transition temperature. This weakens water molecules' hydrogen bonds, lowering the freezing point of the aqueous electrolyte. Molecular dynamic simulations show that the hydrogen bond ratio in water molecules is minimized when $ZnCl_2$ concentration reaches 30 M (Fig. 9b). At extremely low temperatures, the reduced interaction among fewer free H_2O molecules in the battery prevents freezing, thereby maintaining the electrolyte in a liquid state and enabling long cycling performance of 2000 times (Fig. 9c). Furthermore, the use of highly polar solvents mixed with water as additives significantly lowers the freezing point. Nian et al. employed a polarizing microscope to observe the isotropy and anisotropy of the liquid phase pre- and post-freezing, showing that pure water and DMSO begin to freeze at 0 °C and −18 °C, respectively, as depicted in Fig. 9b. The mixed solvent remains unfrozen down to −130 °C, demonstrating its ability to prevent water molecules from forming ordered hydrogen bond networks at specific DMSO/water ratios, making it ideal for low-temperature applications. Furthermore, EG is a commonly used antifreeze additive. Its introduction lowers the freezing point of water, thereby extending the working temperature range of aqueous electrolytes. In aqueous systems, EG serves multiple functions beyond being an antifreeze additive. It is utilized as corrosion inhibitor [194], polyiodide shuttle inhibitor [195], water blocker [196]. Jin et al. combined monomers, crosslinking agents, and EG to create low-temperature self-healing aqueous Zn/polyaniline batteries, as shown in Fig. 9c. EG functions by inhibiting water molecule icing and dynamically adjusting interactions between polymer chains and water. This dual action enhances both antifreeze capabilities and self-healing properties. This aqueous ZIBs with *in-situ* polymerization can maintain 87.3 % of its capacity over 600 cycles at 0.2 A g^{-1} (Fig. 9d). Consequently, various studies on anti-freezing designs in aqueous metal-ion batteries focus on aspects like salt additives, concentration, co-solvents, and hydrogel formation [197,198]. In addition to the extremely cold space, enabling reliable operation of aqueous batteries over a wide temperature range without safety concerns is an urgent prerequisite for being widely used. Kim et al. introduced a novel class of aqueous eutectic electrolyte (AEE), which is based on the colligative property of a LiTFSI-water binary mixture [199]. The maximizes effect of AEE displayed less fraction of free water and average number of hydrogen bonds that of dilute aqueous electrolyte. The AEE can maintain a better ionic conductivity at a broad temperature range from −40 °C and 100 °C, showing good electrochemical stability and feasibility. In aqueous batteries, Yang et al. applied a novel aqueous-salt hydrates DES electrolyte in low-temperature aqueous systems. This approach, utilizing different ligands, was aimed at revealing the superior anti-freezing properties of the electrolyte. The ionic conductivity of the $MgCl_2$ aqueous solution with different concentrations as a function of temperatures through EIS data (Fig. 9e). First, the 4 M $MgCl_2$ solution has the lowest freezing temperature (−62 °C) and highest ionic conductivity (2.77 mS/cm at −50 °C). Second, the mean square displacement (MSD) can elucidate the ion diffusion and solvation structure in $MgCl_2$ electrolytes. The maximum cation and anion MSD values reveal that the $MgCl_2$ system has the faster ion migration than that of $MgSO_4$ and $Mg(CF_3SO_3)_2$ system, which will boost the occurrence of the reversible insertion reactions in MIBs [200]. These results highlight the remarkable anti-freezing performance of low-concentration $MgCl_2$ electrolytes, which afford a wide working temperature range and demonstrate excellent capacity performance at both room temperature and extremely low temperatures (Fig. 9 g). Also, due to the strong acidity allows $ZnCl_2$ to accept donated Cl^- ions to form $ZnCl_4^{2-}$ anions, Yang et al. showed an aqueous $ZnCl_2$ electrolyte with introduced LiCl as supporting salt to form the optimized high-entropy solvation structure (i.e., $Li_2ZnCl_4{\cdot}9H_2O$), sustaining a stable cycling over 800 h between −60 °C and 80 °C [201].

4.3. *Ligand effect of electrolyte salts*

The first paragraph of Section 3.2 highlights the significance of the ZnF_2-rich layer, which is formed by the addition of FEC solvent, in

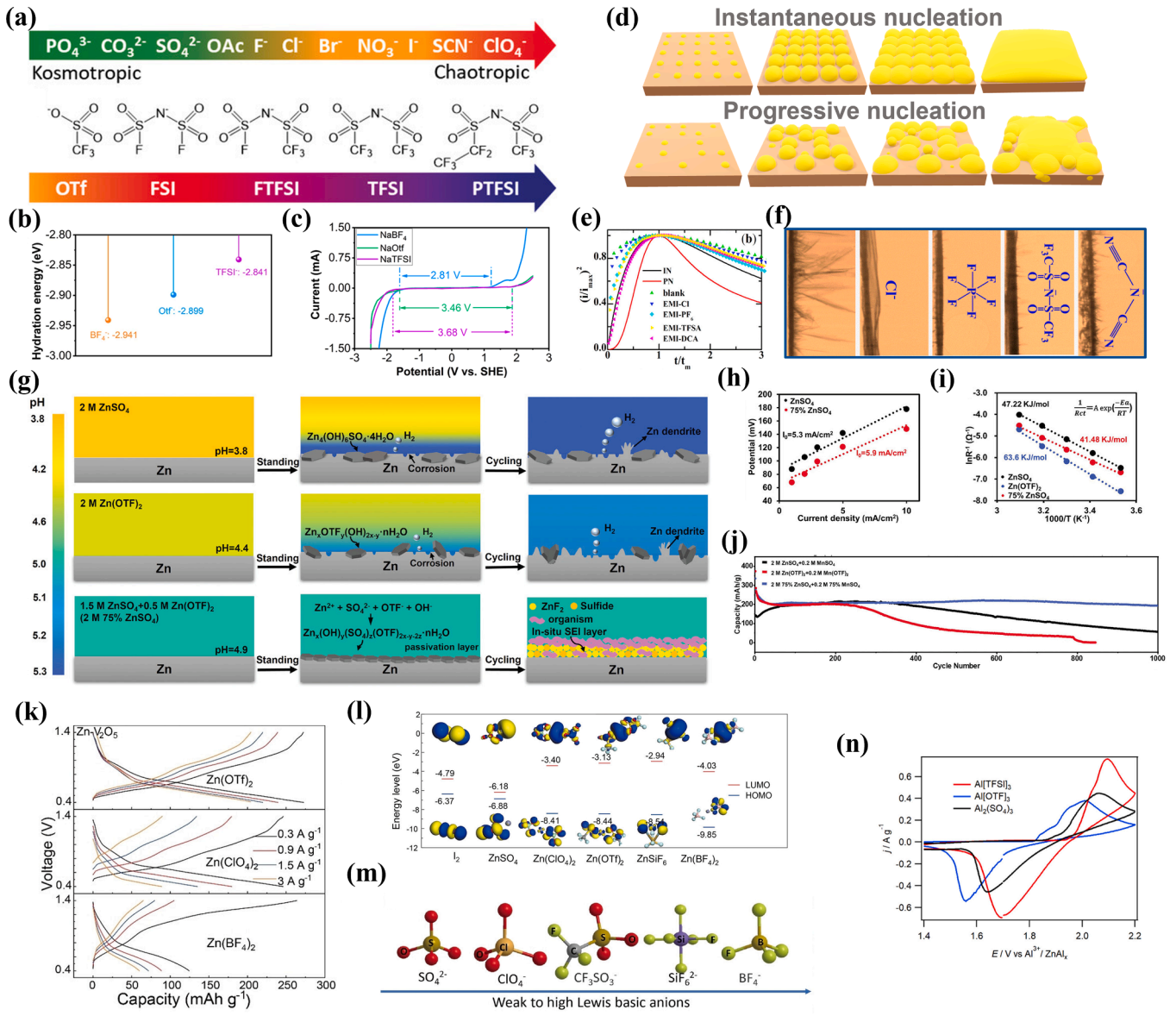

Fig. 10. (a) Typical Hofmeister series for anions in water with kosmotropes on the left and chaotropes on the right end of the series (upper). Chemical structures of the OTf, FSI, FTFSI, TFSI, and PTFSI anions with the colored bar indicating their position in the extended Hofmeister series (lower). Reprinted with permission from Ref. [207] Copyright 2021 Wiley-Blackwell. (b) The hydration energy comparison of BF_4^-, OTf^-, and $TFSI^-$. (c) LSV curves of three electrolytes. Reprinted with permission from Ref. [212] Copyright 2021 Springer Nature. (d) The scheme of instantaneous nucleation and progressive nucleation. (e) X-ray images of Zn deposition at −0.85 V in various electrolytes. (f) Real-time X-ray images of Zn deposition and dendrite formation at various electrolyte. Reprinted with permission from Ref. [213] Copyright 2016 American Chemical Society. (g) Schematic illustration of the interfacial pH evolution of different electrolytes and in situ formation mechanism of the organic-inorganic SEI in the mixed electrolyte. (h) Exchange current density of Zn//Zn symmetric cells with different electrolytes. (i) The fitting Arrhenius curves and the desolvation activation energies for Zn//Zn symmetrical cells with $ZnSO_4$, $Zn(OTf)_2$, and 75 % $ZnSO_4$ electrolytes. (j) Long-term cycle performance of Zn//MnO_2 battery at 1 A g^{-1} with different electrolytes. Reprinted with permission from Ref. [214] Copyright 2022 Wiley-Blackwell. (k) Cycling performances and CEs of Zn−V_2O_5 cells in three different electrolytes at 3 A g^{-1}. (l) LUMO-HOMO energy level diagram of iodine and zinc salts. (m) Structures of anions and their subsequence from weak to high Lewis basic anions. Reprinted with permission from Ref. [215] Copyright 2023 Wiley-Blackwell. (n) Cyclic voltammograms recorded at 0.1 mV s^{-1} in the given electrolyte using MnO_2//Zn–Al cells. Reprinted with permission from Ref. [97] Copyright 2022 American Chemical Society.

significantly enhancing electrode stability and improving energy storage performance. An et al. discovered that the introduction of multifunctional ZnF_2 salt into the aqueous electrolyte results in the formation of a stable F-rich interfacial layer. This layer serves as an inert protective barrier and guides the deposition orientation of the metal [203]. In other words, these anions play a role in coordinating with metal ions in the electrolyte. The solvation structures of metal cations, influenced by the characteristics of anions, are also a tunable factor that can impact battery performance. To date, a wide range of anions in salts have been utilized, including inorganic salts, (SO_4^{2-}, NO_3^-, Cl^-, ClO_4^-, F^-) and organic salts ($CF_3SO_3^-$, $TFSI^-$, CH_3COO^-), etc. Therefore, choosing different anions for electrolyte salts presents a viable approach to addressing challenges in aqueous electrolytes. Their solvation energy, diffusion barrier, and adsorption energy in aqueous electrolytes are dependent on molecular width, functional group, dipole moment. This variation influences factors like mobility, solubility, leveling ability, and reactivity.

Reber et al. described a trend in the critical concentration of anion salts that initiates the precipitation of solvation in aqueous electrolytes (Fig. 10a). Ionic kosmotropes, often small and possessing high charge

density, stand in contrast to chaotropes, which are typically larger and exhibit lower charge density. Kosmotropic anions (structure makers) and chaotropic anions (structure breakers) either construct or disrupt the hydrogen bond network in water, thereby enhancing or diminishing water's interaction with metal cations, respectively [204]. In other words, the chaotropic anions (I^-, $CF_3SO_3^-$) show weaker interactions with H_2O/Zn^{2+} than kosmotropic anions (SO_4^{2-}, NO_3^-, Cl^-). This difference plays a crucial role in determining the solvation structure and hydrogen bond network in aqueous electrolytes. Nevertheless, in organic anions of electrolyte salts, the presence of hydrophobic functional groups (i.e., fluorine) can alter the trend of chaotropicity of these sulfonylimides, pushing water molecules into interaction with metal cations [205]. In fact, on basis of larger size and lower charge density, the chaotropicity of OTf^- is comparable to that of NO_3^-, while the $FTFSI^-$, $TFSI^-$, and $PTFSI^-$ are also more chaotropic than ClO_4^-. That is, the single charge carried by these sulfonylimides tends to delocalize around the molecule. Besides, the kosmotropic anions are not well suited for WIS strategy, as they tend to promote the formation of bulk-like water, resulting in reduction of electrochemical stability of the electrolyte [206]. However, kosmotropic anions, with their higher charge density, exhibit a stronger tendency compared to chaotropic anions to compete with water molecules for placement in the solvation shell of metal cations. As a result, kosmotropic anions release water molecules from the solvation structure of metal cations, leading to high overpotentials for water decomposition. In contrast, chaotropic anions can disrupt the hydrogen bonding between water molecules, thereby providing electrochemical stability [207]. Furthermore, the solvation and binding ability of anions with water molecules can be elucidated through hydration energy. In Fig. 10b, BF_4^- exhibited the lowest hydration energy, while $TFSI^-$ displayed the highest hydration energy. The lower hydration energy of anion salts indicates their easier dissolution in water. Highly soluble salts play a crucial role in regulating the electrolyte towards higher concentrations. Huang's group adopted the saturated concentration of these electrolytes, which is beneficial for suppressing water-related parasitic reactions and for displaying the impact of anions on the working window. Due to reduced H^+ and OH^- activity, the working window can be extended beyond 3.0 V (see Fig. 10c). The anions of ionic liquid type ($TFSI^-$) provide a wider stable window, meaning there is a wider applicable range of electrode materials. Furthermore, dendrite growth and uneven anode surface are also a problem that we can ameliorate through the change of salt anions. As discussed in Section 3.1, achieving a high electrolyte concentration leads to the inclusion of both kosmotropes and chaotropes into the cation solvation shell, which is a critical step in the formation of anion-derived SEI/CEI. Furthermore, due to their lower charge density and larger size, organic anions increase chaotropicity, thereby inhibiting the mobility and nucleation of solvated cations.

Therefore, addition of organic anions may slowdown the nucleation and induction time of metal deposited on the anode. The non-dimensional forms of the Scharifker–Hills model for instantaneous and progressive nucleation are displayed below [208].

$$\left(\frac{J}{J_{max}}\right)^2 = 1.9542\left\{1-\exp\left(-1.2564\left(\frac{t}{t_{max}}\right)\right)\right\}^2\left(\frac{t}{t_{max}}\right)^{-1}$$

$$\left(\frac{J}{J_{max}}\right)^2 = 1.2254\left\{1-\exp\left(-2.3367\left(\frac{t}{t_{max}}\right)^2\right)\right\}^2\left(\frac{t}{t_{max}}\right)^{-1}$$

Fig. 10d illustrates two nucleation mechanisms. The fitting curves in Fig. 10e demonstrate the nucleation behaviors of Cl^-, $PF6^-$, $TFSA^-$ ($TFSI^-$), and DCA^- anion salts. Although the nucleation mechanisms of salt anions reported by Song's group were consistent with the instantaneous nucleation at the initial nucleation state, DCA^- and $TFSI^-$ anions will hold up the induction time, nucleation rate, and number of nucleuses at initial voltage supply. Regarding initial current (i/i_{max}) of nucleation, it's notable that the i/i_{max} value of the blank electrolyte was approximately 0.8. This suggests the absence of solvation ions (aside from water molecules) around metal cations, thus indicating a lack of inhibition of nucleation and growth near the electrode surface. However, due to its hydrophilic property, DCA^- anions exhibit a strong complexing ability with transitional metal cations rather than an adsorption ability on the electrode surface. Additionally, the DCA^- anion in imidazolium ILs will partly aggregate into colloidal films, which disrupt the nucleation and growth of metal, leading to uneven deposition of Zn metal and the formation of voids on the Zn anode. Thus, the slow rate of induction and nucleation does not imply effective adsorption of ligands on the electrode surface to suppress dendrite growth. It is worth noting that both inorganic PF_6^- and organic $TFSI^-$ anions have large steric structure and strong chaotropic effect, thereby leading to simultaneously block the metal deposits and form a complex with metal cations during the charging process [209,210]. Fig. 10f demonstrates that the smooth electrode surfaces and slow induction rates of PF_6^- and $TFSI^-$ support these observations. Conversely, Cl^- acts only as an inhibitor on the anode, leading to rapid reduction of non-solvated metal cations and lateral growth with thicker Zn deposits. In summary, the selection of an appropriate ligand anion capable of forming hydrogen bonds with water molecules, uniformly adsorbing on the anode surface, and controlling the metal cation solvation structure is crucial for enhancing our aqueous electrochemical systems.

Recent research in aqueous electrolytes has shifted focus towards achieving "multifunctional" regulation by employing mixed anion types. This approach aims to simultaneously address various challenges such as water electrolysis, dendrite growth, induction time, and the formation of SEI and CEI films. The choice of ligands in electrolyte salts plays a crucial role in determining the decomposition products, thereby resulting in multifunctional SEI and CEI films. These films offer benefits such as enhanced trapping of active intermediates, robust formation of metal-fluoride compounds, and improved anti-corrosion properties [157]. Furthermore, "Water-in-bisalt" (WIBS) electrolytes will also diminish the fraction of free water molecules, contributing to the stable redox reaction of electrolyte. The hybrid solute strategy not only delivers an excellent combustion resistance, but also boosts growth of robust SEI film to stabilize the electrodes [148]. Consequently, Jin's research group implemented a mixed electrolyte strategy to mitigate metal dendrite formation and side reactions. As shown in Fig. 10 g, the mixed electrolyte of $ZnSO_4$ and $Zn(OTf)_2$ can effectively buffer the pH variation near the electrode surface, simultaneously inducing the organic-inorganic SEI layer ($Zn_x(SO_4)_y(OTf)_z(OH)_{2x-y-z}{\cdot}mH_2O$), thereby eliminating the dendrite growth and by-products formation. As usual, the inorganic layer closer to the metal anode is a compact structure with fully reduced electrolyte salts (e.g., metal fluoride, metal oxide, metal sulfide, metal hydroxide) while the organic layer closer to the electrolyte is a porous structure with partially reduced electrolyte salts (e.g., $ROCO_2$-metal, metal alkoxides, and metal alkylcarbonates). According to the Butler-Volmer equation, the mixed electrolyte exhibits a higher exchange current density compared to $ZnSO_4$, implying faster deposition kinetics for the mixed electrolyte (Fig. 10h). Furthermore, to quantify the de-solvation barrier for transport kinetics of Zn^{2+} ions, the activation energy (E_a) using Nyquist plot and Arrhenius equation demonstrated the optimal kinetic behavior for Zn^{2+} de-solvation and facilitated fast ion transport for the mixed salts. Besides, the transference numbers have been calculated by related formula (see Fig. 10i and Section 2.1), further proving the synergetic effect of mixed electrolytes. Fig. 10j proves that the mixed electrolytes can effectively suppress side reactions and dendrite growth, increasing the CE and cyclability of Zn redox reactions. Additionally, the hydrophobic or hydrophilic nature of the anion leads to two inherently different intermolecular interaction scenarios, thereby directly affecting the solvation structures of cations and hydrogen bond networks [206]. The hydrophobic anions (e.g., $TFSI^-$, ClO_4^- and $CF_3SO_3^-$) hardly interact with water and drive the water molecules to the surrounding cations, which are generally much more hydrophilic. On the other hand, the hydrophilic anions (e.g., CH_3COO^-, Cl^- and NO_3^-)

Table 2
The advantages and disadvantages of various electrolyte anions.

Anion type	Merits	Drawbacks	Ref.
SO_4^{2-}	Low cost, good electrode compatibility, wide window (>2.3 V vs. Zn^{2+}/Zn), high CE in both conversion and insertion-type materials, easy to coordinate with cations (high ESP distribution)	By-products	[211, 215, 216]
BF_4^-	low hydration energy, high ionic conductivity (saturated), Solubility	narrow working window, low CE	[212, 215]
F^-	Low cost, weak oxidative anion, Metal-F-rich SEI layer	Low solubility	[206]
Cl^-	Low cost, weak oxidative anion, easily change solvation shell (hydrophilic)	Thicken metal deposits, narrow window (<0.7 V vs. Zn^{2+}/Zn)	[206, 213]
NO_3^-	Low cost, easily change solvation shell (hydrophilic and high ESP)	Corrosion, oxidative ability, narrow window (<1.25 V vs. Zn^{2+}/Zn)	[206, 211]
ClO_4^-	Low reaction activity	Hardly change the H_2O-H_2O HB bonds	[206]
PF_6^-	large steric structure, thick metal deposition but no dendrite	Air-unstable, solubility	[213]
$CF_3SO_3^-$	Reduced metal-H_2O complexes, weak solvation effect, fast ion mobility, reversibility, wide window, easy to coordinate with cations (mildly hydrophobic but high ESP distribution)	High cost	[211, 212, 216]
CH_3COO^-	Biocompatibility, cheap	Weak alkaline	[50]
$TFSI^-$	wide working window, large steric structure, weaken solvation, Working window, dendrite, fast ion mobility	High cost	[212, 213]
DCA^-	High complexing ability	Dendrite, void	[213]

can compete with cations in interacting with water. For SO_4^{2-}, NO_3^-, and $CF_3SO_3^-$, the sites near the O atoms have the most negative electrostatic potential (ESP), indicating that the hydrogen atoms in water molecules is more likely to bind anions [211]. Table 2 presents a summary of different anions in electrolyte salts, categorizing them based on their ESP, polarity, charge density, and molecular size. This summary also includes each anion's characteristics, functions, and potential drawbacks, providing a comprehensive overview of how these factors influence their performance in electrolyte solutions. Li et al. used five electrolyte salt to perfect the performance of ZIBs and Zn-I_2 system, as given in Fig. 10k. It displayed that 1000-cycles capacity retentions and cycling stability of V_2O_5 in $Zn(OTf)_2$ was better than those in $Zn(ClO_4)_2$, and $Zn(BF_4)_2$ electrolytes. The phenomena can follow the rule of molecular orbitals in Fig. 10l. The $ZnSO_4$ has a higher HOMO energy level than $ZnSiF_6$ and $Zn(BF_4)_2$, which reflects that the anion of $ZnSO_4$ is a better electron donor. Due to the lowest LUMO energy level of I_2, the irreversible shuttling effect of Zn-I_2 batteries can be suppressed by the strong coordination reaction between SO_4^{2-} anion and active materials. The results align with the electronic theory of Lewis acids and bases, which can be used as a judgment method (Fig. 10m). In Fig. 10n, different electrolyte salts in AIBs can change the discharge peak in Al $(TFSI)_3$, which is larger than the other two electrolytes by 0.1 V, showing the faster Al^{3+} migration.

4.4. pH management

Additives in the charge-discharge process can stabilize pH variations, reducing side reactions and by-product formation. The Pourbaix diagram (Fig. 11a) and a modified Nernst equation illustrate how the reaction potential as a function of pH determines the stable working window of pure water [217]. The low stability line (red dashed line) and high stability line (blue dashed line) represent the standard redox potentials of HER and OER versus the SHE. At acidic solution, the E_{HER} and E_{OER} are located at 0 V and 1.23 V, respectively, which is working window of pure water. As the pH increases, both E_{HER} and E_{OER} experience a decrease in reaction overpotentials. It's notable that the overpotentials for O_2 and H_2 evolution at high pH are significantly lower than those at low pH. In essence, water undergoes redox reactions more readily in alkaline solutions compared to acidic solutions. Consequently, the downward shift of the redox potential of water restricts the redox reactions of both the anode and cathode. However, during the cycling process, the side reaction and by-product formation will lead to the uneven distribution and polarization of pH near the electrode surface. This is why we need to concern about the change and distribution of pH during the cycling test.

$$E_{HER} = E^{\theta}_{H2/H2O} + 2.303\frac{RT}{F}(14 - pH)$$

$$E_{OER} = E^{\theta}_{H2O/O2} - 2.303\frac{RT}{F}pH$$

In order to explore the potential factors contributing to the formation of ZHS, a compound sensitive to the pH levels of aqueous electrolytes in ZIBs, Lee et al. conducted an experiment. Their objective was to examine how the pH value of the solution influences the formation of ZHS. As the pH level of the solution was raised to 5.47, it resulted in the formation and dispersion of this by-product of salts within the electrolyte [218]. The inclusion of a pH buffer additive becomes imperative to stabilize pH fluctuations and mitigate the formation of undesirable by-products. However, it is essential to acknowledge that a single additive may offer limited protection to aqueous batteries. Consequently, there is a pressing need to develop multifunctional additives capable of providing comprehensive protection to the entire battery system. As depicted in Fig. 11b, the introduction of a non-metal cation (NH_4^+) can induce an electrostatic shield effect. Nonetheless, this may result in pH polarization, triggering side reactions, corrosion of the Zn anode, and most critically, water decomposition. Introducing OAc^- anions can effectively function as a pH buffer, promoting uniformity in pH values across both the electrode surface and bulk solution. However, these anions alone are insufficient to inhibit the formation of zinc dendrites, ultimately limiting the lifespan of aqueous batteries. By adopting a synergy strategy that incorporates both OAc^- anions and NH_4^+ cation, a dual-functional effect can be achieved, potentially enhancing cyclability and overall battery performance. Fig. 11c and 11d illustrate that maintaining stable high charge-discharge plateaus and reversible capacity can significantly enhance the energy density of ZIBs. A comparable multifunctional additive, $NH_4H_2PO_4$, has been reported to facilitate uniform metal deposition and inhibit the formation of ZHS in dilute aqueous electrolytes. This is attributed to its pH buffering and shielding effects [219]. Nevertheless, the redox pairs of pH buffer additives can result in a narrower working window when attempting to mitigate the formation of ZHS [220]. Hence, the introduction of another additive capable of addressing the limitations induced by pH buffers becomes essential for electrode protection. Zhao's research group utilized acetic acid (HAc) and tetramethylene sulfone (TMS) as a buffering agent and stabilizer, respectively, to establish a stable pH environment and stabilize the metal anode in acidic solutions. Acetic acid effectively buffers the pH increase during the discharge process, thus preventing the formation of side products. However, excessively low pH levels in the solution can lead to electrode and component corrosion, resulting in a narrower working window, as depicted by the black line in Fig. 11e (upper). The hybrid acidic electrolyte (red curve) demonstrates significant inhibition of metal corrosion and the HER with a low pH value of 1.6. Additionally, the inclusion of TMS enhances the activation barrier of the OER, resulting in a wider working window in acid-buffered electrolytes, as depicted in Fig. 11e (lower). In addition to ion-typed pH buffers, the use

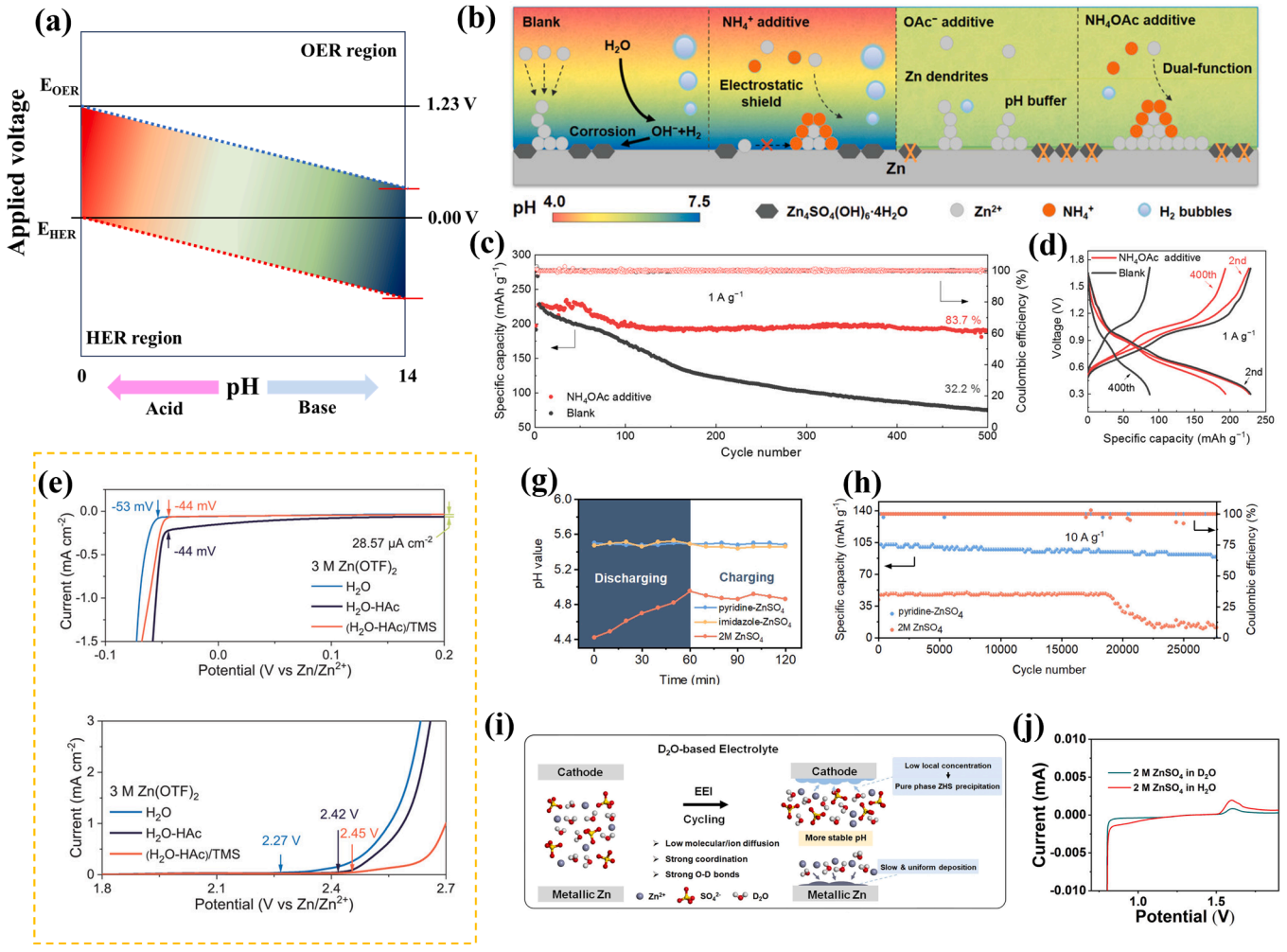

Fig. 11. (a) Pourbaix diagram based on pH variation. (b) Schematic illustration of the reaction and evolution of the Zn surface in different electrolytes with various additives. (c) CV curves and (d) long-term cycling performance of the Zn//Od-NVO full cells in the blank and NH_4OAc-added electrolytes. Reprinted with permission from Ref. [24] Copyright 2022 Wiley-Blackwell. (e) The electrochemical stability window of different aqueous electrolytes was measured using Ti electrodes in the negative (left) and positive voltage range (right), respectively. Reprinted with permission from Ref. [222] Copyright 2022 Wiley-Blackwell. (f) Real-time electrolyte pH near Zn anode during discharge/charge process. (g) Cycling performance in $ZnSO_4$ and pyridine-$ZnSO_4$ at 10 A g^{-1}. Reprinted with permission from Ref. [221] Copyright 2023 Wiley-Blackwell. (h) Schematic diagram illustrating the influence from EEI of D_2O. (i) LSV test of D_2O- and H_2O-based electrolytes in the range of 0.8–1.9 V. Reprinted with permission from Ref. [223] Copyright 2023 Wiley-Blackwell.

of organic pH buffers represents a proposed strategy for stabilizing pH variations. Organic additives such as pyridine and imidazole containing N-heterocyclic functional groups effectively regulate electrolyte pH changes (refer to Fig. 11f). The electrolyte pH remains stable during discharge and charge processes with the incorporation of these organic additives, while significant pH fluctuations occur in cycling tests without them. As the concentration of OH^- increases during discharge, hydrogen ions bound with N-heterocyclic pyridine or imidazole are released, thereby alleviating pH fluctuations. Notably, modified electrolytes demonstrate ultra-stable cycling performance in ZIBs under ultra-fast current densities of 10 A g^{-1}, showcasing outstanding energy and power densities (refer to Fig. 11 g). Leveraging multifunctional additives, this approach can simultaneously inhibit metal dendrites and the shuttle of polyiodide compounds [221]. It is worth noting that Gao et al. introduced a novel approach by incorporating deuterium oxide (D_2O) into the electrolyte, capitalizing on its slower diffusion in the solution and on the Zn anode surface (refer to Fig. 11h). Through strong coordination and O-D bond formation, this method effectively eliminates multiple ZHS phases and modifies the solvation structure of metal ions. Consequently, it leads to a more stable pH, uniform metal deposition, formation of a pure ZHS phase, and reduced gas generation. As illustrated in Fig. 11i, the reduction potential of the electrolyte can be extended towards 0.8 V in D_2O, which is greater than that in H_2O (only ~1.1 V). This extension may lead to a wider working window and higher energy density in aqueous batteries.

5. *Summery and outlook*

Aqueous multivalent metal-ion batteries stand out for their abundant resources, cost-effectiveness, good cyclability, eco-friendly, and high safety. However, critical challenges remain. This review introduces the central theme of electrolyte design, focusing on extending the limits of aqueous batteries in the Ragone plot, addressing key issues like working window, cation transport, and side reactions. It emphasizes managing metal deposition uniformity, SEI/CEI layers, and hydrogen bond regulation, where we summarize various methods for optimizing different types of aqueous batteries.

With the help of versatile strategies, not only are side reactions in aqueous batteries mitigated, but improvements are also seen in ion conductivity, dielectric constant, transference number, and solvation structure. The working principle of each strategy and transport mechanism of electrolytes are thoroughly discussed. Although the

electrochemical performances of multivalent metal-ion batteries can be enhanced via electrolyte design engineering, including salt concentration, pH buffer, additives, hybrid solvents, and hybrid solutes, have been achieved in reported literatures, more efforts prone to promote further progress in both academic and industry applications. On the condition of cost effectiveness and biocompatibility, the review navigates future research directions in electrolyte engineering of aqueous batteries.

5.1. Exploring a quantitatively multifunctional regulator

We prefer using nontoxic, eco-friendly additives or solutions to boost aqueous battery performance. Consequently, a cost-effective and simplified electrolyte production process is favored over multi-step manufacturing. Recent literatures typically address the shortcomings of aqueous batteries by simultaneously adding additives, solvents, and using multiple strategies. A “All-functions-in-one” solvent, solute, and organic molecule, which can simultaneously impact on the energy density and power density, is promising pathway to design electrolytes. In addition to facile process and cost advantages, introduction of one multifunctional agent can easily ensure its recycling procedures and environmental protection. Constantly looking for new organic agents (less than 2 wt.%) and cheap solvents (10 %~50 % content) are important for maximizing efficiency with minimal quantities.

5.2. Designing a high polarity and steric effect of molecule

Organic molecules with low binding and dissociation energies are promising regulators, which usually equipped with high-polarity and large-steric effect such as heterocyclic aromatics. Heterocyclic aromatics (e.g., pyridine [174], furan [224]) or aliphatic heterocyclics (e.g., dioxane [225]) have at least two different elements as a member of its ring. Therefore, other heterocyclic aromatics (e.g., bipyridine, benzofuran, thiophene, carbazole, etc.) and aliphatic heterocyclics (e.g., pyrrolidine, thietane, azetidine, and ethylene oxide, etc.) can be used directly or organically synthesized, which can effectively adhere to the metal surface and coordinate with metal ions to inhibit the corrosion and rapid-reaction-induced uneven deposition.

5.3. Regulating LUMO/HOMO energy level of additives

Most additives can only widen one side of molecular orbital, failing to stabilize SEI film of both cathode and anode and significantly widen the redox potential of water. Simultaneously boosting LUMO (reduction side) and HOMO (oxidation side) can significantly promote the working window, further widening the energy density of aqueous battery. For instance, the structures with the lowest HOMO–LUMO gaps and bifunctional groups (i.e., electron donor and acceptor functional groups) can effectively alter the molecular orbitals, which depends on their number of donor and acceptor functional groups. The electron-donor character is mainly formed by sulfur, nitrogen, and thiol groups, whereas the electron-withdrawing character is predominantly determined through nitro and carbonyl groups assisted by amino and hydroxyl groups [226]. According to molecular orbital theory, the narrow bandgap between the LUMO and HOMO energy levels represents the favorable ability for electron transfer, which will enhance the adsorption of solvent molecules on the metal anode. By changing the energy levels of molecular orbitals and bandgap, the composition of the passivation layer can be effectively adjusted to customize each aqueous battery.

5.4. Eliminating the trade-off between mechanical strength and ionic conductivity

Aqueous batteries hold promise for broader applications such as bendable watches, mobile phones, and portable power supplies. They have the potential to replace memory-effect batteries (such as nickel-cadmium or nickel-metal hydride) and costly lithium-based batteries

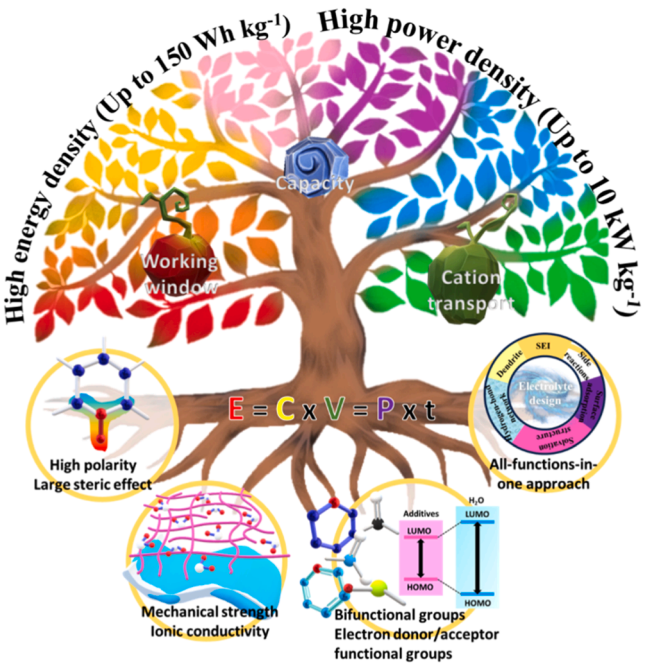

Fig. 12. The schematic illustration of the future research and relationships on electrolyte design for high energy and power density.

(such as lithium-ion or lithium-polymer). The key factors for aqueous batteries in these uses are electrolyte mechanical strength and ion conductivity. Although the water can be distorted in a flexible cell, potential electrolyte leakage will degrade cycling performance. Thus, mechanical strength is crucial in flexibility engineering. Considering the low price of water and some polymers water and some polymers, we suggest that sol-gel matrix derived by organic acid and alcohol is one path to fabricate the polymerized gel with optimal water content, depending on polymerization time, evaporation time, and acid/base catalysis [227]. This "wet gel" electrolyte, coupled with strategic design, can offer both high ionic conductivity and mechanical strength (Fig. 12).

Data availability

No data was used for the research described in the article.

CRediT authorship contribution statement

Yi-Yen Hsieh: Writing – original draft, Investigation, Resources, Writing – review & editing. **Hsing-Yu Tuan:** Supervision, Writing – review & editing.

Declaration of competing interest

The authors declare that they have no known competing financial interests or personal relationships that could have appeared to influence the work reported in this paper.

Acknowledgements

This work was supported by the financial support from the 2030 Cross Generation Young Scholars Program by National Science and Technology Council, Taiwan (NSTC 112-2628-E-007-010 & NSTC 112-2628-E-007-016).

References

[1] F. Zhang, W. Zhang, D. Wexler, Z. Guo, Recent progress and future advances on aqueous monovalent-ion batteries towards safe and high-power energy storage, Adv. Mater. 34 (2022) 2107965.
[2] N. LePan, All the World's Metals and Minerals in One Visualization, Visual Capitalist; Visual Capitalist, Vancouver, WA, USA, 2020.
[3] M. Zhou, Y. Chen, G. Fang, S. Liang, Electrolyte/electrode interfacial electrochemical behaviors and optimization strategies in aqueous zinc-ion batteries, Energy Stor. Mater. 45 (2022) 618–646.
[4] T. Liu, X. Cheng, H. Yu, H. Zhu, N. Peng, R. Zheng, J. Zhang, M. Shui, Y. Cui, J. Shu, An overview and future perspectives of aqueous rechargeable polyvalent ion batteries, Energy Stor. Mater. 18 (2019) 68–91.
[5] Y. Geng, L. Pan, Z. Peng, Z. Sun, H. Lin, C. Mao, L. Wang, L. Dai, H. Liu, K. Pan, Electrolyte additive engineering for aqueous Zn ion batteries, Energy Stor. Mater. (2022).
[6] X. Wang, Z. Zhang, B. Xi, W. Chen, Y. Jia, J. Feng, S. Xiong, Advances and perspectives of cathode storage chemistry in aqueous zinc-ion batteries, ACS Nano 15 (2021) 9244–9272.
[7] J. Xu, Y. Liu, C. Xu, J. Li, Z. Yang, H. Yan, H. Yu, L. Yan, L. Zhang, J. Shu, Aqueous non-metallic ion batteries: Materials, mechanisms and design strategies, Coord. Chem. Rev. 474 (2023) 214867.
[8] G. Li, L. Sun, S. Zhang, C. Zhang, H. Jin, K. Davey, G. Liang, S. Liu, J. Mao, Z. Guo, Developing Cathode Materials for Aqueous Zinc Ion Batteries: Challenges and Practical Prospects, Adv. Funct. Mater. (2023) 2301291.
[9] Z. Wang, C. Wei, H. Jiang, Y. Zhang, K. Tian, Y. Li, X. Zhang, S. Xiong, C. Zhang, J. Feng, MXene-based current collectors for advanced rechargeable batteries, Adv. Mater. (2023) 2306015.
[10] J.B. Goodenough, Y. Kim, Challenges for rechargeable Li batteries, Chem. Mater. 22 (2010) 587–603.
[11] W. Manalastas Jr, S. Kumar, V. Verma, L. Zhang, D. Yuan, M. Srinivasan, Water in rechargeable multivalent-ion batteries: an electrochemical Pandora's box, ChemSusChem 12 (2019) 379–396.
[12] E. Nightingale Jr, Phenomenological theory of ion solvation. Effective radii of hydrated ions, J. Phys. Chem. 63 (1959) 1381–1387.
[13] H.G. Buss, S.Y. Chan, N.A. Lynd, B.D. McCloskey, Nonaqueous polyelectrolyte solutions as liquid electrolytes with high lithium ion transference number and conductivity, ACS Energy Lett. 2 (2017) 481–487.
[14] N. Gavish, K. Promislow, Dependence of the dielectric constant of electrolyte solutions on ionic concentration: A microfield approach, Phys. Rev. E 94 (2016) 012611.
[15] A.-K. Kontturi, K. Kontturi, L. Murtomäki, D.J. Schiffrin, Effect of preferential solvation on Gibbs energies of ionic transfer, J. Chem. Soc., Faraday Trans. 90 (1994) 2037–2041.
[16] J.Y. Kim, D.O. Shin, T. Chang, K.M. Kim, J. Jeong, J. Park, Y.M. Lee, K.Y. Cho, C. Phatak, S. Hong, Effect of the dielectric constant of a liquid electrolyte on lithium metal anodes, Electrochim. Acta 300 (2019) 299–305.
[17] T.S.R.T. Naiwi, M.M. Aung, M. Rayung, A. Ahmad, K.L. Chai, M.L.W. Fui, E.Z. M. Tarmizi, N.A.A. Aziz, Dielectric and ionic transport properties of bio-based polyurethane acrylate solid polymer electrolyte for application in electrochemical devices, Polym. Test. 106 (2022) 107459.
[18] L. Ye, Z. Feng, Polymer electrolytes as solid solvents and their applications, Polym. Electrol. (2010) 550–582. Elsevier.
[19] D. Xie, Y. Sang, D.H. Wang, W.Y. Diao, F.Y. Tao, C. Liu, J.W. Wang, H.Z. Sun, J. P. Zhang, X.L. Wu, ZnF_2-Riched Inorganic/Organic hybrid SEI: in situ-chemical construction and performance-improving mechanism for aqueous zinc-ion batteries, Angew. Chem. Int. Ed. 62 (2023) e202216934.
[20] G. Liang, F. Mo, X. Ji, C. Zhi, Non-metallic charge carriers for aqueous batteries, Nat. Rev. Mater. 6 (2021) 109–123.
[21] F. Yue, Z. Tie, S. Deng, S. Wang, M. Yang, Z. Niu, An ultralow temperature aqueous battery with proton chemistry, Angew. Chem. Int. Ed. 60 (2021) 13882–13886.
[22] Z. Liang, Y.-C. Lu, Critical role of redox mediator in suppressing charging instabilities of lithium–oxygen batteries, J. Am. Chem. Soc. 138 (2016) 7574–7583.
[23] T. Liu, H. Wu, X. Du, J. Wang, Z. Chen, H. Wang, J. Sun, J. Zhang, J. Niu, L. Yao, Water-locked eutectic electrolyte enables long-cycling aqueous sodium-ion batteries, ACS Appl. Mater. Interfaces 14 (2022) 33041–33051.
[24] D. Han, Z. Wang, H. Lu, H. Li, C. Cui, Z. Zhang, R. Sun, C. Geng, Q. Liang, X. Guo, A self-regulated interface toward highly reversible aqueous zinc batteries, Adv. Energy Mater. 12 (2022) 2102982.
[25] V. Soundharrajan, B. Sambandam, S. Kim, S. Islam, J. Jo, S. Kim, V. Mathew, Y.-k. Sun, J. Kim, The dominant role of Mn2+ additive on the electrochemical reaction in ZnMn2O4 cathode for aqueous zinc-ion batteries, Energy Stor. Mater. 28 (2020) 407–417.
[26] Y. Dong, L. Miao, G. Ma, S. Di, Y. Wang, L. Wang, J. Xu, N. Zhang, Non-concentrated aqueous electrolytes with organic solvent additives for stable zinc batteries, Chem. Sci. 12 (2021) 5843–5852.
[27] D. Kang, M. Xiao, J.P. Lemmon, Artificial solid-electrolyte interphase for lithium metal batteries, Batteries Supercaps 4 (2021) 445–455.
[28] Y. Chu, L. Ren, Z. Hu, C. Huang, J. Luo, An in-depth understanding of improvement strategies and corresponding characterizations towards Zn anode in aqueous Zn-ions batteries, Green Energy Environ. (2022).
[29] W. Li, P. Luo, M. Chen, X. Lin, L. Du, H. Song, Y. Lu, Z. Cui, Hedging Li dendrite formation by virtue of controllable tip effect, J. Mater. Chem. A 10 (2022) 15161–15168.
[30] J. Li, S. Zhou, Y. Chen, X. Meng, A. Azizi, Q. He, H. Li, L. Chen, C. Han, A. Pan, Self-smoothing deposition behavior enabled by beneficial potential compensating for highly reversible Zn-metal anodes, Adv. Funct. Mater. (2023) 2307201.
[31] X. Zeng, J. Mao, J. Hao, J. Liu, S. Liu, Z. Wang, Y. Wang, S. Zhang, T. Zheng, J. Liu, Electrolyte design for in situ construction of highly Zn2+-conductive solid electrolyte interphase to enable high-performance aqueous Zn-ion batteries under practical conditions, Adv. Mater. 33 (2021) 2007416.
[32] S. Wu, Z. Hu, P. He, L. Ren, J. Huang, J. Luo, Crystallographic engineering of Zn anodes for aqueous batteries, eScience (2023) 100120.
[33] D. Li, L. Cao, T. Deng, S. Liu, C. Wang, Design of a solid electrolyte interphase for aqueous Zn batteries, Angew. Chem. Int. Ed. 60 (2021) 13035–13041.
[34] L. Cao, D. Li, T. Pollard, T. Deng, B. Zhang, C. Yang, L. Chen, J. Vatamanu, E. Hu, M.J. Hourwitz, Fluorinated interphase enables reversible aqueous zinc battery chemistries, Nat. Nanotechnol. 16 (2021) 902–910.
[35] W. Zhang, G. He, Solid-electrolyte interphase chemistries towards high-performance aqueous zinc metal batteries, Angew. Chem. Int. Ed. 62 (2023) e202218466.
[36] S. Di, X. Nie, G. Ma, W. Yuan, Y. Wang, Y. Liu, S. Shen, N. Zhang, Zinc anode stabilized by an organic-inorganic hybrid solid electrolyte interphase, Energy Stor. Mater. 43 (2021) 375–382.
[37] Y. Li, Z. Yu, J. Huang, Y. Wang, Y. Xia, Constructing solid electrolyte interphase for aqueous zinc batteries, Angew. Chem. (2023) e202309957.
[38] H. Qiu, X. Du, J. Zhao, Y. Wang, J. Ju, Z. Chen, Z. Hu, D. Yan, X. Zhou, G. Cui, Zinc anode-compatible in-situ solid electrolyte interphase via cation solvation modulation, Nat. Commun. 10 (2019) 5374.
[39] S. Di, L. Miao, Y. Wang, G. Ma, Y. Wang, W. Yuan, K. Qiu, X. Nie, N. Zhang, Dual-anion-coordinated solvation sheath for stable aqueous zinc batteries, J. Power Sources 535 (2022) 231452.
[40] L. Geng, J. Meng, X. Wang, C. Han, K. Han, Z. Xiao, M. Huang, P. Xu, L. Zhang, L. Zhou, Eutectic electrolyte with unique solvation structure for high-performance zinc-ion batteries, Angew. Chem. Int. Ed. 61 (2022) e202206717.
[41] X. Shen, R. Zhang, X. Chen, X.B. Cheng, X. Li, Q. Zhang, The failure of solid electrolyte interphase on Li metal anode: structural uniformity or mechanical strength? Adv. Energy Mater. 10 (2020) 1903645.
[42] L. Suo, D. Oh, Y. Lin, Z. Zhuo, O. Borodin, T. Gao, F. Wang, A. Kushima, Z. Wang, H.-C. Kim, How solid-electrolyte interphase forms in aqueous electrolytes, J. Am. Chem. Soc. 139 (2017) 18670–18680.
[43] K. Wang, T. Qiu, L. Lin, X.-X. Liu, X. Sun, A low fraction electrolyte additive as interface stabilizer for Zn electrode in aqueous batteries, Energy Stor. Mater. 54 (2023) 366–373.
[44] Y. Sui, X. Ji, Electrolyte interphases in aqueous batteries, Angew. Chem. Int. Ed. (2023) e202312585.
[45] E. Peled, S. Menkin, SEI: past, present and future, J. Electrochem. Soc. 164 (2017) A1703.
[46] H. Li, Z. Chen, L. Zheng, J. Wang, H. Adenusi, S. Passerini, H. Zhang, Electrolyte strategies facilitating anion-derived solid-electrolyte interphases for aqueous zinc–metal batteries, Small Methods (2023) 2300554.
[47] W. Chen, S. Guo, L. Qin, L. Li, X. Cao, J. Zhou, Z. Luo, G. Fang, S. Liang, Hydrogen bond-functionalized massive solvation modules stabilizing bilateral interfaces, Adv. Funct. Mater. 32 (2022) 2112609.
[48] T. Hu, Z. Ye, Y. Wang, X. Gao, Z. Sun, J. Li, S. Chen, C. Lian, Q. Xu, F. Li, Synergistic effect of h-bond reconstruction and interface regulation for high-voltage aqueous energy storage, Adv. Energy Mater. (2023) 2300567.
[49] H. Bi, X. Wang, H. Liu, Y. He, W. Wang, W. Deng, X. Ma, Y. Wang, W. Rao, Y. Chai, A universal approach to aqueous energy storage via ultralow-cost electrolyte with super-concentrated sugar as hydrogen-bond-regulated solute, Adv. Mater. 32 (2020) 2000074.
[50] C. You, R. Wu, X. Yuan, L. Liu, J. Ye, L. Fu, P. Han, Y. Wu, An inexpensive electrolyte with double-site hydrogen bonding and a regulated Zn^{2+} solvation structure for aqueous Zn-ion batteries capable of high-rate and ultra-long low-temperature operation, Energy Environ. Sci. 16 (2023) 5096–5107.
[51] A.S. Lakhnot, R.A. Panchal, J. Datta, V. Mahajani, K. Bhimani, R. Jain, D. Datta, N. Koratkar, Intercalation Hosts for Multivalent-Ion Batteries, Small Struct. 4 (2023) 2200290.
[52] J. Huang, Z. Guo, Y. Ma, D. Bin, Y. Wang, Y. Xia, Recent progress of rechargeable batteries using mild aqueous electrolytes, Small Methods 3 (2019) 1800272.
[53] M. Rashad, M. Asif, Y. Wang, Z. He, I. Ahmed, Recent advances in electrolytes and cathode materials for magnesium and hybrid-ion batteries, Energy Stor. Mater. 25 (2020) 342–375.
[54] S. Gheytani, Y. Liang, F. Wu, Y. Jing, H. Dong, K.K. Rao, X. Chi, F. Fang, Y. Yao, An aqueous Ca-ion battery, Adv. Sci. 4 (2017) 1700465.
[55] L. Yan, W. Yang, H. Yu, L. Zhang, J. Shu, Recent progress in rechargeable calcium-ion batteries for high-efficiency energy storage, Energy Stor. Mater. (2023) 102822.
[56] M. Mao, T. Gao, S. Hou, C. Wang, A critical review of cathodes for rechargeable Mg batteries, Chem. Soc. Rev. 47 (2018) 8804–8841.
[57] Q. Fu, X. Wu, X. Luo, S. Indris, A. Sarapulova, M. Bauer, Z. Wang, M. Knapp, H. Ehrenberg, Y. Wei, High-voltage aqueous Mg-ion batteries enabled by solvation structure reorganization, Adv. Funct. Mater. 32 (2022) 2110674.
[58] R. Tao, C. Gao, E. Xie, B. Wang, B. Lu, A stable and high-energy aqueous aluminum based battery, Chem. Sci. 13 (2022) 10066–10073.
[59] R. Tao, H. Fu, C. Gao, L. Fan, E. Xie, W. Lyu, J. Zhou, B. Lu, Tailoring interface to boost the high-performance aqueous Al ion batteries, Adv. Funct. Mater. 33 (2023) 2303072.
[60] Y. Liang, H. Dong, D. Aurbach, Y. Yao, Current status and future directions of multivalent metal-ion batteries, Nat. Energy 5 (2020) 646–656.

[61] A. Khairudin, S. Suhaimi, N.A. Mohd Taib, M.I.N. Mohamad Isa, W.Z. Wan Ismail, A review study of binary and ternary ZnO/C composites as anodes for high-capacity lithium-ion batteries, Ionics 29 (2023) 4939–4969.
[62] V.V. Obreja, Supercapacitors specialities-Materials review, in: AIP Conference Proceedings, American Institute of Physics, 2014, pp. 98–120.
[63] A. Manthiram, An outlook on lithium ion battery technology, ACS Central Sci. 3 (2017) 1063–1069.
[64] Y. Zhu, X. Guo, Y. Lei, W. Wang, A.-H. Emwas, Y. Yuan, Y. He, H.N. Alshareef, Hydrated eutectic electrolytes for high-performance Mg-ion batteries, Energy Environ. Sci. 15 (2022) 1282–1292.
[65] K.W. Leong, W. Pan, Y. Wang, S. Luo, X. Zhao, D.Y. Leung, Reversibility of a high-voltage, Cl^--regulated, aqueous Mg metal battery enabled by a water-in-salt electrolyte, ACS Energy Lett. 7 (2022) 2657–2666.
[66] Y. Xu, Z. Liu, X. Zheng, K. Li, M. Wang, W. Yu, H. Hu, W. Chen, Solid electrolyte interface regulated by solvent-in-water electrolyte enables high-voltage and stable aqueous Mg-MnO2 batteries, Adv. Energy Mater. 12 (2022) 2103352.
[67] X. Wang, X. Zhang, G. Zhao, H. Hong, Z. Tang, X. Xu, H. Li, C. Zhi, C. Han, Ether–water hybrid electrolyte contributing to excellent Mg ion storage in layered sodium vanadate, ACS Nano 16 (2022) 6093–6102.
[68] S. Zhang, C. Zhao, K. Zhu, J. Zhao, Y. Gao, K. Ye, J. Yan, G. Wang, D. Cao, An environment-friendly high-performance aqueous Mg-Na hybrid-ion battery using an organic polymer anode, Energy Environ. Mater. 6 (2023) e12388.
[69] M. Huang, X. Wang, J. Wang, J. Meng, X. Liu, Q. He, L. Geng, Q. An, J. Yang, L. Mai, Proton/Mg^{2+} Co-insertion chemistry in aqueous Mg-Ion batteries: from the interface to the inner, Angew. Chem. 135 (2023) e202308961.
[70] M. Karlsmo, R. Bouchal, P. Johansson, High-performant all-organic aqueous sodium-ion batteries enabled by PTCDA electrodes and a hybrid Na/Mg electrolyte, Angew. Chem. Int. Ed. 60 (2021) 24709–24715.
[71] L. Han, J. Li, X. Zhang, H. Huang, Z. Yang, G. Zhu, M. Xu, L. Pan, Low-crystalline akhtenskite MnO2-based aqueous magnesium-ion hybrid supercapacitors with a superior energy density boosted by redox bromide-ion additive electrolytes, ACS Sustain. Chem. Eng. 9 (2021) 9165–9176.
[72] F. Wang, X. Fan, T. Gao, W. Sun, Z. Ma, C. Yang, F. Han, K. Xu, C. Wang, High-voltage aqueous magnesium ion batteries, ACS Central Sci. 3 (2017) 1121–1128.
[73] X. Sun, V. Duffort, B.L. Mehdi, N.D. Browning, L.F. Nazar, Investigation of the mechanism of Mg insertion in birnessite in nonaqueous and aqueous rechargeable Mg-ion batteries, Chem. Mater. 28 (2016) 534–542.
[74] Z. Zhao, J. Lai, D.T. Ho, Y. Lei, J. Yin, L. Chen, U. Schwingenschlögl, H. N. Alshareef, A novel "water-in-ionic liquid" electrolyte for Zn metal batteries, ACS Energy Lett. 8 (2022) 608–618.
[75] M. Han, J. Huang, X. Xie, T.C. Li, J. Huang, S. Liang, J. Zhou, H.J. Fan, Hydrated eutectic electrolyte with ligand-oriented solvation shell to boost the stability of zinc battery, Adv. Funct. Mater. 32 (2022) 2110957.
[76] J. Shi, T. Sun, J. Bao, S. Zheng, H. Du, L. Li, X. Yuan, T. Ma, Z. Tao, Water-in-deep eutectic solvent" electrolytes for high-performance aqueous Zn-Ion Batteries, Adv. Funct. Mater. 31 (2021) 2102035.
[77] T.A. Nigatu, H.K. Bezabh, B.W. Taklu, B.W. Olbasa, Y.-T. Weng, S.-H. Wu, W.-N. Su, C.-C. Yang, B.J. Hwang, Synergetic effect of water-in-bisalt electrolyte and hydrogen-bond rich additive improving the performance of aqueous batteries, J. Power Sources 511 (2021) 230413.
[78] D.E. Ciurduc, C. de la Cruz, N. Patil, A. Mavrandonakis, R. Marcilla, An improved PEG-based molecular crowding electrolyte using $Zn(TFSI)_2$ vs. $Zn(OTf)_2$ for aqueous Zn//V_2O_5 battery, Mater. Today Energy (2023) 101339.
[79] H. Liu, Z. Xin, B. Cao, Z. Xu, B. Xu, Q. Zhu, J.L. Yang, B. Zhang, H.J. Fan, Polyhydroxylated organic molecular additives for durable aqueous zinc battery, Adv. Funct. Mater. (2023) 2309840.
[80] J. Yin, H. Liu, P. Li, X. Feng, M. Wang, C. Huang, M. Li, Y. Su, B. Xiao, Y. Cheng, Integrated electrolyte regulation strategy: Trace trifunctional tranexamic acid additive for highly reversible Zn metal anode and stable aqueous zinc ion battery, Energy Stor. Mater. 59 (2023) 102800.
[81] R. Chen, C. Zhang, J. Li, Z. Du, F. Guo, W. Zhang, Y. Dai, W. Zong, X. Gao, J. Zhu, A hydrated deep eutectic electrolyte with finely-tuned solvation chemistry for high-performance zinc-ion batteries, Energy Environ. Sci. 16 (2023) 2540–2549.
[82] S. Huang, S. He, Y. Li, S. Wang, X. Hou, Hydrogen bond acceptor lined hydrogel electrolyte toward Dendrite-Free aqueous Zn ion batteries with low temperature adaptability, Chem. Eng. J. 464 (2023) 142607.
[83] Z. Li, Y. Liao, Y. Wang, J. Cong, H. Ji, Z. Huang, Y. Huang, A co-solvent in aqueous electrolyte towards ultralong-life rechargeable zinc-ion batteries, Energy Stor. Mater. 56 (2023) 174–182.
[84] Y. Quan, M. Yang, M. Chen, W. Zhou, X. Han, J. Chen, B. Liu, S. Shi, P. Zhang, Electrolyte additive of sorbitol rendering aqueous zinc-ion batteries with dendrite-free behavior and good anti-freezing ability, Chem. Eng. J. 458 (2023) 141392.
[85] H. Du, K. Wang, T. Sun, J. Shi, X. Zhou, W. Cai, Z. Tao, Improving zinc anode reversibility by hydrogen bond in hybrid aqueous electrolyte, Chem. Eng. J. 427 (2022) 131705.
[86] Z. Zha, T. Sun, D. Li, T. Ma, W. Zhang, Z. Tao, Zwitterion as electrical double layer regulator to in-situ formation of fluorinated interphase towards stable zinc anode, Energy Stor. Mater. (2023) 103059.
[87] S. Tian, T. Hwang, S. Malakpour Estalaki, Y. Tian, L. Zhou, T. Milazzo, S. Moon, S. Wu, R. Jian, K. Balkus Jr, A low-cost quasi-solid-state "Water-in-Swelling-Clay" electrolyte enabling ultrastable aqueous zinc-ion batteries, Adv. Energy Mater. (2023) 2300782.
[88] K. Ouyang, S. Chen, W. Ling, M. Cui, Q. Ma, K. Zhang, P. Zhang, Y. Huang, Synergistic modulation of in-situ hybrid interface construction and ph buffering enabled ultra-stable zinc anode at high current density and areal capacity, Angew. Chem. 135 (2023) e202311988.
[89] G. Duan, Y. Wang, B. Luo, L. Sun, S. Zheng, J. Huang, Z. Ye, Taurine-mediated dynamic bridging strategy for highly stable Zn metal anode, Energy Stor. Mater. 61 (2023) 102882.
[90] S. He, J. Wang, X. Zhang, J. Chen, Z. Wang, T. Yang, Z. Liu, Y. Liang, B. Wang, S. Liu, A high-energy aqueous aluminum-manganese battery, Adv. Funct. Mater. 29 (2019) 1905228.
[91] W. Pan, Y. Wang, Y. Zhang, H.Y.H. Kwok, M. Wu, X. Zhao, D.Y. Leung, A low-cost and dendrite-free rechargeable aluminium-ion battery with superior performance, J. Mater. Chem. A 7 (2019) 17420–17425.
[92] T. Dong, K.L. Ng, Y. Wang, O. Voznyy, G. Azimi, Solid electrolyte interphase engineering for aqueous aluminum metal batteries: a critical evaluation, Adv. Energy Mater. 11 (2021) 2100077.
[93] A. Zhou, L. Jiang, J. Yue, Y. Tong, Q. Zhang, Z. Lin, B. Liu, C. Wu, L. Suo, Y.-S. Hu, Water-in-salt electrolyte promotes high-capacity $FeFe(CN)_6$ cathode for aqueous Al-ion battery, ACS Appl. Mater. Interfaces 11 (2019) 41356–41362.
[94] Z. Tong, R. Lian, R. Yang, T. Kang, J. Feng, D. Shen, Y. Wu, X. Cui, H. Wang, Y. Tang, An aqueous aluminum-ion electrochromic full battery with water-in-salt electrolyte for high-energy density, Energy Stor. Mater. 44 (2022) 497–507.
[95] H. Lahan, S.K. Das, Al^{3+} ion intercalation in MoO_3 for aqueous aluminum-ion battery, J. Power Sources 413 (2019) 134–138.
[96] Y. Wang, W. Pan, K.W. Leong, Y. Zhang, X. Zhao, S. Luo, D.Y. Leung, Paper-based aqueous Al ion battery with water-in-salt electrolyte, Green Energy Environ. (2021).
[97] A. Ejigu, L.W. Le Fevre, A. Elgendy, B.F. Spencer, C. Bawn, R.A. Dryfe, Optimization of electrolytes for high-performance aqueous aluminum-ion batteries, ACS Appl. Mater. Interfaces 14 (2022) 25232–25245.
[98] R. Bai, J. Yang, G. Li, J. Luo, W. Tang, Rechargeable aqueous aluminum-FeFe $(CN)_6$ battery with artificial interphase through deep eutectic solution, Energy Stor. Mater. 41 (2021) 41–50.
[99] Z. Hu, Y. Guo, H. Jin, H. Ji, L.-J. Wan, A rechargeable aqueous aluminum–sulfur battery through acid activation in water-in-salt electrolyte, Chem. Commun. 56 (2020) 2023–2026.
[100] Y. Xu, J. Ma, T. Jiang, H. Ding, W. Wang, M. Wang, X. Zheng, J. Sun, Y. Yuan, M. Chuai, Tuning electrolyte solvation structures to enable stable aqueous Al/MnO_2 battery, Energy Stor. Mater. 47 (2022) 113–121.
[101] X. Li, Y. Tang, C. Li, H. Lv, H. Fan, W. Wang, T. Cai, Y. Cui, W. Xing, Z. Yan, Relieving hydrogen evolution and anodic corrosion of aqueous aluminum batteries with hybrid electrolytes, J. Mater. Chem. A 10 (2022) 4739–4748.
[102] C. Lee, S.-K. Jeong, A novel superconcentrated aqueous electrolyte to improve the electrochemical performance of calcium-ion batteries, Chem. Lett. 45 (2016) 1447–1449.
[103] M. Adil, A. Ghosh, S. Mitra, Water-in-salt electrolyte-based extended voltage range, safe, and long-cycle-life aqueous calcium-ion cells, ACS Appl. Mater. Interfaces 14 (2022) 25501–25515.
[104] R. Zhou, Z. Hou, Q. Liu, X. Du, J. Huang, B. Zhang, Unlocking the Reversible Selenium Electrode for Non-Aqueous and Aqueous Calcium-Ion Batteries, Adv. Funct. Mater. 32 (2022) 2200929.
[105] R. Zhou, Z. Hou, K. Fan, C.K. Wun, Q. Liu, T.W.B. Lo, H. Huang, B. Zhang, An advanced organic cathode for non-aqueous and aqueous calcium-based dual ion batteries, J. Power Sources 569 (2023) 232995.
[106] L. Li, G. Zhang, X. Deng, J. Hao, X. Zhao, H. Li, C. Han, B. Li, A covalent organic framework for high-rate aqueous calcium-ion batteries, J. Mater. Chem. A 10 (2022) 20827–20836.
[107] X. Tang, D. Zhou, B. Zhang, S. Wang, P. Li, H. Liu, X. Guo, P. Jaumaux, X. Gao, Y. Fu, A universal strategy towards high–energy aqueous multivalent–ion batteries, Nat. Commun. 12 (2021) 2857.
[108] M. Adil, A. Sarkar, A. Roy, M.R. Panda, A. Nagendra, S. Mitra, Practical aqueous calcium-ion battery full-cells for future stationary storage, ACS Appl. Mater. Interfaces 12 (2020) 11489–11503.
[109] Z. Tong, T. Kang, Y. Wan, R. Yang, Y. Wu, D. Shen, S. Liu, Y. Tang, C.S. Lee, A Ca-ion electrochromic battery via a water-in-salt electrolyte, Adv. Funct. Mater. 31 (2021) 2104639.
[110] F. Qiao, J. Wang, R. Yu, M. Huang, L. Zhang, W. Yang, H. Wang, J. Wu, L. Zhang, Y. Jiang, Aromatic organic small-molecule material with (020) crystal plane activation for wide-temperature and 68000 cycle aqueous calcium-ion batteries, ACS Nano (2023).
[111] T.-C. Liu, S. Sutarsis, X.-Y. Zhong, W.-C. Lin, S.-H. Chou, N. Kirana, P.-Y. Huang, Y.-C. Lo, J.-K. Chang, P.-W. Wu, An interfacial wetting water based hydrogel electrolyte for high-voltage flexible quasi solid-state supercapacitors, Energy Stor. Mater. 38 (2021) 489–498.
[112] Z. Song, H. Duan, D. Zhu, Y. Lv, W. Xiong, T. Cao, L. Li, M. Liu, L. Gan, Ternary-doped carbon electrodes for advanced aqueous solid-state supercapacitors based on a "water-in-salt" gel electrolyte, J. Mater. Chem. A 7 (2019) 15801–15811.
[113] X. Hou, T.P. Pollard, X. He, L. Du, X. Ju, W. Zhao, M. Li, J. Wang, E. Paillard, H. Lin, Water-in-Eutectogel" electrolytes for quasi-solid-state aqueous lithium-ion batteries, Adv. Energy Mater. 12 (2022) 2200401.
[114] X. Li, J. Liang, N. Chen, J. Luo, K.R. Adair, C. Wang, M.N. Banis, T.K. Sham, L. Zhang, S. Zhao, Water-mediated synthesis of a superionic halide solid electrolyte, Angew. Chem. 131 (2019) 16579–16584.
[115] J. Xu, Y. Li, P. Lu, W. Yan, M. Yang, H. Li, L. Chen, F. Wu, Water-stable sulfide solid electrolyte membranes directly applicable in all-solid-state batteries enabled by superhydrophobic Li+-conducting protection layer, Adv. Energy Mater. 12 (2022) 2102348.

[116] X. Peng, H. Liu, Q. Yin, J. Wu, P. Chen, G. Zhang, G. Liu, C. Wu, Y. Xie, A zwitterionic gel electrolyte for efficient solid-state supercapacitors, Nat. Commun. 7 (2016) 11782.
[117] K. Kubota, M. Dahbi, T. Hosaka, S. Kumakura, S. Komaba, Towards K-ion and Na-ion batteries as "beyond Li-ion, Chem. Record 18 (2018) 459–479.
[118] A. Balducci, Ionic liquids in lithium-ion batteries, Ion. Liquids II (2018) 1–27.
[119] K.R. Seddon, A. Stark, M.-J. Torres, Influence of chloride, water, and organic solvents on the physical properties of ionic liquids, Pure Appl. Chem. 72 (2000) 2275–2287.
[120] M. Ishikawa, T. Sugimoto, M. Kikuta, E. Ishiko, M. Kono, Pure ionic liquid electrolytes compatible with a graphitized carbon negative electrode in rechargeable lithium-ion batteries, J. Power Sources 162 (2006) 658–662.
[121] A.P. Abbott, J.C. Barron, K.S. Ryder, D. Wilson, Eutectic-based ionic liquids with metal-containing anions and cations, Chem.–A Eur. J. 13 (2007) 6495–6501.
[122] H. Wang, L. Sheng, G. Yasin, L. Wang, H. Xu, X. He, Reviewing the current status and development of polymer electrolytes for solid-state lithium batteries, Energy Stor. Mater. 33 (2020) 188–215.
[123] K. Wu, J. Huang, J. Yi, X. Liu, Y. Liu, Y. Wang, J. Zhang, Y. Xia, Recent advances in polymer electrolytes for zinc ion batteries: mechanisms, properties, and perspectives, Adv. Energy Mater. 10 (2020) 1903977.
[124] G.S. MacGlashan, Y.G. Andreev, P.G. Bruce, Structure of the polymer electrolyte poly (ethylene oxide)$_6$: LiAsF$_6$, Nature 398 (1999) 792–794.
[125] I. Shaji, D. Diddens, N. Ehteshami, M. Winter, J.R. Nair, Multisalt chemistry in ion transport and interface of lithium metal polymer batteries, Energy Stor. Mater. 44 (2022) 263–277.
[126] L. Long, S. Wang, M. Xiao, Y. Meng, Polymer electrolytes for lithium polymer batteries, J. Mater. Chem. A 4 (2016) 10038–10069.
[127] W.H. Meyer, Polymer electrolytes for lithium-ion batteries, Adv. Mater. 10 (1998) 439–448.
[128] X. Chen, H. Zhang, J.-H. Liu, Y. Gao, X. Cao, C. Zhan, Y. Wang, S. Wang, S.-L. Chou, S.-X. Dou, Vanadium-based cathodes for aqueous zinc-ion batteries: Mechanism, design strategies and challenges, Energy Stor. Mater. 50 (2022) 21–46.
[129] W. Liu, X. Zhang, Y. Huang, B. Jiang, Z. Chang, C. Xu, F. Kang, β-MnO2 with proton conversion mechanism in rechargeable zinc ion battery, J. Energy Chem. 56 (2021) 365–373.
[130] Q. Zhao, A. Song, W. Zhao, R. Qin, S. Ding, X. Chen, Y. Song, L. Yang, H. Lin, S. Li, Boosting the energy density of aqueous batteries via facile grotthuss proton transport, Angew. Chem. 133 (2021) 4215–4220.
[131] X. Gao, H. Wu, W. Li, Y. Tian, Y. Zhang, H. Wu, L. Yang, G. Zou, H. Hou, X. Ji, H+-insertion boosted α-MnO2 for an aqueous Zn-ion battery, Small 16 (2020) 1905842.
[132] M.W. Tsang, S. Holdcroft, Alternative proton exchange membranes by chain-growth polymerization, Polym. Sustain. Environ. Green Energy (2012) 651.
[133] W. Liang, Y. Che, Z. Cai, R. Tang, Z. Ma, X. Zheng, X. Wu, J. Li, H. Jin, C. Zhu, Surface decoration manipulating Zn2+/H+ carrier ratios for hyperstable aqueous zinc ion battery cathode, Adv. Funct. Mater. (2023) 2304798.
[134] Z. Zhao, J. Yin, J. Yin, X. Guo, Y. Lei, Z. Tian, Y. Zhu, O.F. Mohammed, H. N. Alshareef, End-capping of hydrogen bonds: A strategy for blocking the proton conduction pathway in aqueous electrolytes, Energy Stor. Mater. 55 (2023) 479–489.
[135] W. Sun, F. Wang, S. Hou, C. Yang, X. Fan, Z. Ma, T. Gao, F. Han, R. Hu, M. Zhu, Zn/MnO2 battery chemistry with H+ and Zn2+ coinsertion, J. Am. Chem. Soc. 139 (2017) 9775–9778.
[136] X. Chen, X. Hu, Y. Chen, X. Cao, Y. Huang, H. Zhang, J.-H. Liu, Y. Wang, S.-L. Chou, D. Cao, Ultrastable hydrated vanadium dioxide cathodes for high-performance aqueous zinc ion batteries with H+/Zn 2+ Co-insertion mechanism, J. Mater. Chem. A 10 (2022) 22194–22204.
[137] K. Zhu, T. Wu, S. Sun, W. van den Bergh, M. Stefik, K. Huang, Synergistic H+/Zn2+ dual ion insertion mechanism in high-capacity and ultra-stable hydrated VO2 cathode for aqueous Zn-ion batteries, Energy Stor. Mater. 29 (2020) 60–70.
[138] S. Chen, M. Zhang, P. Zou, B. Sun, S. Tao, Historical development and novel concepts on electrolytes for aqueous rechargeable batteries, Energy Environ. Sci. 15 (2022) 1805–1839.
[139] J. Xu, C. Wang, Perspective—electrolyte design for aqueous batteries: from ultra-high concentration to low concentration? J. Electrochem. Soc. 169 (2022) 030530.
[140] L. Suo, O. Borodin, Y. Wang, X. Rong, W. Sun, X. Fan, S. Xu, M.A. Schroeder, A. V. Cresce, F. Wang, Water-in-salt" electrolyte makes aqueous sodium-ion battery safe, green, and long-lasting, Adv. Energy Mater. 7 (2017) 1701189.
[141] L. Chen, L. Cao, X. Ji, S. Hou, Q. Li, J. Chen, C. Yang, N. Eidson, C. Wang, Enabling safe aqueous lithium ion open batteries by suppressing oxygen reduction reaction, Nat. Commun. 11 (2020) 2638.
[142] Y. Shen, B. Liu, X. Liu, J. Liu, J. Ding, C. Zhong, W. Hu, Water-in-salt electrolyte for safe and high-energy aqueous battery, Energy Stor. Mater. 34 (2021) 461–474.
[143] F. Wang, O. Borodin, T. Gao, X. Fan, W. Sun, F. Han, A. Faraone, J.A. Dura, K. Xu, C. Wang, Highly reversible zinc metal anode for aqueous batteries, Nat. Mater. 17 (2018) 543–549.
[144] Y. Zhong, X. Xie, Z. Zeng, B. Lu, G. Chen, J. Zhou, Triple-function Hydrated eutectic electrolyte for enhanced aqueous zinc batteries, Angew. Chem. Int. Ed. 62 (2023) e202310577.
[145] L. Zhao, Y. Li, M. Yu, Y. Peng, F. Ran, Electrolyte-wettability issues and challenges of electrode materials in electrochemical energy storage, energy conversion, and beyond, Adv. Sci. (2023) 2300283.
[146] L. Li, G. Xu, S. Zhang, S. Dong, S. Wang, Z. Cui, X. Du, C. Wang, B. Xie, J. Du, Highly fluorinated Al-centered lithium salt boosting the interfacial compatibility of Li-metal batteries, ACS Energy Lett. 7 (2022) 591–598.
[147] X. He, B. Yan, X. Zhang, Z. Liu, D. Bresser, J. Wang, R. Wang, X. Cao, Y. Su, H. Jia, Fluorine-free water-in-ionomer electrolytes for sustainable lithium-ion batteries, Nat. Commun. 9 (2018) 5320.
[148] F. Wang, O. Borodin, M.S. Ding, M. Gobet, J. Vatamanu, X. Fan, T. Gao, N. Eidson, Y. Liang, W. Sun, Hybrid aqueous/non-aqueous electrolyte for safe and high-energy Li-ion batteries, Joule 2 (2018) 927–937.
[149] Q. Dou, S. Lei, D.-W. Wang, Q. Zhang, D. Xiao, H. Guo, A. Wang, H. Yang, Y. Li, S. Shi, Safe and high-rate supercapacitors based on an "acetonitrile/water in salt" hybrid electrolyte, Energy Environ. Sci. 11 (2018) 3212–3219.
[150] X. Yuan, Y. Li, Y. Zhu, W. Deng, C. Li, Z. Zhou, J. Hu, M. Zhang, H. Chen, R. Li, Low concentration DMF/H2O hybrid electrolyte: a new opportunity for anode materials in aqueous potassium-ion batteries, ACS Appl. Mater. Interfaces 13 (2021) 38248–38255.
[151] Z. Huang, R. Hempelmann, Y. Zhang, L. Tao, R. Chen, Pairing nitroxyl radical and phenazine with electron-withdrawing/-donating substituents in "water-in-ionic liquid" for high-voltage aqueous redox flow batteries, Green Energy Environ. (2022).
[152] Y. Zhang, R. Ye, D. Henkensmeier, R. Hempelmann, R. Chen, Water-in-ionic liquid" solutions towards wide electrochemical stability windows for aqueous rechargeable batteries, Electrochim. Acta 263 (2018) 47–52.
[153] V. Gregorio, P. Jankowski, N. Garcia, J.M. Garcia Lastra, P. Tiemblo, J.H. Chang, Electrolytes for Zn batteries: deep eutectic solvents in polymer gels, ChemSusChem (2023) e202300256.
[154] X. Qin, X. Zhao, G. Zhang, Z. Wei, L. Li, X. Wang, C. Zhi, H. Li, C. Han, B. Li, Highly reversible intercalation of calcium ions in layered vanadium compounds enabled by acetonitrile–water hybrid electrolyte, ACS Nano (2023).
[155] D. Das, S. Manna, S. Puravankara, Electrolytes, additives and binders for NMC cathodes in Li-ion batteries—A review, Batteries 9 (2023) 193.
[156] S. Klein, P. Harte, S. van Wickeren, K. Borzutzki, S. Röser, P. Bärmann, S. Nowak, M. Winter, T. Placke, J. Kasnatscheew, Re-evaluating common electrolyte additives for high-voltage lithium ion batteries, Cell Rep. Phys. Sci. 2 (2021).
[157] J.W. Park, D.H. Park, S. Go, D.-H. Nam, J. Oh, Y.-K. Han, H. Lee, Malonatophosphate as an SEI-and CEI-forming additive that outperforms malonatoborate for thermally robust lithium-ion batteries, Energy Stor. Mater. 50 (2022) 75–85.
[158] J. Xie, Z. Liang, Y.-C. Lu, Molecular crowding electrolytes for high-voltage aqueous batteries, Nat. Mater. 19 (2020) 1006–1011.
[159] M. Peng, L. Wang, L. Li, Z. Peng, X. Tang, T. Hu, K. Yuan, Y. Chen, Molecular crowding agents engineered to make bioinspired electrolytes for high-voltage aqueous supercapacitors, EScience 1 (2021) 83–90.
[160] J. Kong, Y. Wang, Y. Wu, L. Zhang, M. Gong, X. Lin, D. Wang, Toward high-energy-density aqueous lithium-ion batteries using silver nanowires as current collectors, Molecules 27 (2022) 8207.
[161] D. Dong, J. Xie, Z. Liang, Y.-C. Lu, Tuning intermolecular interactions of molecular crowding electrolyte for high-performance aqueous batteries, ACS Energy Lett. 7 (2021) 123–130.
[162] S. Krishnan, D.K. Rai, X. Wang, Boosting the performance of aqueous ammonium-ion batteries by mitigating side reactions using polymer additive, ACS Appl. Polym. Mater. (2023).
[163] C. Lv, Y. Li, Y. Zhu, Y. Zhang, J. Kuang, D. Huang, Y. Tang, H. Wang, Precipitation-free aluminum-air batteries with high capacity and durable service life, Chem. Eng. J. 462 (2023) 142182.
[164] T. Wang, H. Cheng, Z. Tian, Z. Li, Z. Lin, Z. You, Y. Lu, Y. Zhu, W. Li, Y. Yang, Simultaneous regulation on electrolyte structure and electrode interface with glucose additive for high-energy aluminum metal-air batteries, Energy Stor. Mater. 53 (2022) 371–380.
[165] F. Ding, W. Xu, G.L. Graff, J. Zhang, M.L. Sushko, X. Chen, Y. Shao, M. H. Engelhard, Z. Nie, J. Xiao, Dendrite-free lithium deposition via self-healing electrostatic shield mechanism, J. Am. Chem. Soc. 135 (2013) 4450–4456.
[166] Z. Hu, F. Zhang, Y. Zhao, H. Wang, Y. Huang, F. Wu, R. Chen, L. Li, A self-regulated electrostatic shielding layer toward dendrite-free Zn batteries, Adv. Mater. 34 (2022) 2203104.
[167] X. Zhang, J. Chen, H. Cao, X. Huang, Y. Liu, Y. Chen, Y. Huo, D. Lin, Q. Zheng, K. h. Lam, Efficient suppression of dendrites and side reactions by strong electrostatic shielding effect via the additive of Rb2SO4 for anodes in aqueous zinc-ion batteries, Small (2023) 2303906.
[168] X. Guo, Z. Zhang, J. Li, N. Luo, G.-L. Chai, T.S. Miller, F. Lai, P. Shearing, D. J. Brett, D. Han, Alleviation of dendrite formation on zinc anodes via electrolyte additives, ACS Energy Lett. 6 (2021) 395–403.
[169] R. Zhao, H. Wang, H. Du, Y. Yang, Z. Gao, L. Qie, Y. Huang, Lanthanum nitrate as aqueous electrolyte additive for favourable zinc metal electrodeposition, Nat. Commun. 13 (2022) 3252.
[170] Y. Ding, X. Zhang, T. Wang, B. Lu, Z. Zeng, Y. Tang, J. Zhou, S. Liang, A dynamic electrostatic shielding layer toward highly reversible Zn metal anode, Energy Stor. Mater. 62 (2023) 102949.
[171] Z. Wang, M. Zhou, L. Qin, M. Chen, Z. Chen, S. Guo, L. Wang, G. Fang, S. Liang, Simultaneous regulation of cations and anions in an electrolyte for high-capacity, high-stability aqueous zinc–vanadium batteries, Escience 2 (2022) 209–218.
[172] H. Cao, X. Huang, Y. Liu, Q. Hu, Q. Zheng, Y. Huo, F. Xie, J. Zhao, D. Lin, An efficient electrolyte additive of tetramethylammonium sulfate hydrate for Dendritic-Free zinc anode for aqueous Zinc-ion batteries, J. Colloid Interface Sci. 627 (2022) 367–374.

[173] M. Yan, N. Dong, X. Zhao, Y. Sun, H. Pan, Tailoring the stability and kinetics of Zn anodes through trace organic polymer additives in dilute aqueous electrolyte, ACS Energy Lett. 6 (2021) 3236–3243.
[174] J. Luo, L. Xu, Y. Zhou, T. Yan, Y. Shao, D. Yang, L. Zhang, Z. Xia, T. Wang, L. Zhang, Regulating the inner helmholtz plane with a high donor additive for efficient anode reversibility in aqueous Zn-ion batteries, Angew. Chem. 135 (2023) e202302302.
[175] Z. Wang, J. Diao, J.N. Burrow, K.K. Reimund, N. Katyal, G. Henkelman, C. B. Mullins, Urea-modified ternary aqueous electrolyte with tuned intermolecular interactions and confined water activity for high-stability and high-voltage zinc-ion batteries, Adv. Funct. Mater. 33 (2023) 2304791.
[176] M. Wang, Y. Cheng, H. Zhao, J. Gao, J. Li, Y. Wang, J. Qiu, H. Zhang, X. Chen, Y. Wei, A multifunctional organic electrolyte additive for aqueous zinc ion batteries based on polyaniline cathode, Small (2023) 2302105.
[177] T.C. Li, Y. Lim, X.L. Li, S. Luo, C. Lin, D. Fang, S. Xia, Y. Wang, H.Y. Yang, A universal additive strategy to reshape electrolyte solvation structure toward reversible Zn storage, Adv. Energy Mater. 12 (2022) 2103231.
[178] W. Xu, K. Zhao, W. Huo, Y. Wang, G. Yao, X. Gu, H. Cheng, L. Mai, C. Hu, X. Wang, Diethyl ether as self-healing electrolyte additive enabled long-life rechargeable aqueous zinc ion batteries, Nano Energy 62 (2019) 275–281.
[179] W. Deng, Z. Xu, X. Wang, High-donor electrolyte additive enabling stable aqueous zinc-ion batteries, Energy Stor. Mater. 52 (2022) 52–60.
[180] W. Chu, X. Zhang, S. Zhao, M. Tang, S. Li, S. Liu, H. Yu, High-voltage deep eutectic solvent electrolyte with fluorine-substituted acetamide additive for aluminum-ion battery, Adv. Funct. Mater. (2023) 2305194.
[181] P. Samanta, S. Ghosh, N.C. Murmu, T. Kuila, Effect of redox additive in aqueous electrolyte on the high specific capacitance of cation incorporated MnCo2O4@ Ni (OH) 2 electrode materials for flexible symmetric supercapacitor, Compos. Part B: Eng. 215 (2021) 108755.
[182] A.A. Hor, N. Yadav, S. Hashmi, Enhanced energy density quasi-solid-state supercapacitor based on an ionic liquid incorporated aqueous gel polymer electrolyte with a redox-additive trimethyl sulfoxonium iodide, J. Energy Stor. 64 (2023) 107227.
[183] M. Eredia, S. Bellani, M.I. Zappia, L. Gabatel, V. Galli, A. Bagheri, H. Beydaghi, G. Bianca, I. Conticello, V. Pellegrini, High-energy density aqueous supercapacitors: The role of electrolyte pH and KI redox additive, APL Mater. 10 (2022).
[184] Y. Zhang, H. Li, S. Huang, S. Fan, L. Sun, B. Tian, F. Chen, Y. Wang, Y. Shi, H. Y. Yang, Rechargeable aqueous zinc-ion batteries in $MgSO_4/ZnSO_4$ hybrid electrolytes, Micro Nano Lett. 12 (2020) 1–16.
[185] N. Liu, X. Wu, L. Fan, C. Zhao, Z. Guo, A. Chen, Y. Zhang, N. Zhang, Synergistic effect of multi-electron conversion and anion redox media chemistry for high-performance rechargeable aqueous Zn ion batteries, J. Mater. Chem. A 10 (2022) 2807–2812.
[186] R. Sun, D. Han, C. Cui, Z. Han, X. Guo, B. Zhang, Y. Guo, Y. Liu, Z. Weng, Q. H. Yang, A self-deoxidizing electrolyte additive enables highly stable aqueous zinc batteries, Angew. Chem. 135 (2023) e202303557.
[187] C. Zhu, J. Zhou, Z. Wang, Y. Zhou, X. He, X. Zhou, J. Liu, C. Yan, T. Qian, Phase diagrams guided design of low-temperature aqueous electrolyte for Zn metal batteries, Chem. Eng. J. 454 (2023) 140413.
[188] Q. Nian, J. Wang, S. Liu, T. Sun, S. Zheng, Y. Zhang, Z. Tao, J. Chen, Aqueous batteries operated at− 50°C, Angew. Chem. Int. Ed. 58 (2019) 16994–16999.
[189] Q. Zhang, Y. Ma, Y. Lu, L. Li, F. Wan, K. Zhang, J. Chen, Modulating electrolyte structure for ultralow temperature aqueous zinc batteries, Nat. Commun. 11 (2020) 4463.
[190] K. Zhu, Z. Li, Z. Sun, P. Liu, T. Jin, X. Chen, H. Li, W. Lu, L. Jiao, Inorganic electrolyte for low-temperature aqueous sodium ion batteries, Small 18 (2022) 2107662.
[191] Y. Hu, R. Shi, Y. Ren, W. Peng, C. Feng, Y. Zhao, S. Zheng, W. Li, Z. Sun, J. Guo, A "Two-in-One" strategy for flexible aqueous batteries operated at− 80°C, Adv. Funct. Mater. 32 (2022) 2203081.
[192] D. Feng, Y. Jiao, P. Wu, Proton-reservoir hydrogel electrolyte for long-term cycling Zn/PANI batteries in wide temperature range, Angew. Chem. 135 (2023) e202215060.
[193] Y. Yan, S. Duan, B. Liu, S. Wu, Y. Alsaid, B. Yao, S. Nandi, Y. Du, T.W. Wang, Y. Li, Tough hydrogel electrolytes for anti-freezing zinc-ion batteries, Adv. Mater. 35 (2023) 2211673.
[194] T. Nguyen Thanh Tran, M. Zhao, S. Geng, D.G. Ivey, Ethylene glycol as an antifreeze additive and corrosion inhibitor for aqueous zinc-ion batteries, Batteries Supercaps 5 (2022) e202100420.
[195] J. Zhang, Q. Dou, C. Yang, L. Zang, X. Yan, Polyiodide shuttle inhibition in ethylene glycol-added aqueous electrolytes for high energy and long-term cyclability of zinc–iodine batteries, J. Mater. Chem. A 11 (2023) 3632–3639.
[196] N. Wang, Y. Yang, X. Qiu, X. Dong, Y. Wang, Y. Xia, Stabilized rechargeable aqueous zinc batteries using ethylene glycol as water blocker, ChemSusChem 13 (2020) 5556–5564.
[197] Y. Zhao, Z. Chen, F. Mo, D. Wang, Y. Guo, Z. Liu, X. Li, Q. Li, G. Liang, C. Zhi, Aqueous rechargeable metal-ion batteries working at subzero temperatures, Adv. Sci. 8 (2021) 2002590.
[198] Y. Sui, M. Yu, Y. Xu, X. Ji, Low-temperature aqueous batteries: Challenges and opportunities, J. Electrochem. Soc. 169 (2022) 030537.
[199] H.-I. Kim, E. Shin, S.-H. Kim, K.M. Lee, J. Park, S.J. Kang, S. So, K.C. Roh, S. K. Kwak, S.-Y. Lee, Aqueous eutectic lithium-ion electrolytes for wide-temperature operation, Energy Stor. Mater. 36 (2021) 222–228.
[200] G. Yang, X. Xu, G. Qu, J. Deng, Y. Zhu, C. Fang, O. Fontaine, P. Hiralal, J. Zheng, H. Zhou, An aqueous magnesium-ion battery working at− 50°C enabled by modulating electrolyte structure, Chem. Eng. J. 455 (2023) 140806.
[201] C. Yang, J. Xia, C. Cui, T.P. Pollard, J. Vatamanu, A. Faraone, J.A. Dura, M. Tyagi, A. Kattan, E. Thimsen, All-temperature zinc batteries with high-entropy aqueous electrolyte, Nat. Sustain. 6 (2023) 325–335.
[202] X. Jin, L. Song, C. Dai, H. Ma, Y. Xiao, X. Zhang, Y. Han, X. Li, J. Zhang, Y. Zhao, A self-healing zinc ion battery under-20°C, Energy Stor. Mater. 44 (2022) 517–526.
[203] Y. An, Y. Tian, K. Zhang, Y. Liu, C. Liu, S. Xiong, J. Feng, Y. Qian, Stable aqueous anode-free zinc batteries enabled by interfacial engineering, Adv. Funct. Mater. 31 (2021) 2101886.
[204] S. Moelbert, B. Normand, P. De Los Rios, Kosmotropes and chaotropes: modelling preferential exclusion, binding and aggregate stability, Biophys. Chem. 112 (2004) 45–57.
[205] J.C. Biffinger, H.W. Kim, S.G. DiMagno, The polar hydrophobicity of fluorinated compounds, Chembiochem 5 (2004) 622–627.
[206] J. Han, A. Mariani, S. Passerini, A. Varzi, A perspective on the role of anions in highly concentrated aqueous electrolytes, Energy Environ. Sci. 16 (2023) 1480–1501.
[207] D. Reber, R. Grissa, M. Becker, R.S. Kühnel, C. Battaglia, Anion selection criteria for water-in-salt electrolytes, Adv. Energy Mater. 11 (2021) 2002913.
[208] B. Scharifker, G. Hills, Theoretical and experimental studies of multiple nucleation, Electrochim. Acta 28 (1983) 879–889.
[209] K.I. Assaf, W.M. Nau, The chaotropic effect as an assembly motif in chemistry, Angew. Chem. Int. Ed. 57 (2018) 13968–13981.
[210] D. Bastos-González, L. Pérez-Fuentes, C. Drummond, J. Faraudo, Ions at interfaces: the central role of hydration and hydrophobicity, Curr. Opin. Colloid Interface Sci. 23 (2016) 19–28.
[211] Q. Zhang, K. Xia, Y. Ma, Y. Lu, L. Li, J. Liang, S. Chou, J. Chen, Chaotropic anion and fast-kinetics cathode enabling low-temperature aqueous Zn batteries, ACS Energy Lett. 6 (2021) 2704–2712.
[212] Z. Huang, Y. Hou, T. Wang, Y. Zhao, G. Liang, X. Li, Y. Guo, Q. Yang, Z. Chen, Q. Li, Manipulating anion intercalation enables a high-voltage aqueous dual ion battery, Nat. Commun. 12 (2021) 3106.
[213] Y. Song, J. Hu, J. Tang, W. Gu, L. He, X. Ji, Real-time X-ray imaging reveals interfacial growth, suppression, and dissolution of zinc dendrites dependent on anions of ionic liquid additives for rechargeable battery applications, ACS Appl. Mater. Interfaces 8 (2016) 32031–32040.
[214] S. Jin, F. Duan, X. Wu, J. Li, X. Dan, X. Yin, K. Zhao, Y. Wei, Y. Sui, F. Du, Stabilizing interface pH by mixing electrolytes for high-performance aqueous Zn metal batteries, Small 18 (2022) 2205462.
[215] P. Li, Y. Wang, Q. Xiong, Y. Hou, S. Yang, H. Cui, J. Zhu, X. Li, Y. Wang, R. Zhang, Manipulating coulombic efficiency of cathodes in aqueous zinc batteries by anion chemistry, Angew. Chem. 135 (2023) e202303292.
[216] N. Zhang, F. Cheng, Y. Liu, Q. Zhao, K. Lei, C. Chen, X. Liu, J. Chen, Cation-deficient spinel $ZnMn_2O_4$ cathode in Zn $(CF_3SO_3)_2$ electrolyte for rechargeable aqueous Zn-ion battery, J. Am. Chem. Soc. 138 (2016) 12894–12901.
[217] S. Glasstone, An Introduction to Electrochemistry, Read Books Ltd., 2011.
[218] B. Lee, H.R. Seo, H.R. Lee, C.S. Yoon, J.H. Kim, K.Y. Chung, B.W. Cho, S.H. Oh, Critical role of pH evolution of electrolyte in the reaction mechanism for rechargeable zinc batteries, ChemSusChem 9 (2016) 2948–2956.
[219] W. Zhang, Y. Dai, R. Chen, Z. Xu, J. Li, W. Zong, H. Li, Z. Li, Z. Zhang, J. Zhu, Highly reversible zinc metal anode in a dilute aqueous electrolyte enabled by a pH buffer additive, Angew. Chem. Int. Ed. 62 (2023) e202212695.
[220] C. Dong, F. Xu, L. Chen, Z. Chen, Y. Cao, Design strategies for high-voltage aqueous batteries, Small Struct. 2 (2021) 2100001.
[221] Y. Lyu, J.A. Yuwono, P. Wang, Y. Wang, F. Yang, S. Liu, S. Zhang, B. Wang, K. Davey, J. Mao, Organic pH buffer for dendrite-free and shuttle-free Zn-I_2 batteries, Angew. Chem. Int. Ed. 62 (2023) e202303011.
[222] X. Zhao, X. Zhang, N. Dong, M. Yan, F. Zhang, K. Mochizuki, H. Pan, Advanced buffering acidic aqueous electrolytes for ultra-long life aqueous zinc-ion batteries, Small 18 (2022) 2200742.
[223] X. Gao, Y. Dai, C. Zhang, Y. Zhang, W. Zong, W. Zhang, R. Chen, J. Zhu, X. Hu, M. Wang, When It's heavier: interfacial and solvation chemistry of isotopes in aqueous electrolytes for Zn-ion batteries, Angew. Chem. Int. Ed. 62 (2023) e202300608.
[224] X. Zhang, X. Liu, H. Zhang, Z. Wang, Y. Zhang, G. Li, M.-j. Li, G. He, Robust chalcogenophene viologens as anolytes for long-life aqueous organic redox flow batteries with high battery voltage, ACS Appl. Mater. Interfaces 14 (2022) 48727–48733.
[225] T. Wei, Y. Ren, Y. Wang, L.e. Mo, Z. Li, H. Zhang, L. Hu, G. Cao, Addition of dioxane in electrolyte promotes (002)-textured zinc growth and suppressed side reactions in zinc-ion batteries, ACS Nano 17 (2023) 3765–3775.
[226] J.L. Teunissen, F. De Proft, F. De Vleeschouwer, Tuning the HOMO–LUMO energy gap of small diamondoids using inverse molecular design, J. Chem. Theory Comput. 13 (2017) 1351–1365.
[227] S. Dervin, S.C. Pillai, An Introduction to Sol-Gel Processing For aerogels, Sol-gel materials For energy, Environment and Electronic Applications, Springer, 2017, pp. 1–22.